Title: Improved sample utilization in thermal ionization mass spectrometry isotope ratio measurements: refined development of porous ion emitters for nuclear forensic applications

Author(s): Baruzzini, Matthew Louis

Intended for: PhD Dissertation

Issued: 2017-05-08

Improved sample utilization in thermal ionization mass spectrometry isotope ratio measurements: refined development of porous ion emitters for nuclear forensic applications

A Dissertation Presented for the
Doctor of Philosophy
Degree
The University of Tennessee, Knoxville

Matthew Louis Baruzzini
May 2017

To my parents, Louis and Deborah Baruzzini, for their unwavering support

and encouragement over the years

Acknowledgements

I would like to thank Floyd Stanley and Khalil Spencer of the Actinide Analytical Chemistry Group (C-AAC) at Los Alamos National Laboratory (LANL) for their mentoring and guidance while completing the research for this dissertation. I would also like to express my gratitude to my current group management, Dave Hayes and Bill Myers, of the Advanced Nuclear Technology Group (NEN-2) at LANL for providing feedback and allowing me time to work on my dissertation. I would like to extent thanks to Howard Hall for chairing my committee and serving as my advisor during my time at the University of Tennessee – Knoxville. I would like to thank my committee members, Dr. Lawrence Heilbronn, Dr. Steven Skutnik, and Dr. Michael Sepaniak for their service and review of this work. I would also like to thank Dr. John Auxier for taking time out of his busy schedule to review this work and offer his expertise. Finally, I would like to gratefully acknowledge the support of the U.S. Department of Homeland Security under

Grant Award Number, 2012-DN-130-NF0001-02. The views and conclusions contained in this document are those of the authors and should not be interpreted as necessarily representing the official policies, either expressed or implied, of the U.S. Department of Homeland Security. The U.S. Department of Energy/National Nuclear Security Administration Office of Nonproliferation and Verification Research and Development and the U.S. Department of Energy through the LANL/LDRD Program provided additional support.

Abstract

The precise and accurate determination of isotopic composition in nuclear forensic samples is vital for assessing origin, intended use and process history. Thermal ionization mass spectrometry (TIMS) is widely accepted as the gold standard for high performance isotopic measurements and has long served as the workhorse in the isotopic ratio determination of nuclear materials. Nuclear forensic and safeguard specialists have relied heavily on such methods for both routine and atypical efforts. Despite widespread use, TIMS methods for the assay of actinide systems continue to be hindered by poor ionization efficiency, often less than tenths of a percent; the majority of a sample is not measured. This represents a growing challenge in addressing next-generation nuclear detection needs by limiting the ability to analyze ultra-trace quantities of high priority elements that could potentially provide critical nuclear forensic signatures. Porous ion emitter (PIE) thermal ion sources were developed in response to the growing need for new TIMS ion source technologies. By simultaneously incorporating multiple, previously developed strategies for improved ionization efficiency, PIEs have proven to be simple to implement, straightforward approach to boosting ion yield.

This work serves to expand the use of PIE techniques for the analysis of trace quantities of plutonium and americium. PIEs exhibited superior plutonium and americium ion yields when compared to direct filament loading and the resin bead technique, one of the most efficient methods for actinide analysis, at similar mass loading levels. Initial attempts at altering PIE composition for the analysis of plutonium proved to enhance sample utilization even further. Preliminary investigations of the instrumental fractionation behavior of plutonium and uranium analyzed via PIE methods were conducted. Data collected during these initial trial indicate that PIEs fractionate in a consistent, reproducible manner; a necessity for high precision isotope ratio measurements. Ultimately, PIEs methods were applied for the age determination of various uranium isotopic standards. PIEs did not exhibit significant advantages for the determination of model ages when compared to traditional filaments; however, this trial was able to provide valuable insight for guiding future investigations.

Table of Contents

List of Tables

List of Figures

Acronyms

%RSD percent relative standard deviation. 82, 127

AMDC Atomic Mass Data Center. 98

CRM certified reference material. 72, 93, 100, 103, 111, 119

DDEP Decay Data Evaluation Project. 97

DI deionized. 71, 72, 94, 119, 126, 143

DOE Department of Energy. 4, 147

FWHM full width at half maximum. 18

GUM evaluation of measurement data – guide to the expression of uncertainty in measurement. 130

HECS high efficiency cavity source. 52, 53, 55

IAEA International Atomic Energy Agency. 20

ICP-MS inductively coupled plasma mass spectrometry. 116

IDMS isotope dilution mass spectrometry. 120, 122, 125, 129

IRM isotopic reference material. 93, 105, 107, 111, 122

IRMM Institute for Reference Materials and Measurements. 93

IRMS isotope ratio mass spectrometry. 7, 89

IUPAC International Union of Pure and Applied Chemistry. 15

JCGM Joint Committee for Guides in Metrology. 130

LANL Los Alamos National Laboratory. 68, 73, 94, 119

MC-ICP-MS multi-collector ICP-MS. 91, 132, 135

MC-TIMS multi-collector TIMS. 19, 53

NBL New Brunswick Laboratory. 15, 72, 93, 119, 131, 132, 135, 137, 140

NBS National Bureau of Standards. 46, 50, 119

NIST National Institute of Standards and Technology. 15

NNSA National Nuclear Security Administration. 4, 147

PIE porous ion emitter. 3, 5–11, 20, 55–60, 64–69, 71–75, 77–80, 82, 84–86, 88, 92–94, 100, 103, 107, 111, 112, 114, 118, 122, 125–128, 131–140, 142–145, 147–149

PMT photomultiplier tube. 174

RF radio frequency. 48, 49

SEM scanning electron microscope. 59, 82

SEM/EDS scanning electron microscopy with energy dispersive X-ray spectroscopy. 56, 84

SID surface ionization-diffusion. 49, 50

SRM standard reference material. 119, 144

TE total evaporation. 95, 96, 121

TIC thermal ion cavity. 6, 51, 52, 54, 55, 66, 75

TIMS thermal ionization mass spectrometry. 2–7, 11, 13–16, 18–21, 24, 25, 27, 29, 30, 37, 38, 41, 45, 52, 54, 58, 61, 64–66, 82, 84, 86, 88, 90–92, 94, 96, 111, 118, 120, 121, 125, 135, 139, 140, 142, 145, 147, 148, 168

TOF time of flight. 52

WARP	wide aperture retarding potential. 73, 74, 95, 125, 126, 176

List of Symbols

H_3PO_4 phosphoric acid. 45, 46, 124, 128, 138, 144

HCL hydrochloric acid. 123, 124

HNO_3 nitric acid. 93, 120, 124, 144

LN_2 liquid nitrogen. 74, 95, 121, 125

Pt/Re platinum and rhenium in a 50/50, by mass, mix. 57, 69, 71, 74, 75, 79, 80, 82, 84–86, 88, 148

$SiCl_4$ silicon tetrachloride. 143

Chapter 1

Introduction

1.1 Background

Thermal ionization mass spectrometry (TIMS) is internationally accepted as a benchmark technique for obtaining highly precise and accurate data on isotope amount ratios and concentrations of samples containing actinides present in levels ranging from ultra-trace to bulk. In addition to excellent accuracy and precision, TIMS offers advantages such as mass spectra that are essentially free from background interferences and relatively minimal fractionation effects when compared to other isotope ratio techniques; despite these advantages TIMS methodologies are hampered by inadequate sample utilization. This represents a growing challenge in addressing next-generation nuclear detection needs, namely, measuring trace and ultra-trace forensic signatures and characterizing the age of young materials with minute progeny in-growth. Ionization efficiencies for high priority elements like uranium and thorium, for example, are below a few tenths of a percent, leaving the vast majority of a tediously prepared sample completely unmeasured [1, 2]. Unfortunately, efforts aimed at addressing this need through ion source redesign have yet to match the spectacular progress made in electronic, vacuum, and ion detection technologies.

1.2 Objective and impacts of this work

This research was conducted to address the need for state-of-the-art mass spectrometry approaches that exhibit improved sample utilization during isotope ratio measurements. During this work several advancements were pursued through systematically augmenting the current design and application of porous ion emitters (PIEs) as TIMS sources. The capabilities developed herein have expanded the set of mass spectrometry techniques employed to detect useful nuclear forensic signatures, ensure international treaty compliance, and monitor environmental presence of actinides. Additionally, this work includes a comprehensive review of features associated commonly employed TIMS ion source technologies, the basis for thermal ionization, and various efforts that have sought to improve sample utilization during TIMS analyses. Throughout this work, the terms sample utilization, ionization efficiency, and ion yield will be used interchangeably to describe the ratio of the number of neutral atoms of an isotope loaded on the filament to the number of ions counted by the detection system.

This work is intended to expand the use of PIEs to the analysis of trace quantities of actinides, capitalize on the enhanced sample utilization associated with PIEs to address current challenges in uranium chronometry, and refine existing TIMS source preparation methods to improve ionization for a range of actinides. Key deliverables form this work include developing novel TIMS methods capable of detecting critical materials signatures while utilizing lower sample quantities than previously possible and improved chronometric analysis capabilities for furthering investigations of nuclear material provenance and interrogation samples containing only trace levels of uranium progeny. These enhanced capabilities offer the potential to greatly facilitate investigations of actinide systems in the field of nuclear forensics. Though nuclear forensic applications are the central focus of this dissertation, the majority of the concepts presented herein are undoubtedly of high value in an array of fields employing TIMS isotopic measurement strategies.

1.3 Summary

This dissertation is comprised of a series of stand-alone manuscripts summarizing the work performed to satisfy the tasks specified in a proposal funded in by the United States Department of Energy (DOE) National Nuclear Security Administration (NNSA) Office of Proliferation Detection Research & Development (NA-22) entitled "Improved sample utilization in TIMS isotopic ratio measurements via refined development and application of porous ion emitters". While each chapter is presented as an individual work, the knowledge gleaned from the ionization efficiency and fractionation effects experiments served as crucial building blocks for the age-dating work. A brief introduction to the concepts of this dissertation are presented below.

1.3.1 Literature review

This work begins with a comprehensive review of TIMS ion source technologies. To the extent of our knowledge, a review of this magnitude has never been undertaken and was completed at the request of the sponsor. Topics covered in this evaluation include the history and basis for thermal ionization, features associated with commonly employed ion sources, and various efforts that have sought to improve sample utilization during TIMS analyses. Filament materials, geometry, and additives used in TIMS sources are discussed in detail; sample utilization numbers and sample sizes are presented when available in order for comparison of source technologies. This review culminates in section outlining PIEs, a new ion source technology designed to boost ion yield by combining previously employed strategies that have been proven to enhance ionization. Throughout this work, the terms ionization efficiency, sample utilization, utilization efficiency, and ion yield will be used interchangeably to describe the ratio of the number of neutral atoms of an isotope loaded on the filament to the number of ions counted by the detection system.

1.3.2 Enhanced ionization efficiency

Traditional filament loading techniques are associated with ionization efficiencies in the tenths-of-a-percent range for actinide-bearing samples; actinides are not easily thermally ionized due to their relatively high ionization potentials and refractory nature. Such low sample utilization considerably limits the ability to make accurate and precise measurements of such high priority elements as americium, plutonium, uranium, and thorium that could potentially provide critical nuclear forensic signatures. Over the past several decades, numerous TIMS strategies for enhancing ionization efficiency have been proposed and tested; the majority of which involve the sample being chemically reduced via the addition of carbon. Carbon can be introduced in the form of collodium, water-based colloidal graphite, ion exchange resin beads, or filament carburization for example. Indeed, the resin bead technique has proven to be one of the most effective methods for the analysis of actinides via TIMS. Drawbacks of the resin bead approach include long preparation time and tediousness of securing a pre-loaded bead atop the filament. More recently, thermal ion cavity (TIC) sources have been proposed as a method to improve sample utilization in TIMS. While enhanced sample utilization has been demonstrated using TIC, costly modifications to the sample turret, or to the source housing, or to both are often necessary [3]. PIEs have been proposed as an alternative approach to boosting ion yields without the need for modifications to the mass spectrometer's ion source. Increased ionization surface contact area, superior ion optical properties, and ion bombardment by the PIE material itself have been proposed as mechanisms of improved sample utilization. Neutral atoms incur multiple interactions with the ionizing surface as they diffuse through the PIE structure thus limiting their rapid escape and increasing the probability of ionization.

1.3.3 Mass fractionation effects

Instrumental fractionation represents a significant source of error in isotope ratio mass spectrometry (IRMS). Fractionation is the term used to describe the combination of effects in a mass spectrometer that lead to a difference between the measured and the true isotope ratio(s) of a sample. In TIMS, the rate at which each isotope evaporates from the hot metal filament depends on its abundance, mass, and on the the temperature of the filament. As analysis proceeds, a sample tends to become enriched in heavier isotopes; the result is a time-dependent variation in measured isotope ratios. The time dependence of measured isotope ratios precludes the accurate determination of a sample's true isotope ratios via direct measurement. Additionally, the accuracy of measured isotope ratios is limited because the effect of mass bias cannot be totally controlled and reproduced.

Correcting for instrumental mass fractionation can be accomplished by normalizing a measured isotope ratio to a known or accepted reference ratio. Measured isotope ratios are commonly corrected by applying one of the well known mass fractionation correction laws that appear in the literature [4–8]. All fractionation correction laws assume that evaporation and ionization of a sample occurs in a single, homogeneous point on a filament. In reality, a sample is not well represented as a point source and the temperature gradient across the filament compounds the effects of fractionation. Previous studies have demonstrated that PIEs fully contain the sample and do not permit sample migration across the filament [9, 10]. The ability of PIEs to more accurately represent a point source suggests that they may potentially reduce the effects of mass bias associated with the thermal gradient across the filament when compared to other single filament techniques.

The objective of this study is to evaluate the fractionation effects of uranium and plutonium isotopic reference standards using PIEs. Fractionation effects will be analyzed, then corrected for, using the commonly employed empirical mass bias correction laws. This portion of the project focuses on the efficacy of existing empirical laws to adequately correct fractionation exhibited using PIE sources.

1.3.4 Nuclear forensic age-dating

Determining the age of a nuclear sample can provide valuable information about a material such as origin, process history, and intended use [11, 12]. In the context of nuclear forensics a material's age refers to the time elapsed since a parent radionuclide of interest was chemically or physically separated from its decay products. The ^{230}Th/^{234}U daughter-parent isotope pair provides one of the most valued and widely used chronometers in modern nuclear forensic and nuclear safeguards research [11, 13]. These two isotopes represent the longest-lived intermediate decay products of the radium (4n + 2) decay series. The relatively rapid ingrowth of ^{230}Th has enabled this chronometer to be successfully applied for the determination of sample with ages ranging from a few years to several hundred thousand years old [2, 14, 15]. The accuracy of model-ages determined using the ^{230}Th/^{234}U chronometer rely heavily on the following assumptions: 1) the parent isotope has been completely separated form daughter products and any residual impurities, 2) the system remains closed after purification, and 3) the measured isotope ratios values are accurate.

The focus of this study is to capitalize on the enhanced thorium sample utilization associated with PIE thermal ion sources demonstrated by Stanley et al. [10] in an effort to improve precision and accuracy of model-age determination of uranium materials using the ^{230}Th/^{234}U chronometer containing trace quantities of thorium. Stanley et al. reported that in addition to exhibiting a trend of increased sample utilization as sample size decreases, a relative enhancement in sample utilization was observed as analyte loading levels were reduced [10]. These findings indicate that PIE filaments should significantly outperform traditional filaments in their ability to produce ions at femtogram mass loading levels of thorium. This boost in ion yield should translate to a more stable ion beam at higher target intensity yielding more precise and accurate isotope ratios.

1.3.5 Lead analyses

Knowing the origin of an unknown nuclear material is crucial for purposes of nuclear security, such information can be derived from the isotopic signatures of radiogenic lead. The isotopic composition of radiogenic lead in samples have long been used by geologists for the age determination of geological structures and by mining companies to assess the commercial viability of a mine from sample. Lead is composed of four stable isotopes; ^{204}Pb, ^{206}Pb,

^{207}Pb, and ^{208}Pb; only ^{204}Pb is entirely primordial and nonradiogenic. The remaining three isotopes are the end products of the ^{238}U, ^{235}U, and ^{232}Th decay chains, respectively. Natural variations of uranium and thorium isotopic composition, based on global position, coupled with large differences in their half-lives, have resulted in ore deposits with distinct lead signatures based on geolocation. Determination of geographic origin of uranium samples based on lead signatures have previously been demonstrated [16–22]. Signatures from anthropogenic lead produced from fossil fuel combustion such as industrial processes and automobile exhaust can provide additional information about geographic origin as the isotopic composition will differ from that of naturally occurring deposits. Due to the relevance of lead isotopic signatures in the field of nuclear forensics, preliminary experiments were conducted to investigate the ability of a PIE to improve ionization efficiency for the analysis of lead samples via TIMS.

Chapter 2

Evolution of the thermal ionization mass spectrometer source

This chapter, entitled “Evolution of the thermal ionization mass spectrometer source”, has been reviewed and approved for release under institutional number LA-UR-15-27578

Abstract

TIMS has served as the workhorse in the isotopic ratio determination of nuclear materials for decades and is widely regarded as the benchmark for such analyses; however, TIMS methods for the assay of actinide systems are hindered by poor ionization efficiencies (i.e., the ratio of ions detected to the total number of atoms loaded on the filament). Most of the sample remains unmeasured. For example, traditional direct filament loading techniques in TIMS are associated with analyte ionization efficiencies less than 0.1 % for actinide bearing systems [1]. The use of resin bead techniques, one of the most efficient methods for such analyses, has been shown to improve upon these values, but still yield only efficiencies, ranging from 0.5–2 %. Such low efficiencies significantly limit the ability to detect highly refractory elements (e.g., uranium and thorium) that could potentially provide critical signatures in nuclear forensic, non-proliferation and safeguards efforts. This limitation, coupled with the desire to analyze progressively smaller samples, will drive development of state-of-the-art TIMS approaches that exhibit

improved sample utilization and expand the current set of mass spectrometry techniques. This will require the development of ion sources that maximize analyte-to-filament interaction while minimizing sample spreading and ion energy distribution for enhanced abundance sensitivity.

In response to the growing need for new TIMS ion source technologies, this work provides a review of the basis for thermal ionization, features associated with commonly employed sources, and various efforts that have sought to improve sample utilization during TIMS analyses. Particular emphasis has been placed on nuclear-related applications, though most concepts are applicable to numerous other fields employing TIMS isotopic measurement strategies. Additionally, this work highlights rising developments exhibiting improved sample utilization and the attributes associated with successful approaches.

2.1 Introduction

Thermal ionization, also referred to as surface ionization, is the general process through which ions are produced by subjecting a material to elevated temperatures. TIMS exploits this process as a sample introduction method for purified solids undergoing isotopic analysis. This technique, in conjunction with relevant detection [23, 24] and sample preparation strategies [25], offers excellent precision and accuracy, relatively minimal fractionation effects, and mass spectra that are essentially free from background interferences.

Since its inception, TIMS has been used for isotopic investigations in such fields as geochemistry, archeology, and cosmochemistry. Additionally, nuclear forensics, safeguards, and fuel cycle specialists have relied heavily on such methods for both routine (e.g., nuclear fuel characterization) and atypical (e.g., illicit trafficking response) efforts. In fact, this nuclear connection has existed for decades, as demonstrated by Alfred Nier's early uranium studies [26]. TIMS is now an accepted standard for high-performance isotopic measurements and is the method of choice in establishing many material reference values [27]. For example, most International Union of Pure and Applied Chemistry (IUPAC) standard atomic weights are based on TIMS isotopic measurements [28], as are the certificate values for commonly used nuclear material standards produced by the National Institute of Standards and Technology (NIST) and the New Brunswick Laboratory (NBL).

Despite the rich history associated with TIMS methodologies, inadequate sample utilization (i.e., low analyte ion yield) represents a growing challenge in addressing next-generation nuclear detection needs, such as measuring ultra-trace (sub $\mu g \, g^{-1}$ levels) forensic or proliferation signatures, and characterizing the age of young materials with minute progeny in-growth. Ionization efficiencies for high priority species like uranium and thorium, for example, continue to fall below even the few tenths of a percent mark, leaving the vast majority of a tediously prepared sample completely unmeasured [1, 2]. Unfortunately, efforts aimed at addressing this need through source redesign have yet to match the successes observed in upgrades to other instrument components, such as detectors, vacuum pumps and controlling electronics.

2.1.1 A brief history of TIMS

The discovery of positive thermal ion emission from a heated metal surface was first documented in 1873 by Frederick Guthrie, who observed the emission of positive ions from a two inch diameter cast iron ball heated to a dull red glow at atmospheric pressure in air [29, 30]. It wasn't until 1918 that the utility of a thermal ion source was applied in the emerging field of mass spectroscopy by A. J. Dempster [31]. He successfully developed the first TIMS, establishing the fundamental theory and design used in modern-day TIMS instrumentation. His machine was a 180-degree, single-focusing magnetic sector thermal ion mass spectrograph illustrated in Figure 2.1. Samples were loaded as salts atop single platinum filaments. Positive ions were produced thermally by resistively heating the filament (A); the platinum filament ion source is still routinely employed in present-day TIMS analyses of selected elements. The

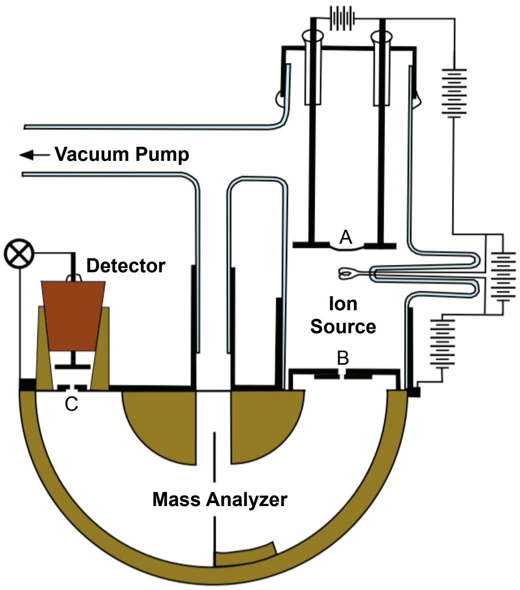

Figure 2.1: An illustration of the first thermal ionization mass spectrograph developed by A. J. Dempster, adapted from Dempster [31]. Components of Dempster's mass spectrograph relevant to contemporary TIMS are: The platinum filament upon which the sample was loaded is labeled (A), the entrance and exit slits are labeled (B) and (C), respectively.

ion beam was extracted from the source housing via high voltage and passed through an adjustable slit (B) in to the mass analyzer, also referred to as the magnetic sector. In the mass analyzer, the beam was directed around a 180-degree path resulting in separation of ions according to ions mass-to-charge ratio (m/z). Finally, ions were passed through a second adjustable exit slit (C) for detection. Unlike contemporary TIMS instrumentation, isotopic separation was achieved by varying the acceleration potential; the magnetic field was held constant. Dempster's rudimentary TIMS was capable of measuring isotopic compositions and abundances with a mass resolving power of 100. Resolving power is defined as $m/\Delta m$, where the mass is denoted by m and Δm is the width of the peak, measured at full width at half maximum (FWHM) for this specific case, required for separation at mass m.

Since its inception, TIMS has played an integral role in the discovery of isotopes and the determination of isotopic abundances. However, due to advancements in isotopic separation technology made during World War II, the mass spectrometer was no longer a tool just for physicists; its application was extended to other fields such as chemistry, biology, and the petroleum industry. Commercial applications of TIMS sparked the need for increased sample throughput. In 1954, Frederick A. White was the first to patent a device for rapid sample changes titled, "Multiple Cartridge

Source for Mass Spectrometer" [32]. His design consisted of six cartridges, allowing for the analysis of up to six samples before opening the source housing [33] and breaking vacuum; source evacuation proved to be very time-consuming. The first commercially available multi-sample TIMS, the model MM30VG manufactured by VG Micromass (Now IsotopX: Middlewich, Cheshire; UK), was introduced in 1973. The next major milestone in instrument development came in the early 1980s with the debut of the Finnegan-MAT 261 (Now Thermo Scientific: Waltham, MA: USA); the first commercial multi-collector TIMS (MC-TIMS). Multiple detectors permitted the simultaneous measurement of several isotopes, as well as for oligo-element analysis. The advent of multi-isotope collection allowed for improvements in the speed, precision, and accuracy of mass spectrometer analyses.

In the late 1950s and early 1960s several techniques were pioneered to enhance sample utilization and reduce required sample size. Filament additives such as silica gel for the analysis of lead and carbon for uranium and plutonium analyses were established. The use of multiple filaments for the analysis of a single sample was also developed around this time. Further ionization enhancements were demonstrated in the 1970s with the introduction of the canoe filament and the resin bead method for the analysis of actinides. A steady rise in the number of events involving illicit trafficking of nuclear materials, began in the mid-1990s. In response to increasing concerns, substantial efforts have been put forth in developing analytic methods relevant to international safeguard and nuclear forensic investigations. Such investigations require TIMS strategies that could further reduce the sample size of uranium and plutonium required for analysis while simultaneously improving analytic precision. The thermal ion cavity source was adapted to address this need in support of International Atomic Energy Agency (IAEA) safeguards and nonproliferation efforts [34, 35]. The most recent development in ion source technology is the PIE. This method is still new, but has exhibited promise for enhancing ionization efficiencies of uranium and thorium.

Notwithstanding considerable efforts, enhancements in thermal ion sources have been unable to keep pace with improvements associated with advancements in vacuum, detector, and instrument electronics technologies. The current generation of TIMS offers state-of-the-art electronics and the convenience of full-computer automation, resulting in a significantly improved ease of use while making high-precision measurements. These improvements have established TIMS as the gold standard for the isotopic analysis of many high priority elements such as uranium, plutonium, thorium, americium, strontium, neodymium, and lead as well as high precision isotope dilution analysis of parent-daughter systems.

2.1.2 Instrument operating principles

Much like the initial design by Dempster, a modern TIMS, illustrated in Figure 2.2, consists of three main components: 1) the ion source, 2) the mass analyzer, and 3) an ion collector. Samples, often in the form of nitrate or chloride salts, are loaded onto a refractory metallic filament, mounted onto a sample turret and placed into the ion source housing. The entire system is then evacuated to high vacuum, approximately 10^{-8} mbar. Ions are produced in the source housing, by resistively heating the sample loaded metallic filament, accelerated with an applied electric potential up to 10 kV and focused into a narrow rectangular beam by the collimator (i.e., a series of slits and electrostatically charged plates), also known as an ion lens. The collimated beam is directed down the flight tube and into the mass analyzer, where the ion beam is separated according to the mass-to-charge ratio governed by Equation 2.1;

$$\frac{m}{z} = \frac{R^2B^2}{2V}, \tag{2.1}$$

where m and z are the mass and charge of the ion, respectively (in the case of TIMS, z is almost always equal to one as thermal ionization is a soft ionization method); B and R are the magnitude and radius of the magnetic field; and V is the ion accelerating voltage. See Appendix A for a detailed derivation of

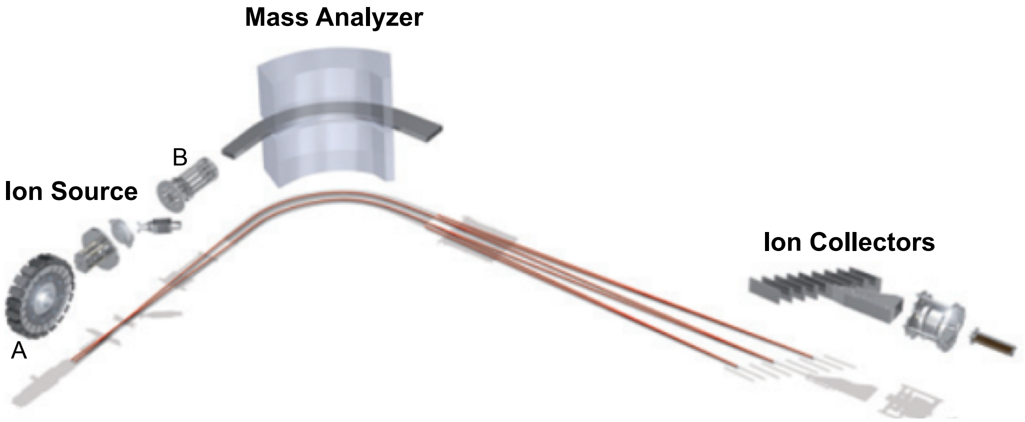

Figure 2.2: An exploded view illustration of a modern TIMS instrument. Much like Dempster's design, contemporary TIMS instruments are composed of three main components: the ion source, mass analyzer, and the ion collector(s). The sample turret is labeled (A) and the ion optic lenses are labeled (B) are contained in the source housing. This figure was adapted from Thermo Fisher Scientific [36]

Equation 2.1. The mass-resolved beam is then directed to the ion collection system where the ion beam(s) will be measured, either sequentially (i.e., single collector) or simultaneously (i.e., multi-collector), and isotope ratios are calculated.

2.1.3 Theory of surface ionization

The majority of the groundwork for surface ionization theory was developed in the early 1920s by Langmuir and Kingdon [37]. This phenomenon was ultimately explained through the thermodynamic derivation of the Saha-Langmuir equation, which was based on the work of Meghnad Saha [38, 39].

The Saha-Langmuir equation calculates the ion emission ratio, the number of ions (n) to the number of neutrals (n^0), vaporizing from a hot metal surface, with which the analyte atoms are in thermal equilibrium. In its simplest form, the Saha-Langmuir equation for positive ion emission can be expressed as Equation 2.2;

$$\frac{n^+}{n^0} = \frac{g^+}{g^0} exp\left[\frac{\phi - \Delta E_I}{kT}\right], \tag{2.2}$$

where ϕ is the work function (in eV) of the ionizing surface, ΔE_I is the ionization energy (in eV) of the element to be analyzed, k is the Boltzmann constant, $8.617\,330\,3(50) \times 10^{-5}\,\mathrm{eV\,K^{-1}}$ [40], and T is the temperature (in K) of the metal ionizing surface. The ratio of the statistical weight of the ionic and atomic states, g^+/g^0, is generally not known for electronically complex atoms (e.g., plutonium) and commonly assigned a value of one. Upon inspection of Equation 2.2, it is evident that the degree to which a material can be ionized is strongly dependent on the work function and temperature of the filament, as well as the ionization potential of the element of interest; therefore, it is desirable to select a filament material with a high work function and high melting temperature in order maximize the probability of ion formation.

A caveat of the Saha-Langmuir equation is that it was originally derived to describe the behavior of neutral atoms impinging on a hot metal surface. It doesn't account for the lack of thermal equilibrium or chemical changes that occur in a sample when loaded directly on a filament. Therefore, it is much less useful for describing the ionization behavior associated with a traditional TIMS single filament arrangement in which evaporation and ionization duties are carried out atop the same surface [41]. Furthermore, for many applications, the agreement between theory and experiment is more qualitative than quantitative. Equation 2.2 is generally useful for order-of-magnitude actinide ionization efficiency estimates and for comparing ionization efficiencies of various elements.

2.2 Sources and applications

2.2.1 Filament material selection

Popular filaments materials include rhenium, platinum, tungsten and, to a lesser extent, tantalum. In addition to being highly refractory and possessing desirable work functions, these materials are chemically inert. Electron work functions, and melting points of these metals are summarized in Table 2.1. The work function values listed in Table 2.1 are averages; a material's work function can vary significantly depending on factors such as crystal orientation, temperature and surface conditions (e.g., oxidized or carburized filament

Table 2.1: Melting points and average work functions [42] of metals commonly used for TIMS filaments.

Filament material	Work function (eV)	Melting point (K)
Platinum (Pt)	5.61 ± 0.13	2041
Rhenium (Re)	5.37 ± 0.10	3455
Tungsten (W)	5.15 ± 0.05	3695
Tantalum (Ta)	4.96 ± 0.22	3293

surface). For a comprehensive list of work functions associated with the numerous crystal orientations of the metals in Table 2.1 see reference [43].

Due to its favorable work function and melting temperature, the most common filament material used for modern TIMS analyses is zone-refined rhenium. Rhenium has the added advantage that it retains its ductility at high temperatures and, due to advancements in zone-refining techniques, is now commercially available in exceptionally high purity (99.999 %); this is especially important when analyzing small samples because it limits background interferences (e.g., hydrocarbons, uranium and thorium contamination). In addition, zone-refined rhenium has been shown to exhibit a higher work function than polycrystalline rhenium, a characteristic likely attributed to the preferential formation of the basal plane (i.e., the 0001 crystal orientation) during the refining process [43–45], illustrated in Figure 2.3. Platinum has a higher work function than rhenium, but its utility is limited in applications involving highly refractory elements such as uranium or thorium, which

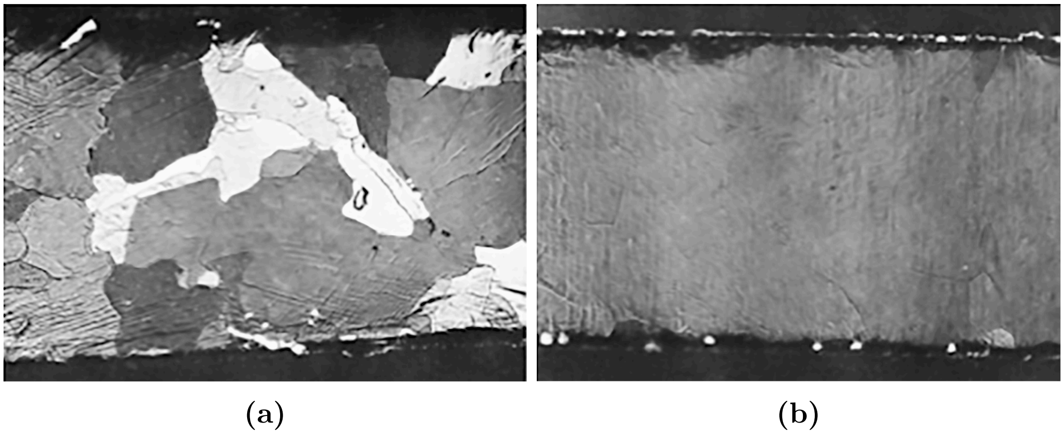
(a) (b)

Figure 2.3: (a) An image of a standard, untreated polycrystalline rhenium filament. (b) An image of a zone-refined rhenium filament; this illustrates that zone refining rhenium promotes the formation of a desirable, high work function monocrystalline surface. The figures were adapted from reference [44]

generally require temperatures above the melting point of platinum for adequate evaporation and ionization. Tungsten has a similar work function to rhenium and a higher melting point but becomes brittle at elevated temperatures, rendering it inferior to rhenium. Tantalum exhibits the lowest work function of all the metals listed in Table 2.1 and has a lower melting temperature than rhenium or tungsten; as a result its most common use is as an evaporation filament in multi-filament setup where these parameters are less critical.

In the early 1970s Sasaki et al. proposed an alternative to the traditional metal single filament. In an effort to capitalize on the enhanced emission of ions associated with the use of carbon additives, Sasaki and his colleagues investigated the use of a graphite filament in lieu of a standard metal one [46]. When loaded with uranium this filament was reported to produce an intense, stable beam of ions. This can be explained by the high permeability of graphite; the uranium sample is incorporated into the filament where it can readily form a refractory uranium carbide. Though not addressed in this paper, it's worth considering the porous nature of graphite may promote sample spreading uniformly throughout the filament which could potentially destroy good abundance sensitivity. While Sasaki reported no quantitative results, the claim was made that the uranium metal ion (i.e., U^+) beam was much greater than that of uranium oxide ions (i.e., ${UO_2}^+$) generated from the samples loaded in oxide form atop a tungsten filament. While interesting, this method has not appeared in subsequent literature and seems to have been abandoned. The high cost of filament fabrication and lack of commercial availability are likely reasons this technology have been abandoned.

2.2.2 Filament configuration

Modern TIMS sources typically employ single, double or triple, flat ribbon filaments to vaporize and ionize a sample; ionization efficiencies associated with a variety of thermal ion sources and configurations are summarized in Table 2.2. The single filament is the simplest and oldest form of TIMS

Table 2.2: Actinide and lead ionization efficiencies associated with a variety of commonly used filament configurations, materials and additives.

Element	Filament config.	Filament/ additives	Sample size (pg)	Median IE (%)	Ref.
Am	Single	Re/C	10–100	0.07	3.3.1
		Resin bead/C	0.174–0.29	0.16	[1]
		Re cavity/bead/C	0.29	0.63	[1]
		PIE	10–100	0.81	3.3.1
Pu	Single	Re/C	1–2690	0.05	[1]
		Re/Pt SID	1000	0.34	[47]
		Resin bead/C	0.05–10	0.54	[1]
		Re cavity/bead/C	0.82 - 330	8.00	[35]
			0.93–10	1.33	[1]
		PIE	10–100	0.83	**??**
		Pt PIE	10	1.03	**??**
	Triple	Re	∼30000	0.22	[48]
U	Single	Re/C	10	0.08	[48]
		Resin bead/C	7–605	0.58	[1]
		Re + Pt SID	10000	0.02	[49]
		Re “V”	1000–100000	0.003	[50]
		Re “V”/H	1000–100000	0.45	[50]
		Re “V”/C_6H_6	1000	0.66	[50]
		Dimpled Re/C	0.04–400	0.6–1.2	[51]
		Re cavity/bead/C	100–500	5.8	[35]
		Re cavity/C	50–75	0.021	[1]
		PIE/C_6H_6	0.2–10	1.7	[9]
	Triple	Re	∼200000	0.1	[48]
Th	Single	Re/C	1000	0.05	[2]
			100	0.12	[2]
			30	0.13	[2]
		PIE/C_6H_6	1000	0.022	[10]
			100	0.13	[10]
			30	0.31	[10]
		PIE	1000	0.017	[10]
			100	0.11	[10]
			30	0.26	[10]
	Triple	Re	200000–1000000	0.02–0.04	[52, 53]
Pb	Single	Re/Silica gel/H_3PO_4	300	6.10	[54]

ion source currently in use, dating back nearly 100 years to the first TIMS developed by Dempster. Sample evaporation and ionization rates are not mutually exclusive and, therefore not easily controlled when using a single filament. The temperature of the filament must be carefully monitored; a compromise between ionization efficiency and sample analysis time must be reached. This issue prompted the conception of the triple filament ion source as a means of improving sample utilization by separating the evaporation and ionization duties. Because double and triple filament configurations operate on the same principle they will therefore be addressed as a single category.

Single filament ion source

Using a single filament configuration, illustrated in Figure 2.4, sample material is loaded directly onto the ionizing surface (i.e., the filament) where it is heated and volatilized into a cloud composed of ions and neutral atoms. A single filament source produces ions only when the analyte is in direct contact with the filament surface. Because the filament must be analyzed under high vacuum, it is unlikely that evaporated neutral atoms will interact with the filament upon leaving the immediate proximity of the filament surface; they are therefore permanently. As a result, the primary sample loss mechanism associated with the single filament is the direct evaporation

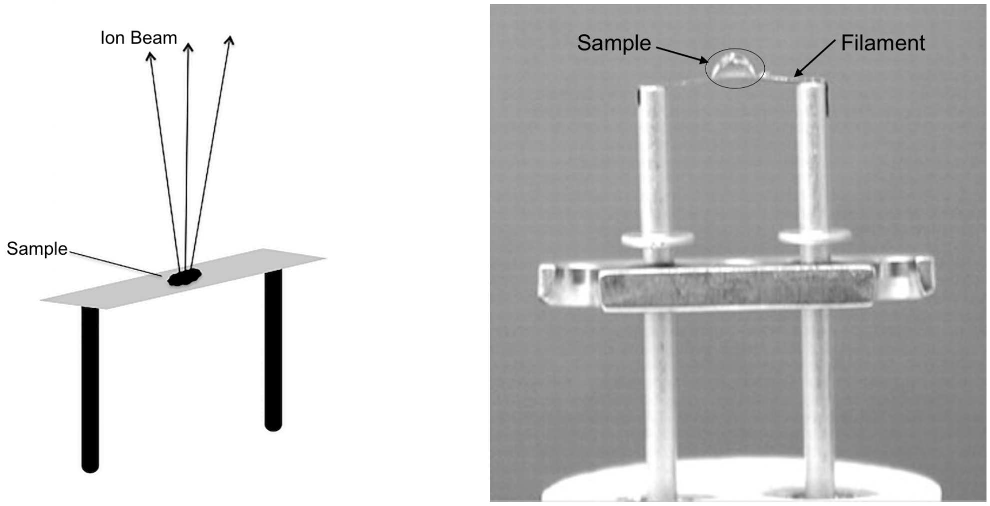

(a) **(b)**

Figure 2.4: (a) Schematic of a single filament thermal ion source, (b) photograph of a filament assembly with liquid sample loaded atop the filament ribbon adapted from reference [55]; the filament will be gently heated to dry the sample to a thin, solid film prior to being placed in the mass spectrometer.

of neutral atoms prior to ionization. In order to prevent sample blow-off, resulting in the complete loss of sample, single filament analyses are started at relatively low temperatures where ionization is less probable. During the course of an analysis the filament temperature is slowly raised in an effort to maintain a stable ion beam. The use of a bare single filament (i.e., no activator or additive) limits the elements and quantities of sample that can be analyzed by TIMS. Special sample loading techniques, or the incorporation of ionization enhancers added during sample loading, or both have been shown to improve ionization efficiencies and ion beam stability during single filament analyses. The use of ionization enhancers in conjunction with a single filament source has expanded their use to a variety of difficult-to-ionize elements as well as significantly reduced the required sample sizes for such analysis. These techniques will be discussed in detail in subsequent sections. Well-devised single filament strategies offer several advantages when compared to a multi-filament alternative. Such advantages include simplicity, a more stable ion beam when analyzing small samples, a significantly lower baseline, and increased ion transmission due to superior ion optical and geometric (i.e., less issues due to filament warping) properties.

Multi-filament ion source

In an effort to combat difficulties encountered with single filament analysis, an alternative configuration was proposed in 1953 by Inghram and Chupka [56]. They incorporated three separate filaments into a single ion source design instead of one filament. In a multi-filament arrangement, analyte is loaded onto the outer filament(s) and evaporated as a neutral gas onto the nearby center filament, where it is then ionized; this process is illustrated in Figure 2.5. The process of ion formation can be divided into four basic steps: 1) A neutral atom approaches a hot metal surface; its electrons and the nuclei of the filament metal are attracted to one another, resulting in the formation of a electric dipole in each, 2) The neutral atom is adsorbed on the metal

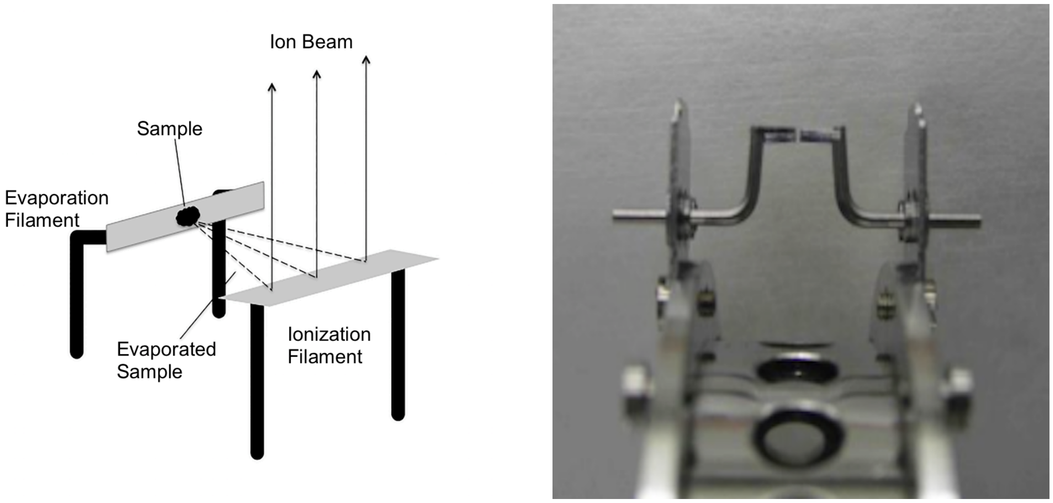

(a)

(b)

Figure 2.5: (a) Illustration of a double filament assembly; the sample is loaded on the side (i.e., evaporation) filament where it is heated and evaporated onto the neighboring ionization filament. (b) Photograph of a double filament assembly mounted on the sample turret, adapted from reference [57].

surface and held in place by the dipole field, 3) The adsorbed atom and metal are quickly brought into thermal equilibrium, broadening the valence shell of the sample atom. If broadened to the point where the Fermi levels of the atom and metal overlap, there is an intense electron exchange between the atom and the metal 4) If the surface of the metal is hot enough the atom will desorb as an ion with some probability. The current to each filament can be adjusted independently; separating evaporation and ionization duties allows for more precise control over the sample evaporation rate. Additionally, the ionizing filament in a multi-filament array can be held at much higher temperatures than possible during single filament analysis, typically improving the ionization efficiency. Disadvantages to the multi-filament setup include an expected sample loss—known as the geometric loss—that occurs during the transfer of sample between filaments. The geometric loss was reported to be approximately 20 % Wilson and Daly [58]. Furthermore, ion emission occurs across the entire length and width of a filament, voltage drop across a filament can be several volts [59], resulting in an ion energy spread greater than 1 eV. The spread in ion energy results in additional ion losses and a reduction in abundance sensitivity. A recent study reports the triple filament arrangements exhibits an approximate tenfold reduction in abundance sensitivity when compared to the porous ion emitter single filament technique discussed in a following section [9]. The losses associated with multi-filament limit the applications to relatively large sample sizes. Despite these drawbacks, the multi-filament arrangement exhibits an increase in ionization efficiency when compared to traditional, bare single filament analyses. Typical ionization efficiency numbers of actinides analyzed by a multi-filament arrangement are; approximately 0.22 % for plutonium, 0.10 % for uranium, and 0.04 % for thorium [52] in the nanogram mass loading range. Details regarding sample, ionization efficiency, and filament additives for multi- and single filament configurations are listed in Table 2.2.

In the early 1960s, prior to the widespread availability of a multi-sample turret, an interesting variation of the standard triple filament arrangement was developed and implemented by Patterson and Wilson [60]. They designed a parallel triple filament arrangement, thus enabling the analysis of two consecutive samples from the same bead by loading a different sample onto each of the outer filaments. The outer filaments could be heated independently, allowing for a direct comparison of two different samples under the same source conditions. Patterson and Wilson reported a threefold improvement in accuracy as well as an increase in sample utilization due to the larger cross section of the ionization filament when compared to a standard triple filament setup.

2.2.3 Variation of filament geometry

Varying the geometry of the standard flat single filament as a method to increase ionization efficiency was first suggested by White et al. in 1955 [61]. A V-shaped filament was devised to boost ion yield in an effort to find new, naturally occurring trace isotopes. The design consisted of a standard tungsten filament ribbon folded in half lengthwise, along the long axis, prior to being welded to supporting posts; the sample is deposited at the center of the “V”. This type of source, illustrated in Figure 2.6, is also known as a canoe or

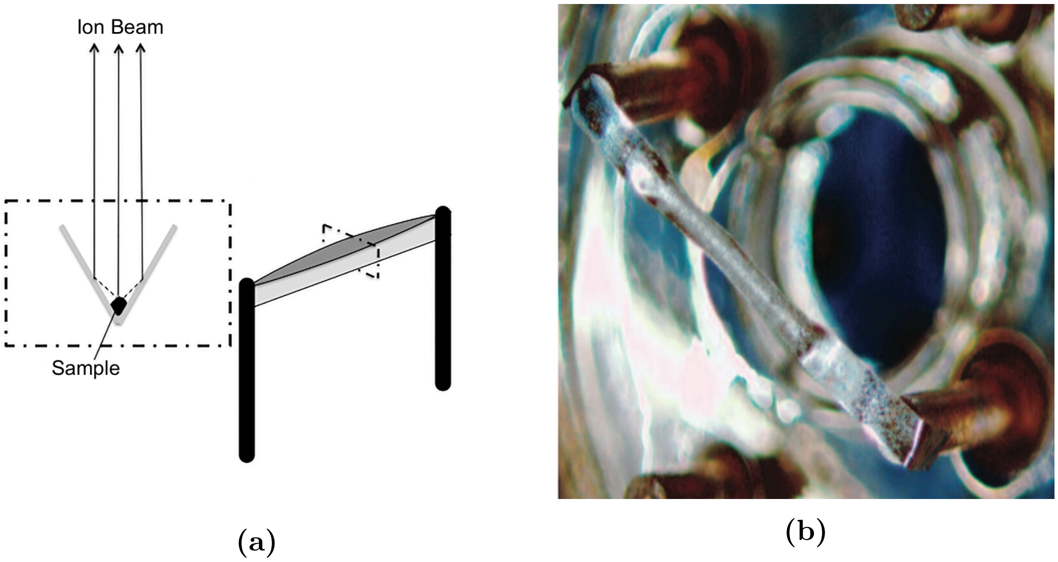

Figure 2.6: (a) A schematic of a V-type filament. The sample is loaded at the bottom of the trough, as the filament is heated, evaporated neutral atoms have multiple chances to interact with the filament surface; this increases the probability that a neutral atom will be ionized. (b) A photograph of a filament with V-shaped indentation, adapted from reference [62].

boat-type filament. The theory for improved ionization efficiency associated with the use of the canoe filament is that the V-shaped indentation gives evaporated neutral atoms additional opportunities for interaction with the hot filament surface thereby increasing the probability of ionization before being lost. Unlike a standard flat single filament, ionization efficiency associated with the canoe shaped filament can, in theory, be more closely approximated as a Saha-Langmuir interaction (i.e. the beam of evaporated neutral atoms will strike the hot walls of the filament). Additionally, the "V" geometry has been shown to exhibit superior ion beam focusing properties when compared to the standard flat filament promoting greater ion transmission through the collimator [63]. Despite the potential advantages associated with the V-shaped, early filament fabrication was difficult, time consuming, and filament uniformity was an issue. An average ionization efficiency of approximately 0.003 % for 1–100 ng mass loading levels of uranium on bare, untreated "V" filaments was reported by Fenner [50]. The unexpectedly low efficiency was investigated and findings indicated that roughly 90 % of the sample migrated to the filament support posts at the ends of the canoe. McHugh reported sample utilization efficiencies raging from 0.0035–1.1 % for an approximate 80 fg sample mass loading of uranium; his results were highly contingent on filament geometry (i.e., height and angle of the sides) [44]. Filament uniformity and sample migration issues were eventually circumvented with the development of a filament fabrication fixture [64]. This jig was capable fabricating filaments with consistent geometry; sample spreading was mitigated by pressing a V-shaped trough in the center (i.e., the center of the long and short axes) of the filament. Boat-type filaments are now commercially available. In modern TIMS analyses the V-type filament is most commonly used in conjunction with additives to elicit further enhancements in ionization efficiency. These will be discussed in detail in subsequent sections of this review.

Esat et al. introduced the dimpled filament in 1979 as an improvement to the canoe filament [65]. The dimple serves to contain the sample, preventing spreading, as well as increase the analyte-filament contact area. The design was fabricated from a standard flat rhenium filament ribbon with a 200-micron hemispherical dimple stamped in the center of the ribbon. This style of filament was initially developed for reducing required sample size and improving ionization efficiency for magnesium analyses. Chen and Wasserburg adopted the dimpled filament for uranium analyses; ionization efficiencies of 0.6–1.2 % for 0.04–400 pg mass loadings were reported [51]. Esat used a dimpled filament for thorium analysis using a charge collection thermal ion mass spectrometer, an ionization efficiency of 4 % for 15 pg loads was reported [66]. Dimpled rhenium filaments were employed by Bürger et al. as a base for the resin bead analyses of uranium, plutonium, and americium with reported ionization efficiencies ranging from 0.16–0.54 % [1].

2.2.4 Additives/activators/ionization enhancers

It is widely known that conventional flat filaments suffer from low sample utilization especially during the analysis of difficult to ionize elements, namely actinides (e.g., uranium, plutonium, and thorium). During the analysis of such samples, ionization enhancers can be employed to boost ion production through three primary mechanisms: 1) concentrating the analyte at the center of a filament so a point source can be more closely approximated for improved ion focusing, 2) promoting the formation of elemental ions and impeding the formation of less desirable species that may complicate analyses, and 3) boosting the effective work function of the ionizing surface thus increasing the probability of ion formation. The combination of these mechanisms promotes the emission of a more stable and intense ion beam resulting in improved precision and accuracy, translating to lower detection limits.

In addition to promoting improved sample utilization, an effective emitter must provide reproducible running conditions and mass fractionation patterns as well as a low analytical blank. Commonly used ionization enhancers in modern TIMS analyses are carbon, ion exchange resin beads and molten glass.

Surface ion diffusion techniques are used to a much lesser extent, however the underlying principles are relevant in the development of more contemporary sources and will therefore be discussed.

Carbon-based additives

The addition of carbon has been shown to boost ionization efficiency in two main ways: 1) by reducing an oxide sample to metal ions and 2) increasing the work function of the filament surface. Carbon additives have also been shown to counteract analyte diffusion across the filament surface [67, 68]. Carbon can be introduced in several forms such as colloidal graphite, collodion, sugar or sucrose, benzene or hexane vapor saturation, and ion exchange resin beads (discussed in a subsequent section). Most carbon additives are added to the filament surface in liquid form and evaporated to dryness; however, benzene and hexane are introduced in gas form, detailed methods for carburizing filaments can be found in previous literature [68–72]. Despite the fact that the ion formation mechanisms are not fully understood, it has long been known that the addition of carbon to a single filament source increases the ion yield of plutonium, uranium, and a variety of other elements [70, 73, 74]. Typical ionization efficiencies of actinides in the picogram to nanogram range using carbon additives and flat rhenium filament are as follows: thorium, uranium, plutonium, and americium efficiencies are approximately 0.02 % [2, 53, 75], 0.08 % [48], 0.05 % [1], and 0.07 % [3.3.1], respectively.

The first account of the use of carbon additives to improve ion yield occured in a 1962 [70]. Studier et al. investigated the effects of reducing and oxidizing agents on the filament and in the surrounding atmosphere during the isotopic analysis of uranium from a single filament ion source. Prior to the introduction of carbon, single filament uranium analyses exhibited a high degree of variability in ion beam stability and intensity as well as inconsistencies in which species were emitted from the filament. The addition of carbon, in the form of sucrose or benzene vapor, to a sample loaded on rhenium or tungsten filaments was found to greatly increase the thermal emission of uranium metal ions [70]. Studier and his colleagues observed that in the presence of carbon, uranium ions didn't appear until temperatures in excess of 1800 °C, well above normal volatilization temperature of uranium metal. This observation suggests the formation of a uranium metal-carbide as an intermediate species prior to decomposition to uranium metal; a theory that has since been confirmed [76, 77]. The formation of refractory metal carbides delays sample volatilization allowing for analysis at higher temperatures than would normally be achievable lending to increased ion yield [68, 73, 74, 76, 77].

Following the work of Studier, Fenner used atomic hydrogen gas mixed with oxygen, as a reducing agent in lieu of benzene, in an effort to reduce the hydrocarbon background [50]. He found that treatment with hydrogen unexpectedly boosted the production of oxides as well as metal ions; benzene on the other hand produced no oxide. An average ionization efficiency ($N = 10$ for each mass loading) of 0.42 %, 0.53 %, and 0.40 % was reported for 100 ng, 10 ng and 1 ng samples of uranium loaded on canoe type filaments treated with hydrogen. This translates to an approximate 150-fold improvement over the untreated boat filaments and a tenfold boost over the triple filament arrangement. The hydrogen treatment technique has been abandoned by the TIMS community due to superior ion yields associated with benzene treated filaments at smaller loading levels; an approximate 200 % increase at the 1 ng loading level.

Since the discovery of carbon's utility for increasing ion production, there have been several studies devoted to gaining a more thorough understanding of the complex mechanisms of ion formation in the presence of a carbon activator [67–69, 74, 76–79]. In 1971, Smith investigated the desorption parameters of uranium ions and neutrals from carburized rhenium and compared them to bare polycrystalline rhenium. Smith concluded that carburized rhenium is a much more efficient ionizer of uranium than bare metal rhenium [69, 78–80] due to the formation of an electric double-layer [81]—the creation of an induced electrical dipole field, illustrated in Figure 2.7—at the metal-carbon interface resulting in a boost to the effective work function of the filament surface [78]. The positive charge residing on or near the surface of the filament increases the difficulty of removing an electron from the filament metal (i.e., the work function) making it more likely to remove an electron from the sample atoms (i.e., more likely to form an ion). Due to its success as ionization enhancer, the use of carbon additives is in widespread use today.

The resin bead method

The resin bead loading method for mass spectrometry analysis was first suggested in 1970 by Freeman [82], and was first used implemented by Walker et al. for the simultaneous determination of plutonium and uranium isotopic composition of spent nuclear reactor fuel samples [83]. By far, the largest application of the resin bead method is in the analyses of actinides (i.e., uranium and plutonium), but has found use in the analyses of other elements relevant to the nuclear field such as zirconium [84] and technetium [85]. Unfortunately, no ionization efficiency numbers were reported in either paper.

Typically, the resin bead method involves placing a single bead pre-loaded with analyte at the center of the trough of a V-type filament and securing

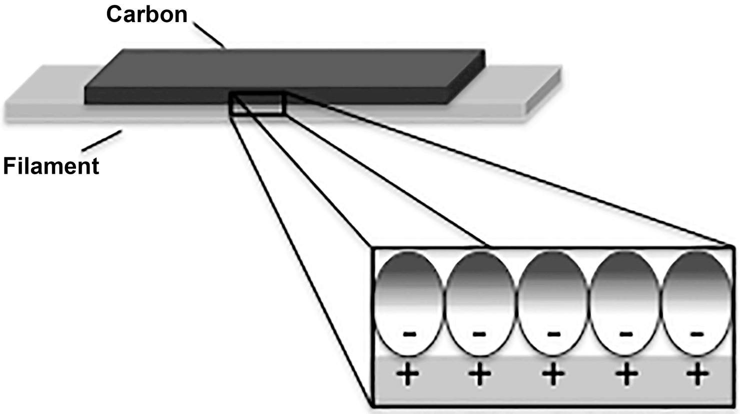

Figure 2.7: Illustration of the dipole formation at the carbon/filament interface.

it with a gluing agent (usually a collodion solution). However, Buesseler and Halverson [86] report using two beads to help insure against sample loss after being loaded into the source housing. Resin bead sample preparation methods have been widely reported in the literature [1, 83, 87–89]. The resin bead acts as a reservoir, concentrating the analyte at the center of the filament, effectively creating a point source vital for ion transmission. As the filament is heated, the resin bead is pyrolysed leaving behind a carbon "skeleton". The carburized bead acts as a reducing agent promoting the emission of metallic ions in lieu of less desirable oxide ions; however, the amount of carbon produced by the bead is too small to have much effect on filament work function so a supplementary source of carbon is required.

In the early 1980s, Smith and Carter investigated the effectiveness of adding pure rhenium powder, and later a slurry of rhenium powder and carbon, in the form of a sucrose solution, over the top of a resin bead in an effort to further enhance ionization [80]. Smith and Carter adopted this idea from the surface ion diffusion-type source described in references [47, 90], however chose to use a slurry of rhenium powder, water and sucrose due to technical challenges encountered with the original source. They found that the addition of rhenium significantly boosted ion yields to 0.5 % (N=3) for 0.3–0.5 ng uranium loadings, a four to five-fold improvement over the uncoated bead. A three-fold improvement over the uncoated bead was reported in the analysis of 1 ng samples of uranium. A more recent study conducted by Smith et al. circa 1994, reports ionization efficiencies of 4–9 % for plutonium samples ranging in sized from 5–16 fg, loaded on resin beads coated with the rhenium carbon slurry previously described.

The resin bead method offers superior ionization efficiency, reduced effects of isotopic fractionation, and increased precision when compared to direct, single and multi-filament loading techniques. Disadvantages of this method include long preparation time, the tediousness of placing and securing a bead atop the filament, and a relatively high chance of losing a valuable sample prior to analysis [71].

Molten glass ion emitters: the silica gel method

Use of the silica gel method as an ionization enhancer for TIMS isotopic analysis of lead can be traced back to 1957 [91]. This technique has since been extended to the analyses of several other elements that have relatively high ionization energies but are quite volatile [92–94] and are readily reduced to elemental form by the molten glass [93, 94]. Prior to the advent of silica gel activators, mass spectrometry isotopic analyses of lead required large sample sizes and suffered from excessive effects of thermally induced mass fractionation. The enhanced efficiency associated with use of silica gel emitters has permitted lead based chronometric investigations of samples contain trace amounts of lead. Additionally, lead isotopic information can provide valuable insight into geographical origin of a sample useful in nuclear forensic and nuclear safeguard applications [95].

Akishin et al. successfully demonstrated that lead ions could be readily produced when a sample was deposited on silica-zirconia gel washed with phosphoric acid (H_3PO_4) and distilled water. The gel developed by Akishin proved difficult to prepare in sufficiently pure form and excessive lead and hydrocarbon background were observed during the analysis of nanogram samples of lead. This prompted Cameron et al. to develop an improved method of silica gel production [96]. During this study Cameron and his colleagues concluded that silica gel in the absence of zirconium was much easier to prepare in sufficiently pure form and worked just as well as the silica-zirconia ion source. Cameron initially omitted the addition of H_3PO_4 to the emitter; however, it was quickly discovered that the addition of H_3PO_4 was necessary for lead ion formation. The only rationale cited for the requisite addition of H_3PO_4 was the possible formation of lead phosphate. A new silica gel emitter was developed by Gerstenberger and Haase using a commercially available colloidal silicic acid solution manufactured by Merck (article no: 12475) mixed with dilute H_3PO_4 [97]. An ionization efficiency range of 8.5–11.6 % was reported for 10 ng mass loading levels of National Bureau of Standards (NBS) NBS-981 lead isotopic standard; a significant improvement over the traditional silica gel activator [98, 99] which was reported to have an ion yield of 1.2–1.8 % at the same sample mass loading level. The silica gel produced by Gerstenberger and Haase is regarded as the most effective and widely used activator for lead isotopic measurements [54]. Because the Merck colloidal silicic acid solution is no longer produced, focus has shifted to find a suitable replacement. Kani and Nohda proposed a method using fused silica gel [100], however, they noted that this activator did not produce a sufficiently stable ion beam to measure low abundance samples. Miyazaki et al. focused on methods of producing a silica gel with a small particle size proposed to increase ionization efficiency and reduced fractionation effects [97, 101–103]. Nohda et al. proposed doping standard colloidal silica with germanium and rhenium as a means of improving ion yield [103]. Despite the germanium-rhenium ratio not being optimized, ionization efficiencies of 1.46 %, 1.32 %, 4.79 % and 4.28 % were reported for lead loadings of 10 pg, 5 pg, 5 pg and 2.5 pg, respectively. None of the emitters, developed during the above investigation, were able to match the performance of that developed by Gerstenberger and Haase. Most recently, Huyskens et al. investigated the suitability of several commercially available silica gels for lead isotopic analysis to replace the Merck gel [54]. The Sigma-Aldrich silica gel (article no: 701491) was found to be a suitable replacement for the Merck silica gel, with an average ionization efficiency (N=21) of 6.1 %.

The fundamental mechanisms by which these processes produce ions are only partially understood. Some ionization mechanisms have been suggested [54, 92–94], the most likely being that increased ion emission is due to the extent in which the rhenium filament is dissolved and oxidized by the molten glass. The resulting rhenium-oxide migrates to the surface of the glass creating a high work function surface, as high as 7.2 eV [45, 104], atop the molten glass from which ions are emitted [92–94].

Diffusion-based thermal ion sources

The concept of encapsulating a sample in a high work function material as a means to improve ionization efficiency of a single filament ion source was first presented in 1969 by Myers and White [105]. This method serves to contain the thermally volatilized sample, limiting the prompt loss of sample as a neutral gas until a sufficient temperature is reached for the analyte atoms to diffuse through the ionizing material. The time required for atoms to diffuse through the ionizing surface allows for elevated analysis temperature where essentially all molecular species are dissociated and the emission of elemental ions is exclusively observed.

Myers and White attempted three sample encapsulation methods for analyzing nanogram quantities of uranium. These included: 1) sandwiching sample between rhenium filaments, 2) depositing the sample in a tubular rhenium filament, and 3) vapor depositing rhenium over the top of the sample loaded atop a standard rhenium filament. The most successful technique in the study was a vapor distillation method; however, problems were encountered in controlling the thickness of the rhenium coating, a critical parameter. Rec et al. sought to improve on the method by radio frequency (RF) diode sputtering a high work function coating over a sample loaded filament [106]. Rhenium, nickel, and tungsten coatings were evaluated; rhenium was deemed to be the only suitable material. The RF sputtering technique proved superior to vapor deposition for controlling the plating thickness. Reported utilization efficiencies for coated plutonium samples loaded onto zone-refined rhenium filaments were 0.16 %, 0.10 %, 0.13 %, and 0.4 % for mass loadings of 1.2 pg, 0.12 pg, 12 fg, and 1.2 fg, respectively. Efficiencies for uncoated samples for the same sample sizes were reported to be 0.05 %, 0.02 %, and 0.01 %; the signal from the 1.2 fg sample was indistinguishable from background. Perrin et al. did not find the sputtering technique capable of producing a sufficiently pure coating and devised a method of electroplating a thin rhenium coating over the top of samples that were electrodeposited on rhenium filaments dubbed the surface ionization-diffusion (SID)-type source. Electrodeposition served as an additional purification step for the sample and the coating. In their first study Perrin et al. analyzed nanogram quantities of plutonium [90]. During this study two significant complications were encountered: 1) optimal overplating conditions varied from filament to filament resulting in an excessive failure rate and 2) the maximum count rate was reached prior to the ion beam reaching maximum stability. For a follow-up study they decided to switch to a platinum SID source [47]; the use of platinum corrected the deficiencies encountered with rhenium. Perrin reported mean ionization efficiency of 0.34 % (N=36) for 1 ng loadings of various plutonium isotopic standards. The platinum SID was also adapted for the analysis of nanogram quantities of uranium [49]. A mean ionization efficiency of 0.015 % (N=17) for a 10 ng load of uranium isotopic standard (NBS U-500) spiked with approximately 1 ng of ^{233}U was reported. This technique has also been used to measure neptunium, americium and ruthenium [47, 107]. Efurd et al. report an ionization efficiency of 1 % for 0.1 ng neptunium samples [107], no ionization efficiency numbers were reported for americium or ruthenium.

Advantages of the SID technique include enhanced ionization efficiency and improved precision when compared to direct filament loading as well as predictable isotope fractionation patterns [47, 49]. Despite the advantages, the SID source is hindered by the need for extremely clean samples. This technique is very sensitive to impurities that might co-plate with the sample or over-plate the sample, significantly depressing ion beam intensity. The requisite for a special apparatus for sample and coating electrodepsition on the filament and the need for clean rooms and clean benches render this technique impractical to implement in many labs.

2.2.5 Thermal ion cavity sources

Pioneering research on hot cavity ion sources as a means of isotope separation first began in the early 1970s [108, 109]. It was quickly discovered that ion formation in a hot cavity was very efficient, considerably higher than the values predicted by the Saha-Langmuir equation (2.2) for surface ionization [110], suggesting that there are multiple ion production mechanisms at work. Enhanced ionization efficiencies are theoretically achieved with an increased surface area-to-volume ratio and confined geometry increasing sample retention time allowing for higher operating temperatures and promoting multiple neutral interactions between neutral atoms and the ionizing surface [3, 108, 109, 111–113].

Cesario et al. were the first to adapt a TIC as the ion source for a magnetic sector mass spectrometer [114]. Their TIC source consisted of sharpened rod (samples were electrodeposited on the tip) that was inserted into the end of a rhenium tube. The rod-tube assembly was heated via electron bombardment; electrons were emitted from a heated tantalum wire surrounding the cavity. Ion current was adjusted by increasing or decreasing the distance between the tip of the sample rod and heated end of the rhenium tube. Ionization efficiencies of 0.143 %, 0.02 %, and 0.05 % were reported for 40 ng, 200 ng, and 300 ng loadings of uranium on a tantalum rod, a 4–28-fold enhancement in ion yield relative to uranium atop conventional rhenium filaments. Duan et al. sought to make a simpler TIC source designed specifically for use in mass spectrometry [113, 115]. This source could be coupled with an isotope separator or a quadrupole mass spectrometer with no modifications. The "crucibles" were made from tungsten rods with a cavity drilled in one end and heated by electron impact from a tantalum wire. Initial ionization studies were conducted using the TIC-isotope separator on "tens of milligrams" samples of uranium and thorium; utilization efficiencies of 8 % for uranium and 2 % for thorium were reported [115]. A follow-up study using the TIC-quadrupole mass filter combination achieved efficiencies of 8.5 % and 3.6 % for 1 µg loadings of uranium with and without graphite respectively. Plutonium utilization efficiencies were reported to be 8 % for 100 pg plutonium loads. Wayne et al. adapted the TIC source developed by Duan to a time of flight (TOF) mass spectrometer, obtaining total efficiencies of 1–3 % for 0.075–25 ng loadings of thorium [3, 116].

In the early 2000s, Riciputi et al. developed a completely new high efficiency cavity source (HECS) and coupled it with a Finnigan MAT 262 single-collector TIMS [35]; this new HECS is illustrated in Figure 2.8, A standard multi-sample turret was modified to accommodate thirteen HECS. Unlike previous TIC sources, this design was completely interchangeable with a standard TIMS source. The HECS consists of a rhenium rod with a cavity drilled in one end; the sample is loaded on a resin bead, placed in the cavity and covered with graphite prior to analysis. Sample heating is achieved by electron

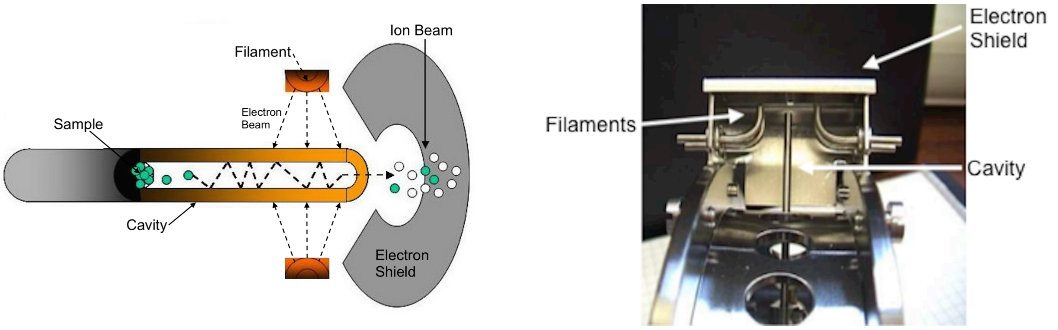

(a) (b)

Figure 2.8: (a) An illustration of an HECS, the cavity is heated via electron bombardment; electrons are generated from restively heated standard rhenium filament ribbons. (b) Photograph of an HECS mounted on a standard sample turret. Figures were adapted from reference [34].

bombardment. Riciputi et al. report that this combination produced an average ionization efficiency of 5 % for 100 pg and 500 pg uranium loads and 9 % for 20 pg and 165 pg plutonium loads. More recently, Bürger et al. [1, 117] assembled an identical HECS on the sample turret of a ThermoFisher 'Triton' MC-TIMS (successor to the MAT 262), but were unable to reproduce the results reported by Riciputi [35]. A total median efficiency of 1.33 % ($N = 30$) was achieved for 0.093–10 pg resin bead loadings of plutonium using a rhenium cavity and a supplemental carbon additive. Uranium resin bead loads coated with graphite in rhenium cavities were also studied but no quantitative results were given, citing that this method "yielded significantly lower ionization efficiencies than expected" due to tungsten heating filament failure prior to achieving adequate temperature for analyses. Trials using uranium liquid loads with a carbon additive in a rhenium cavity were conducted successfully; however, they were only able to achieve a median efficiency of 0.021 % ($N = 4$) for 50–70 pg mass loadings. Reasons for the discrepancy in the uranium and plutonium ionization efficiencies reported by Bürger [1] and Riciputi [35] were not documented in this paper. During this study, repeat trials were carried out to determine ionization efficiencies in TICs using the same sample loading method previously described. An average efficiency of 0.63 % ($N = 6$) was reported for 0.29 pg samples, this compared to 0.16 % efficiency achieved for of 0.17–0.29 pg samples of americium loaded on resin bead atop a dimpled filament and covered with carbon.

In an effort to reduce background and eliminate the formation of multiply charged ions [113, 116] during trace element analysis, Li-Hua et al. developed a Joule heated TIC ion source coupled with a magnetic sector mass spectrometer [118]. In contrast to previous designs that employed electron bombardment as the heating method, Li-Hua's design is resistively heated much like a traditional TIMS filament. His system consists of a rhenium "ionizer" tube inserted into a tantalum "evaporator" tube. The ionizer and evaporator could be independently allowing for sample retention while the ionizer was being preheated. Li-Hua et al. reported total efficiencies of 4–9 % for 0.1–30 pg loadings of plutonium and 0.5–2 % for 12–50 ng loadings of uranium. This source requires a new sample wheel to be designed and manufactured prior to implementation. Furthermore, this TIC design exhibited a lack of durability when compared to the electron bombardment heating method.

Despite reports of the potential for significant improvements in ionization efficiency associated with the TIC type source, there are significant disadvantages that deter its widespread use. Arguably the most notable drawback is the need for source modifications—sometimes quite extensive and costly—makes this technology impractical for many users/laboratories. Another concern is the lack of reproducibility in isotopic fractionation patterns, rendering this method ineffective for applications requiring high precision isotope ratios. In addition, inconsistencies in reported ionization efficiencies for the HECS requires further investigation.

2.2.6 Porous ion emitters

Recently developed PIE techniques simultaneously take advantage of multiple strategies discussed in previous sections of this review to boost ion production. These include the use of high work function rhenium and platinum metal powders, carbon additives, increased surface area for greater interaction between the analyte and ionizing surface. Additionally, the small footprint of the PIE serves to concentrate the analyte at the center of the filament for enhanced ion transmission. Currently, PIEs are constructed from a 50/50 mix, by mass, of rhenium and platinum powders, and, depending on application, carburized; prior to the sample introduction a few drops of dilute liquid ion exchange resin is added to the PIE for enhanced actinide incorporation. A detailed description of PIE construction can be found in [71]. The PIE is a hemispherical metal "bead" illustrated in Figure 2.9. The small footprint of the PIE, approximately 700-microns in diameter and roughly 75-microns in height, serves to localize the analyte loading area at the center of the filament such that the instrument optics will behave as if each sample were a point source for greater ion transmission through the ion lens. Localized loading also leads to a reduced ion energy spread as a function of voltage drop across the filament surface, leading to enhanced abundance sensitivity when compared other techniques [9]. A study conducted by Watrous et al. revealed that ions are most frequently emitted from the center (i.e., the thickest part) of the PIE and no ions were emitted from the surrounding filament [9]; the resin bead technique allows for analyte diffusion across the filament surface. Additionally, scanning electron microscopy with energy dispersive X-ray spectroscopy (SEM/EDS) analysis of PIE filaments loaded with analyte have indicated that no sample is present on the surface of the emitter; the analyte is fully contained within the highly porous microstructure [10]. As a result, neutral analyte atoms are

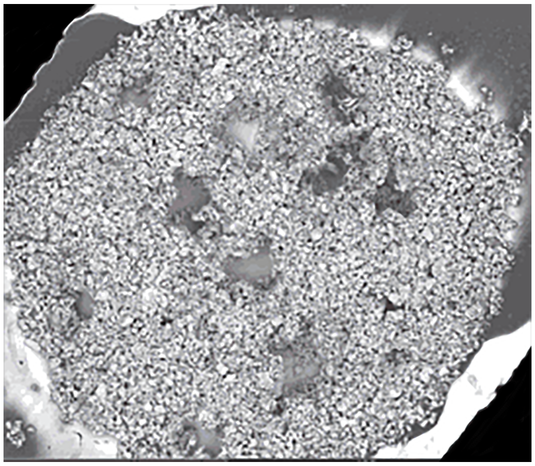

Figure 2.9: An SEM image of a PIE mounted atop a standard zone-refined rhenium filament.

forced to interact with the hot Pt/Re "alloy" as they migrate through the PIE structure increasing the likelihood that evaporated neutrals be ionized prior to escaping. Thus far PIE techniques have been applied to the analysis of picogram quantities of uranium and thorium with great success.

Preliminary investigations have demonstrated that, despite a lack of refinement in PIE construction, PIEs consistently exhibit superior sensitivity and increased reliability during uranium analyses at the low picogram level when compared to the well-established direct loading and resin bead methods. For initial uranium trials carburized PIEs constructed from 325-mesh (0.044 mm nominal sieve opening) rhenium and platinum powders provided the best overall average efficiency; 1.7 % ($N = 4$) for 10 pg loads of uranium. This translates to as much as a 2200 % improvement in ionization efficiency over direct filament loading and an approximate 200 % increase over resin beads for similar mass loadings [71]. PIEs made with the larger 200-mesh (0.074 mm nominal sieve opening) rhenium powder were only capable of achieving sample utilization efficiencies of 0.2–0.6 % at the same uranium mass loading level. These findings indicate that smaller pore size, a function of rhenium powder mesh size, and increased surface area are significant factors in the increased ionization efficiency associated with the use of PIEs. All PIE equipped filaments used in this study were carburized; therefore, the full impact of carburization and PIEs is unknown at this time. It was stated that PIE filaments subjected to higher temperatures during carburization outperformed those subjected to lower pre-treatment temperatures.

A recent investigation conducted by Stanley et al. focused the application PIE of techniques to thorium analyses [10]. Thorium is notoriously difficult to ionize via thermal mechanisms and is arguably the worst-case scenario with regard to TIMS analysis. Repeat ionization efficiency trials (N = 8–10) were conducted for various loadings of thorium; utilization efficiencies of 0.022 %, 0.13 % and 0.31 % were reported for 1000 pg, 100 pg and 30 pg thorium loads on carburized PIEs. All loading levels were reported to show a clear improvement in ionization efficiency ranging from 220–410 % when compared to values for similar mass loading levels using traditional single filaments previously reported in literature. Upon review, however, it was discovered that Stanley et al. [10] and Wayne et al. [3] erroneously interpreted the plot presented by Edwards et al. [2] and reported thorium ionization efficiencies that were significantly lower than the actual values. At the 1000 pg loading level traditional filaments exhibited ionization efficiency of approximately 0.05 %, a two-fold enhancement in ionization efficiency when compared to PIEs. PIE and standard filaments performed equally well at the 100 pg loading level with an ionization efficiency of approximately 0.12 %. The only marked improvement in ionization efficiency was during the analysis of the 30 pg samples; PIE equipped filaments outperformed the standard filaments (ionization efficiency of 0.13 %) by roughly 240 %. This finding suggests that additional thorium trials should be extended to mass loadings less than 30 pg in order to explore the utility of PIE analyses of samples containing trace quantities of thorium. The impact of filament carburization was also investigated during this study; a small (0.005–0.05 %), consistent, yet statistically insignificant improvement in ionization efficiency was demonstrated at every mass loading when using carburized filaments. No attempts were made to optimize carburization conditions or PIE composition for thorium analyses during this investigation.

Scanning electron microscope (SEM) investigations of PIE filaments during this study have shown that the PIE composition is vastly altered throughout the course of analysis. Platinum currents were measured to be in the tens of millivolts level during the early stages of thorium analysis; the platinum supply from the PIE structure was entirely consumed within the first fifteen minutes of thorium analysis. This observation supports the theory of increased sample utilization due to platinum ions impacting the cloud of evaporated neutral analyte atoms surrounding the filament. Due to the refractory nature of thorium and the fact that most of the platinum is consumed during the early stages of analysis, it can be inferred that platinum ion impact is probably not as significant in thorium analyses as it would for more volatile actinides (i.e., americium and plutonium). However, rhenium ions may perform a similar function at elevated temperatures required during the analysis of thorium samples.

Due to the relative nascence of PIE techniques, additional investigations are necessary to further elucidate the exact functioning of PIE sources for enhanced sample utilization. Initial investigations have demonstrated the utility of employing PIE techniques for the analyses of trace quantities of uranium and thorium. Additionally, the use of PIEs requires no special source modifications, allowing PIE filaments to be run in conjunction with traditional filaments. Efforts to alter PIE composition, dimension and carburization conditions to target specific analytes should be conducted in order to maximize ionization efficiencies for a variety of actinides that require different analysis conditions.

2.3 Conclusions

Since its inception, TIMS has been used in isotopic investigations in a variety of fields. TIMS is now an accepted "gold standard" for high-performance isotopic measurements and is the method of choice in establishing many material reference values. TIMS, coupled with relevant detection [23, 24] and sample preparation strategies [119], offers several advantages such as exceptional precision and accuracy, relatively minimal effects from isotopic fractionation, and mass spectra that are essentially free from background interferences. Despite instrumental advantages, low sample utilization associated TIMS analysis of actinide-bearing samples continues to hinder the application of TIMS. This is especially important in applications such as nuclear forensics and safeguards where samples might contain ultra-trace quantities of high priority analytes. It's important to mention that the vast majority of improvements associated with TIMS based analyses have stemmed from advancements in vacuum system, detector and instrument electronics technologies. Improvements to source ion production have evolved much more slowly, often stagnating for decades at a time. Techniques employing the use of ionization enhancers such as silica gel and carbon have been around for nearly sixty years with little to no enhancement. This body of work serves not only as a comprehensive summary of commonly employed ion sources and various efforts to improve sample utilization, but also highlights significant shortcomings of contemporary thermal ion sources.

Chapter 3

Enhanced plutonium and americium ionization efficiency using porous ion emitters

This chapter is based on a published manuscript [120]:

Matthew L. Baruzzini, Howard L. Hall, Matthew G. Watrous, Khalil J. Spencer, and Floyd E. Stanley, "Enhanced ionization efficiency in TIMS analyses of plutonium and americium ionization efficiency using porous ion emitters", International Journal of Mass Spectrometry 412 (2017) 8–13, DOI: `http://dx.doi.org/10.1016/j.ijms.2016.11.013`

My contributions to this work include: Preparation of PIE stock materials; traditional and PIE filament preparation; sample preparation and loading; conception and development of platinum PIEs; mass spectrometric analyses; processing, analyzing, and interpretation of experimental data; and the writing of the manuscript.

The institutional number for this chapter, entitled "Enhanced plutonium and americium ionization efficiency using porous ion emitters", is LA-UR-15-27578

Abstract

Investigations of enhanced sample utilization in TIMS using PIE techniques for the analyses of trace quantities of americium and plutonium were performed. Repeat ionization efficiency (defined as the ratio of the number of ions detected to atoms loaded on the filament) measurements were conducted on sample

sizes ranging 1–100 pg for plutonium and 10–100 pg for americium using PIE and traditional (i.e., a single, zone-refined rhenium, flat filament ribbon with a carbon ionization enhancer) TIMS filament sources. When compared to traditional filaments, PIEs exhibited an average boost in ionization efficiency of ∼550 % for plutonium and ∼1100 % for americium. A maximum average efficiency of 1.09 % was observed at a 1 pg plutonium sample loading using PIEs. Supplementary trials were conducted using newly developed platinum PIEs to analyze 10 pg mass loadings of plutonium. Platinum PIEs exhibited an additional ∼134 % boost in ion yield over standard PIEs and ∼736 % over traditional filaments at the same sample loading level.

3.1 Introduction

TIMS has long been the method of choice for the isotopic ratio determination of nuclear materials and is widely considered the gold standard for such analyses. However, traditional filament loading techniques are associated with ionization efficiencies of less than 0.1 % for actinides [1]; the majority of the sample is not measured. Such low efficiencies significantly limit the ability make accurate and precise measurements of high priority elements (e.g., americium, plutonium, uranium and thorium) that could potentially provide critical signatures in nuclear forensic, non-proliferation, and safeguards efforts.

For decades, the TIMS resin bead technique has proven to be one of the best methods for the analysis of actinide samples. However, despite several advantages, the resin bead approach suffers from long preparation time and tediousness of securing a pre-loaded bead atop the filament increasing the chance of losing a valuable sample. More recently, the use of TIC sources have been proposed as a method to improve sample utilization. While enhancements in ionization efficiency have been demonstrated using TIC, there are significant drawbacks to implementing this method; namely, costly instrument modifications and sample dedication [3].

PIEs have been proposed as an alternative approach for boosting ion yields. Theses sources have demonstrated significant enhancements in ionization efficiency during the analysis of trace quantities (e.g.,$\leq$30 pg) of uranium [9] and thorium [10]. Unlike TIC sources, PIEs can be implemented with no modifications to the mass spectrometer. Proposed mechanisms of improved sample utilization associated with the use of PIE sources include increased ionizing surface contact area, superior ion optical properties, and bombardment by ions emitted by the PIE material itself [10]. Neutral atoms incur multiple interactions with the ionizing surface as they traverse the PIE structure thus limiting their rapid escape, increasing the probability of ionization. PIEs have been shown to eliminate sample migration across the filament; as a result, they exhibit superior abundance sensitivity when compared to multi-filament and resin bead techniques [9]. Concentrating the sample at the center of a filament is essential for maximizing ion beam focusing and transmission, as magnetic sector instruments are very sensitive to the location of ion production on a filament. Previous research suggests that additional ions may be generated via collisions between escaped neutral atoms with platinum ion emitted as the PIE material is consumed during heating [10]. The extent to which each mechanism contributes to the overall boost in ionization efficiency is unknown at this time.

3.2 Experimental methods and equipment

3.2.1 Filament pre-treatment

Prior to the addition of any ionization enhancers, all filaments used during this experiment were pre-treated in a GV Instruments Ltd. (now Isotopx: Middlewich, Cheshire; UK) filament bake-out unit evacuated to approximately 10^{-7} mbar ($\sim10^{-5}$ Pa). The filaments were slowly heated to 4.5 A and held at this temperature for roughly 10 min to remove any impurities (e.g., hydrocarbons, environmental uranium, etc.) that may be present in or on the filament ribbons. Traditional and those intended for use with PIEs were subjected to identical heating and cooling conditions prior to sample loading.

Standard filament preparation

Traditional filaments were prepared by pipetting 1 µL of a colloidal graphite solution (Ultra Carbon Corporation; Bay City, MI) atop each zone-refined rhenium filament ribbon (H. Cross Co.; Moonachie, NJ). Extreme care was taken to localize the graphite solution to the center of the filament surface during application. The graphite solution was partially dried via resistive heating at 1 A for approximately 15 s.

PIE stock preparation

All PIE stock material used herein was prepared in-house, at Los Alamos National Laboratory (LANL). Standard PIE stock was made by combining equal parts, by mass, of platinum powder (325 mesh, Sigma Aldritch; St. Louis, MO), rhenium powder (325 mesh, Sigma Aldritch; St. Louis, MO), and a hot melt gluing agent (not well characterized). The hot glue was melted atop a quartz glass microscope slide using a laboratory hot plate; the platinum and rhenium powders were added to the melted hot glue and thoroughly mixed. Stock material for platinum PIEs was fabricated by incorporating platinum powder (325 mesh, Sigma Aldritch; St. Louis, MO) and hot melt glue in a two-to-one ratio, by mass. The platinum powder and glue were amalgamated in the manner previously described for standard PIE material. The stock mixtures were loaded into a custom built extruder specially designed to reproducibly expel the PIE stock material into a small diameter rope. A custom built extruder was used to reproducibly each PIE stock material into a small, ~550 µm, diameter rope. Images of the extruder and a PIE rope atop a quartz glass plate are illustrated in Figure 3.1.

PIE filament preparation

Sections of PIE stock material, approximately 100 µm in height, were secured to the center of each outgassed rhenium filament ribbon via gentle heating at 1 A for approximately 5 s. The filaments were then placed in the bake-out unit were the PIE stock was sintered; the result is a three-dimensional porous bead approximately 700 µm in diameter and ~75 µm in height. Details of the sintering process of platinum/rhenium Pt/Re PIEs and platinum PIE filaments are provided below.

Pt/Re PIEs. The filaments were loaded in the filament bake-out unit, placed under vacuum, ~10^{-7} mbar (~10^{-5} Pa), and slowly heated to ~1700 °C; the filaments were held at for this temperature for approximately 20 min. The

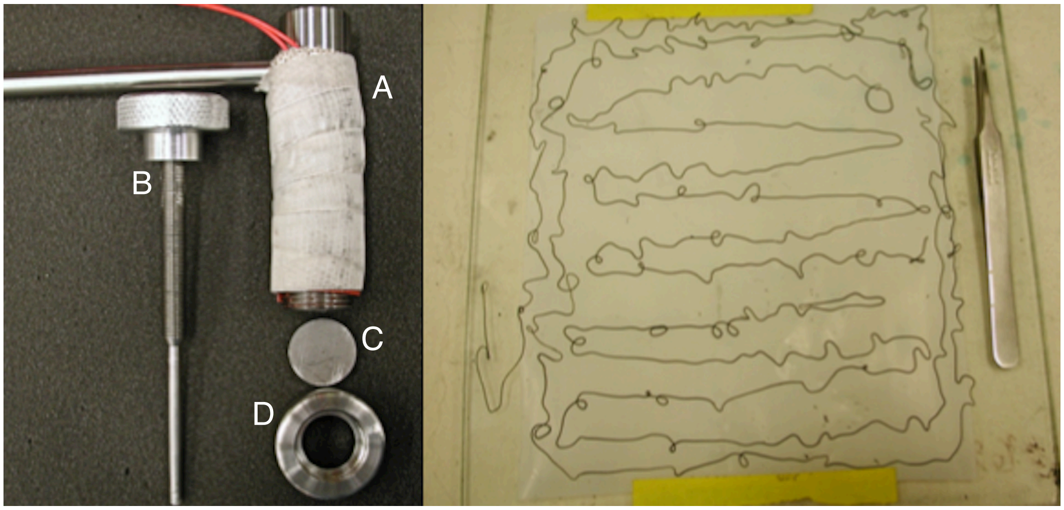

Figure 3.1: Photographs of the custom fabricated extruder, on the left, and a PIE stock rope extruded onto a quartz glass plate, on the right. The PIE stock material is loaded in the extruder body (A) which is warmed via heat tape: the temperature is controlled using a Variac. The threaded plunger (B) is slowly turned, forcing the stock material through a small conical hole in the die (C); the die is held in place with a threaded ring (D). *Photographs courtesy of Matthew Watrous at Idaho National Laboratory.*

baking process serves two purposes; 1) to volatilize the glue and 2) sinter the PIE to itself and to the filament surface. The pressure in the bake-out unit was carefully monitored to ensure that there were no pressure spikes as the glue volatilized during the sintering process. Rapid volatilization of the glue could result in the PIE blowing-off the prior to fusing itself to the filament or the in formation of large pores in the PIE structure. Explicit details for preparation of Pt/Re PIEs can be found in reference [71].

Platinum PIEs. Filaments were mounted in the filament bake-out unit which was then evacuated to ~10^{-7} mbar (~10^{-5} Pa). Attempts at making platinum PIEs using the heating method described in 3.2.1 resulted in failure; either the PIE material was melted into a solid, non-porous, mass of platinum or was completely lost due to being volatilized from the filament surface. The most desirable results were produced by gradually heating the filaments at a rate of 0.25 A min^{-1} until reaching a temperature of ~1450 °C. Filaments were held at this temperature for approximately 10 min.

Prior to sample loading, two drops of poly(4-styrenesulfonic acid) cation exchange polymer (M_W=75 000, 18 wt% in H_2O: Sigma Aldritch; St. Louis, MO), diluted in 18 MΩ deionized (DI) water to a concentration of approximately 3 % by mass, were added to each PIE and dried by heating at 1 A for approximately 15 s. The ion exchange resin was added in an effort to enhance sample incorporation into the PIE.

In an effort to limit systematic errors that may be introduced by irregularities in PIE construction, great care was taken to select a set of filaments exhibiting similar characteristics. Each PIE filament was examined using an optical microscope; criterion used in filament selection included diameter, height, and consistency in pore size (i.e., no large cavities created as the hot glue was volatilized) of the PIE.

3.2.2 Sample application

Americium sample stock for sampling was prepared from a well-characterized ^{243}Am spike; certified reference material (CRM) 144 (NBL; Chicago, IL), was used to prepare the plutonium stock solution. Aliquots of each stock solution were prepared in concentrations ranging from 2–200 $\mathrm{ng\,g^{-1}}$ using Optima™ grade nitric acid (Fisher Scientific, Pittsburgh, PA; USA) diluted to 1 $\mathrm{mol\,L^{-1}}$ using 18 MΩ DI water to limit loading volume to 0.5 µL. The small aliquot size allowed for precise application of the analyte on the filament as well as minimizing sample diffusion across the filament. Samples were deposited directly onto the PIE or atop the damp colloidal graphite solution using a

2.5 µL capacity pipette and dried completely in preparation for subsequent analysis.

3.2.3 TIMS instrumentation

All measurements were made using an Isoprobe-T™ from GV Instruments Ltd. (now Isotopx: Middlewich, Cheshire; UK) at LANL. The ion collection system consists of nine, variable-position, Faraday cup detectors equipped with $10^{11}\,\Omega$ resistors and a static ion counting Daly detector at the axial position mounted behind a wide aperture retarding potential (WARP) energy filter; additional details about Faraday cup and Daly detectors can be found in Appendix B.1 and Appendix B.2, respectively. Mass spectrometer performance and programming were controlled via the GV Instruments IonVantage software package installed on a Dell Optiplex PC (Rock Round, TX; USA). To ensure maximum measurement precision, the mass spectrometer was warmed for at least one hour under electronic conditions similar to those employed during sample analysis. Following warm-up, primary instrument tuning (e.g., ion optic lens, peak shape, and peak centering adjustments) was conducted using the $^{187}\mathrm{Re}^{+}$ ion beam from an outgassed bare zone-refined rhenium filament. Fine-tuning was conducted at the mass number of interest before the analysis of each sample. Due to the long runtime of PIE equipped filaments, additional fine-tunings were conducted, as needed, during sample analysis to compensate for any drift in electronics that may occur. Pressure in the source housing was kept as low as possible, $\sim 10^{-8}$ mbar ($\sim 10^{-6}$ Pa), with the aid of the LN_2 added to the cold trap as needed.

3.3 Results and discussion

Side-by-side ionization efficiency measurements were conducted using Pt/Re PIEs, platinum PIE, and standard single rhenium filament assemblies. Sample ion beams were monitored exclusively using the Daly detector in conjunction with the WARP filter. Integrated signals were determined off-line, post-analysis and used to calculate ionization efficiencies. All samples were run to signal exhaustion, approximately 500 cps.

3.3.1 Americium ionization efficiency

Repeat sample utilization measurements were conducted at 10 pg, 50 pg, and 100 pg mass loading levels of americium. An average $^{243}Am^{+}$ ion yield of 0.81 % was achieved using Pt/Re PIE equipped filaments compared to 0.07 % using tradition single filament assemblies; this translates to an approximate 1100 % enhancement in sample utilization at all sample loading levels tested.

Additionally, PIEs exhibit superior ion yield when compared to published ionization efficiency values for americium using both the resin bead and TIC sources. Bürger et al. [1] report average efficiencies of 0.16 % for the resin bead method and 0.63 % for resin beads with carbon additive loaded in rhenium cavities at americium loading levels of 0.17–0.29 pg and 0.29 pg, respectively. Data for individual trials are plotted in Figure 3.2; the shaded regions indicate theoretical americium ionization efficiencies, predicted by the Saha-Langmuir equation (2.2), using standard polycrystalline rhenium filaments and filaments made from a Pt/Re alloy. A filament temperature range of 2024–2324 K, rhenium work function of 4.98 eV [3], americium first ionization potential of 5.9738(2) eV [121], and Pt/Re alloy (50 at% platinum composition) work function of 5.30 eV were used in calculation theoretical ion yields. The Pt/Re alloy work function was theoretically determined using the method described by Chrzanowski et al. [122]; the work function of the alloy was used to predict performance of Pt/Re PIEs, which are a mechanical mixture of platinum and rhenium and not a true alloy. Figure 3.2 clearly illustrates that Pt/Re PIEs consistently produced americium ion yields exceeding that predicted by the Saha-Langmuir equation (2.2) for thermal ionization using conventional, flat polycrystalline rhenium filaments. Average americium ionization efficiency data collected during the present investigation is presented in Table 3.1. A

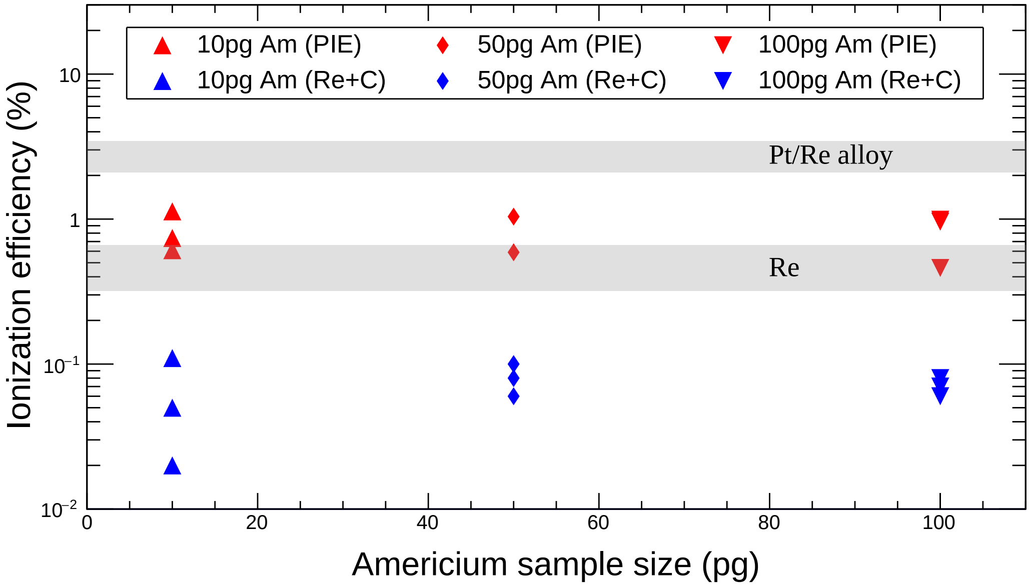

Figure 3.2: Americium ionization efficiency data acquired using Pt/Re PIE and traditional single filaments. The shaded areas indicate theoretical americium ionization efficiencies atop rhenium and Pt/Re alloy filaments as predicted by the Saha-Langmuir equation.

Table 3.1: A summary of average americium ionization efficiency data collected using PIE and traditional filaments as ion sources.

Am sample size (pg)	Ionization Efficiencies (%)		Enhancement (%)
	PIE	Traditional	
100	0.80	0.07	~1143
50	0.81	0.08	~1013
10	0.83	0.07	~1186

tendency of increased ionization efficiency with decreasing sample size was not observed in data acquired over the mass loading range, a commonly observed phenomenon attributed to analyte atoms competing for filament surface area [2, 3]. However, this trend may become evident if analyses were conducted over a broader range of sample sizes. At 50 pg and 100 pg sample mass loading levels both standard and PIE filaments were able to produce stable ion beams; however, at 10 pg loading levels traditional filaments were unable to maintain aiming intensity. Traditional filaments were run at aiming intensities ranging from 40 000–100 000 cps, PIEs were analyzed at ion beam aiming intensities of 120 000–300 000 cps. Figure 3.3 shows that, for 10 pg americium sample loadings, PIEs exhibit greater ability to generate a stable ion beam at a much higher intensity than did their standard filament equivalents. Inspection of Figure 3.3 also reveals that PIEs were able to generate a stable ion beam much more quickly (i.e., at a lower temperature) than traditional filaments; we attribute this to the higher work function of PIEs, through the addition of platinum, as well as a substantial increase in surface area associated with PIE sources. The larger surface area increases the probability that evaporated neutral atoms will be ionized as they migrate through the porous structure by promoting multiple interactions with the PIE; this proves significant at lower temperatures where ionization is less likely to occur.

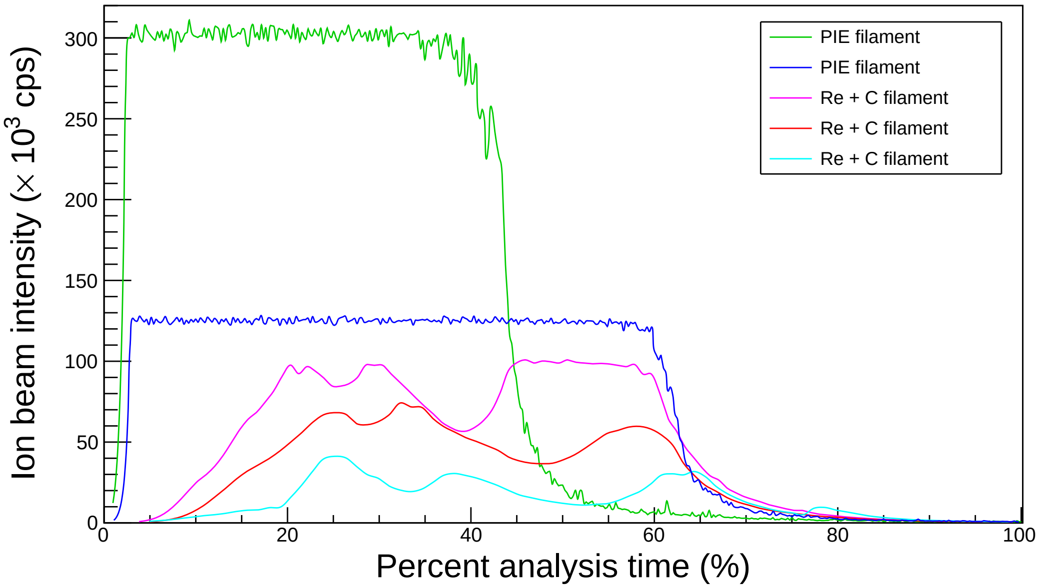

Figure 3.3: Ion beam intensity as a function of percent runtime representative of PIE and traditional filaments at a 10 pg americium loading level.

Intensity curves associated with PIE seem to exhibit more "noise" than the traditional filament intensity curves for 10 pg americium sample loadings, as illustrated in Figure 3.3. This noise was originally thought to be a result of the changing morphology of the PIE as it disintegrates during heating; however, analysis of ion beam intensity curves for larger americium samples reveled that this noise is present in intensity curves of PIE and traditional filaments. Figure 3.4 shows the signal noise in plateau region of aiming intensity curves for 100 pg americium samples acquired using PIE and traditional filament sources.

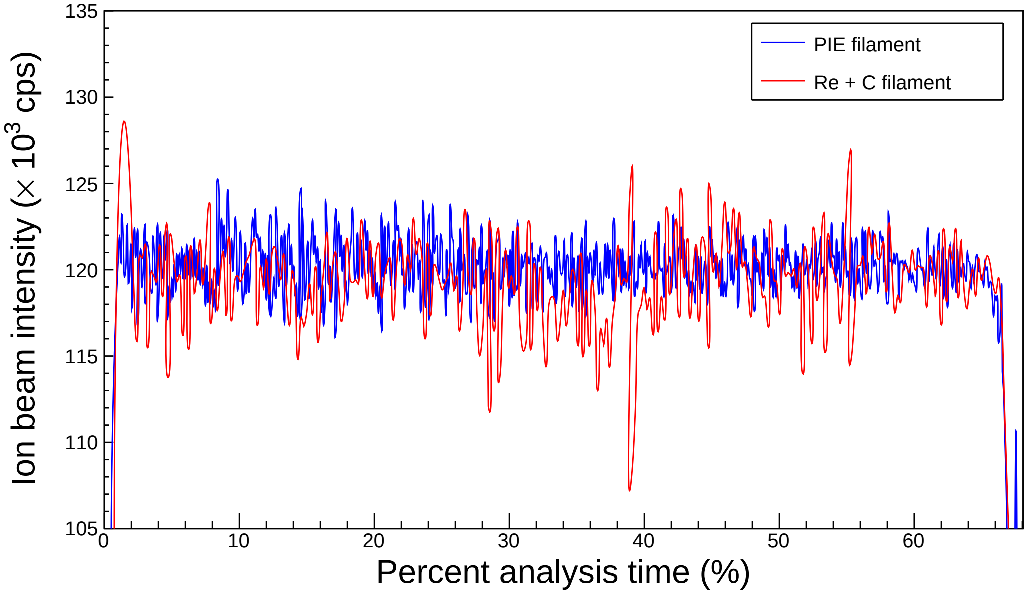

Figure 3.4: Plateau region of ion beam intensities, as a function of percent runtime, representative of PIE and traditional filaments at a 100 pg americium loading level.

3.3.2 Plutonium ionization efficiency

Plutonium ionization efficiency measurements were performed on sample mass loadings of 1 pg, 10 pg, 50 pg, and 100 pg; multiple trials (N=3–11) were conducted at each sample size. The $^{242}\mathrm{Pu}^{+}$ ion beam was monitored for these measurements. Ion yield was relatively constant for plutonium mass loadings ranging from 10–100 pg using Pt/Re PIE sources, with an average efficiency of 0.83 %. This translates to an approximate 460 % improvement in ion yield over traditional filaments and a roughly 154 % increase in ionization efficiencies reported for the resin bead technique [1]. A maximum average sample utilization of 1.09 % was realized at a 1 pg mass loading on Pt/Re PIEs. The ionization efficiency at the 1 pg plutonium sample loading achieved during this study employing PIEs is a marked improvement over utilization efficiency of 0.23 % for 0.1 pg plutonium samples reported by Watrous [123]. Data for trials at 1 pg plutonium sample loadings using traditional filaments are not presented as each filament failed rapidly. Data presented in Figure 3.5 suggests a possible trend of enhanced sample utilization with decreased sample size beginning at 1 pg loading levels of plutonium; however, additional trials conducted at sample sizes less than 1 pg are required to confirm this hypothesis. The shaded areas in Figure 3.5 indicate theoretical plutonium ionization efficiencies atop rhenium and carburized rhenium predicted by the Saha-Langumir equation (2.2); a first ionization energy of 6.0260 eV [124] for plutonium, work function values of 4.98 eV and 5.36 eV [3] for rhenium and carburized rhenium, respectively. and a filament temperature range of 2024–2324 K were used in calculating ion yield. As with americium, PIEs were able to produce plutonium ion yields that routinely exceeded those predicted by the Saha-Langumir equation (2.2) using standard bare rhenium filaments.

Additional ionization efficiency measurements (N=3) were conducted at 10 pg loading levels of plutonium using newly developed PIE sources made completely from platinum. Platinum PIEs demonstrated a additional 134 %

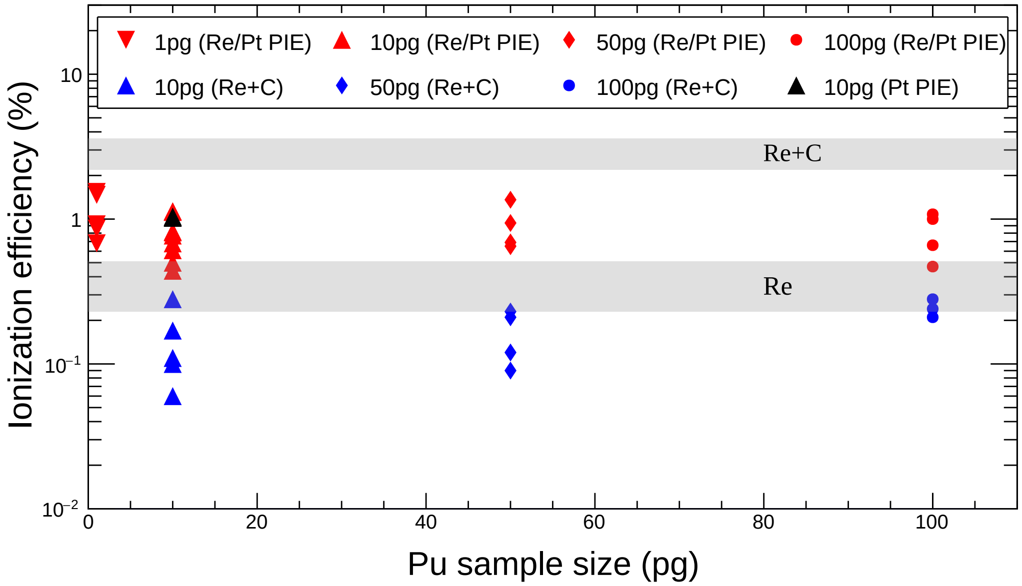

Figure 3.5: Plutonium ionization efficiency data obtained using Pt/Re PIEs, platinum PIEs, and traditional filaments. The shaded areas indicate theoretical plutonium ionization efficiencies atop bare rhenium and rhenium with a carbon additive as predicted by the Saha-Langmuir equation.

increase in sample utilization over their Pt/Re PIE counterparts. This boost in ion yield can likely be attributed to two primary factors: 1) the work function of platinum is higher than that of rhenium [42] and 2) increased ionization surface contact area; the pores in the platinum PIEs, observed using an optical microscope, appeared to be smaller and more uniform in size than those in PIEs made from a combination of platinum and rhenium powders. Smaller pores allow for increased contact between the analyte and filament which has proven to be a significant contributor for increased sample utilization associated with PIEs [71]. Figure 3.6 is a SEM image illustrating the large pores, 50–100 µm in diameter, found in Pt/Re PIEs. The homogeneity in micro-porous structure of platinum PIEs appears to have the added benefit of increased measurement precision. In this study, percent relative standard deviation (%RSD) in ionization efficiency measurement results made using platinum PIEs were significantly lower than those made using Pt/Re PIEs or traditional TIMS sources; platinum PIEs exhibited a measurement precision of 1 %RSD whereas ionization efficiency measurements made using Pt/Re PIEs and traditional filaments demonstrated a precision of >20 %RSD. Averaged plutonium ionization efficiency data for each sample size analyzed is listed in Table 3.2

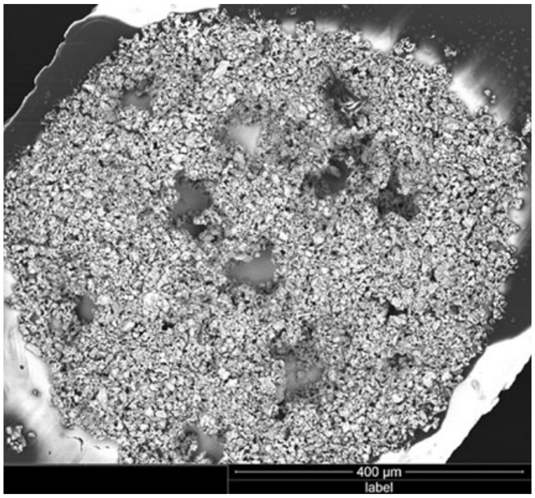

Figure 3.6: An SEM image of a Pt/Re PIE mounted atop a standard, zone-refined rhenium filament. The larger intermittent pores range in size from 50–100 μm in diameter. This figure was adapted form reference [10].

Table 3.2: A summary of average plutonium ionization efficiency data collected using PIE and traditional filaments as ion sources.

Pu sample size (pg)	Ionization Efficiencies (%)		Enhancement (%)
	PIE	Traditional	
100	0.80	0.24	∼333
50	0.91	0.16	∼569
10	0.77	0.14	∼550
1	1.09	–	–
10[a]	1.03	0.14	∼736

---

[a] sample analyzed with platinum PIE

3.3.3 Additional considerations

The extent to which an element can be ionized is highly contingent on the work function of the ionizing surface. This process can be described by the Saha-Langmuir equation (2.2). Platinum has a higher mean work function than rhenium and should produce ions more easily for a given temperature and analyte. At this point, the work function of platinum-rhenium mechanical mixture has not been studied; however, SEM/EDS analyses have shown that platinum-rhenium composition and, as a result, Pt/Re PIE work function are dynamic. During thorium trials the PIEs platinum supply was nearly exhausted within the first fifteen minutes of analyses [10]. Due to the highly refractory nature of thorium, TIMS analyses of thorium are conducted at much higher temperatures than those for plutonium. As such, the rate of platinum consumption at lower analysis temperatures is unknown at this time. The increased work function does not seem to be a significant driver in thorium analyses; however, it may prove significant in the analysis of actinides with lower ionization potentials (e.g., americium and plutonium).

3.3.4 Recommendations for future work

Filament carburization is a proven method of effectively boosting ionization efficiency of actinides. Uranium analyses using carburized PIEs have been conducted: however, the effects of carburization were not tested. Side-by-side thorium trials using carburized and non-carburized PIEs showed a small but consistent boost in ionization efficiency when using carburized PIEs; no attempts at optimizing carburization conditions were attempted. No attempts at analyzing americium or plutonium using carburized PIE filaments were made during this study. It is likely that, given the proper carburization conditions, analyses of more volatile actinides such as americium and plutonium using PIEs would benefit from filament carburization. Currently, all PIEs incorporate a liquid cation exchanger that does provides a small source of carbon; however, like the resin bead, the amount of carbon is so small that its effects, if any, are limited.

Further investigations should be conducted to optimize platinum PIE construction. A 2-to-1 ratio of platinum-to-glue was used in this study, but due to issues with the PIE spreading across the filament a higher concentration of metal might be preferred; this may help to concentrate the PIE in an even smaller footprint as its heated. Side-by-side studies should be conducted comparing flat platinum filament ribbons, rhenium filaments and PIEs (i.e., platinum and Pt/Re) to aid in elucidating PIE functioning. Such trials may give an indication of the extent to which platinum ion bombardment, work function and ionization surface area plays in enhanced ionization efficiency.

A variety of actinides should be investigated, as the contribution of each mechanism is undoubtedly different depending on the element.

3.4 Conclusions

This work represents an initial investigation into enhanced ionization efficiency of americium and plutonium using PIEs as TIMS sources. PIE techniques consistently demonstrated substantial improvements in sample utilization during the analyses of americium and plutonium in the 1–100 pg mass loading range when compared to traditional TIMS ion sources. Initial trials, conducted using 10 pg samples of plutonium, suggest that PIEs constructed of 100 % platinum can further enhance ion yield, with greater precision, when compared to Pt/Re PIEs. Subsequent investigations of enhanced sample utilization using platinum PIEs, carried out over a broader range of sample sizes and elements, are required to fully explore the efficacy of these sources. Americium ionization efficiency measurements using platinum PIE sources were not investigated during this work.

Chapter 4

Isotopic mass fractionation behavior of uranium and plutonium using porous ion emitters as TIMS sources

This chapter is based on a manuscript that is in preparation for submission to, *Analytical Chemistry*, to be considered for publication: Matthew L. Baruzzini, Howard L. Hall, Khalil J. Spencer, and Floyd E. Stanley, "Isotopic fractionation studies of uranium and plutonium using Pt/Re porous ion emitters as TIMS sources".

My contributions to this work include: Preparation of PIE stock materials; PIE filament preparation; sample preparation and loading; mass spectrometric analyses; processing, analyzing, and interpretation of experimental data; and the writing of the manuscript.

The institutional number for this chapter, entitled "Isotopic mass fractionation behavior of uranium and plutonium using porous ion emitters as TIMS sources", is LA-UR-16-23969

Abstract

An investigation of the isotope fractionation behaviors of plutonium and uranium reference standards was conducted employing Pt/Re PIEs sources, a relatively new TIMS ion source strategy. The suitability of commonly employed mass bias correction laws (i.e., the Power, Exponential, and Linear laws) for correcting such isotope ratio data was determined. Plutonium trials were conducted using 5 ng and 10 ng; the data indicate an approximate

25 % reduction in fractionation factor per atomic mass unit (‰ amu^{-1}) when sample size was halved. Corrected plutonium isotope ratio data, regardless of mass bias correction scheme, were statistically identical to that of the certificate value once expanded uncertainty was accounted for; however, the process of isotope fractionation behavior of plutonium using the adopted experimental conditions was determined to most accurately described by the Power law. Uranium trials were limited to 50 ng samples. Analysis of the data indicate that the fraction behavior of uranium, under the current analytical conditions, is also most suitably modeled using the Power law, though the Linear and Exponential laws for mass bias correction rendered uranium isotope ratio results that were identical, within uncertainty, to the certificate value. Uncertainties for experimentally determined isotope ratios are reported at the 1σ level, where σ is the standard deviation of the population.

4.1 Introduction

Instrumental bias represents a significant source of error in IRMS; the ability to make precise and accurate isotopic ratio measurements is critical for nuclear forensic efforts. In the context of mass spectrometry, the term *bias* is used to describe a combination of effects, that occur in a mass spectrometer, leading to a difference between the measured and true isotope ratio(s) of a sample.

Such effects may occur during the formation, transmission, and detection of ions. In TIMS, mass fractionation occurs as the sample is heated by the metal filament. The rate at which each isotope evaporates from the hot metal filament depends on its abundance in the sample and on its mass. Lighter isotopes are preferentially evaporated relative to heavier isotopes in the thermal ion source; this is a result of the higher translational velocities of lighter isotopes, for a given kinetic energy, and the tendency of heavier isotope to form stronger chemical bonds [125]. The result is a time-dependent variation in measured isotope ratios; the sample reservoir (i.e., the sample remaining on the filament at a given time) tends to become relatively enriched in heavier isotopes as the analysis proceeds. Another significant factor influencing mass bias is the size of the sample. As sample size increases, competition between analyte atoms for filament surface area also increases [2, 3]. This effect is magnified in traditional single filament analysis where analyte atoms are evaporated and ionized by the same filament. The result is a substantial loss of analyte as evaporated neutral atoms, biased in favor of lighter isotopes, at relatively low filament temperatures where ionization is less likely to occur.

This time-dependent behavior of measured isotope ratios hinders the accurate determination of the true isotope ratio of a sample through individual direct measurement because the effects of mass bias cannot be totally controlled and reproduced. In TIMS, typical mass bias is on the order of ∼1 ‰ amu^{-1} for high mass elements (i.e. ≥180 amu), whereas mass bias associated with multi-collector ICP-MS (MC-ICP-MS) can be expected to be approximately an order of magnitude larger for the same mass range [126]. However, correcting for instrumental mass fractionation can be accomplished by normalizing the measured ratio of interest to a known or accepted reference ratio. Measured isotope ratios are commonly corrected for fractionation by applying one of the well known mass bias correction laws that appear in the literature. These include the Linear law [4, 5], the Power law [4–6], the Exponential law [4–7] and Rayleigh's distillation law[5–8]. Several studies of isotopic fractionation behavior during TIMS analysis have centered around creating source specific models for correcting mass bias [127–130]. Andreasen and Sharma have concluded that isotope ratios corrected for mass fractionation using the Exponential law are fully satisfactory given the current level of precision obtainable in TIMS analyses [130]. As precision of isotope ratio measurements continues to improve, it may become advantageous to apply or develop fractionation models that are source specific.

All fractionation laws assume that evaporation and ionization of a sample occurs in a single, homogeneous domain atop a filament. In reality, this assumption isn't well justified as a sample loaded atop a filament, either single or multi-filament geometries, is not a point source and a temperature gradient exists across the filament; mass fractionation behavior is temperature dependent. Recently introduced PIE techniques have been shown to address such issues. Watrous et al. have demonstrated that PIEs are very effective at containing a sample within the porous structure and do not permit sample migration across the filament [9] The small footprint of the PIE serves to localize the analyte at the center of the filament such that the instrument optics behave as if each sample were a point source. Localized loading leads to a reduction in ion energy spread as a function of voltage drop and temperature gradient across the filament surface resulting in ion transmission through the ion optics and enhanced abundance sensitivity when compared to other techniques [9]. The PIE's ability to more accurately represent a point source suggests that they may potentially reduce the effects of mass bias associated with the thermal gradient across the filament when compared to other single filament techniques. The objective of this investigation is to evaluate the fractionation effects arising from the use of PIEs as TIMS sources in the measurement of uranium and plutonium isotopic systems. Fractionation effects were evaluated according to each of the mass correction strategies introduced above (Linear, Power, and Exponential mass bias correction laws) and distinctions in applicability are discussed.

4.2 Experimental

4.2.1 Isotopic standards and reagents

Samples were prepared from CRM 144 (NBL: Argonne, IL; USA) plutonium isotopic standard and isotopic reference material (IRM) 199 (Institute for Reference Materials and Measurements (IRMM): Joint Research Centre; Geel, Belgium) uranium isotopic reference standard. Platinum and rhenium metal powders, both 325-mesh, as well as the water soluble poly(4-styrene-sulfonic acid) ion exchange solution (M_w=75 000, 8 wt% in H_2O) were procured from Sigma Aldrich (St. Louis, MO). High-purity, zone-refined rhenium filament ribbons were acquired form H. Cross Co. (Moonachie, NJ; USA). Optima™ grade nitric acid (HNO_3) was purchased from Fisher Scientific (Pittsburgh, PA; USA).

4.2.2 PIE stock material and filament preparation

PIE stock material was prepared by incorporating equal parts, by mass, of platinum powder, rhenium powder, and melted hot glue. Once throughly integrated, the stock mixture loaded into a specially designed extruder and expelled as a small diameter rope onto a quartz glass plate. After cooling, sections approximately 100 µm in height were cut from the stock material rope, as needed, and affixed to standard, high-purity, zone-refined rhenium single TIMS filament assemblies via gentle heating at 1 A for ~5 s. The PIE stock was sintered to the filament using a GV Instruments Ltd. (now Isotopix: Middlewich) filament bake-out unit evacuated to ~10^{-7} mbar (~10^{-5} Pa); the temperature was slowly increased, ~0.25 A min^{-1}, to 1700 °C and held for 20 min. A detailed description of PIE filament fabrication has been described by Watrous et al. [71].

4.2.3 Sample loading

Two drops, ~1 µL each, of poly(4-styrenesulfonic acid) water soluble cation exchange resin, diluted to a concentration of approximately 3 % by mass using 18 MΩ DI water, were added to eachPIE. The ion exchange resin was dried by heating at 1 A for ~15 s. The water soluble cation exchange resin was added to promote sample incorporation into the PIE. Samples were loaded directly to the PIE in nitrate form using a 2.5 µL capacity pipette and dried via gentle heating at 1 A for ~15 s.

4.2.4 TIMS instrumentation

Mass spectrometric analyses were carried out using a GV Instruments Ltd. (now Isotopx: Middlewich, Cheshire; UK) IsoProbe T™ multi-collector

TIMS at LANL. This mass spectrometer is equipped with a 20-position sample turret, a single-focusing magnetic sector fitted with a 54 cm magnet, nine fully adjustable Faraday cup collectors, a Daly detector ion-counting system, and a WARP filter positioned between the main collector array and rear ion counting Daly detector. Programming and performance of the mass spectrometer was controlled via the GV Instruments IonVantage software package installed on a Dell Optiplex PC (Round Rock, TX; USA). Amplifier gains cross-calibrations are conducted on a weekly basis; automated corrections are built into the software. To ensure maximum measurement precision, the instrument was warmed for at least an hour under electronic conditions similar to those employed during sample analysis. Preliminary instrument tuning was conducted each day, prior to sample analyses, using the ^{187}Re^{+} beam from a bare rhenium filament. Fine tuning of the mass spectrometer was carried out using a low intensity beam of the major isotope present in each sample immediately preceding analysis. The liquid nitrogen (LN_2) cold trap was filled, as needed, to improve vacuum in the ion source housing maximizing ion transmission and reducing abundance sensitivity.

Mass spectrometric analysis. Uranium and plutonium isotope ratio measurements were conducted using a total evaporation (TE) technique similar to the method described by Callis and Abernathey [23] and Fiedler et al. [131]. The TE method was developed for multi-filament TIMS analysis where the sample is deposited on the evaporation filament which is placed in close proximity (an ~1 mm gap) to the ionizing filament. The temperature of the evaporation and ionizing filaments are controlled independently of one another. During analysis the ionizing filament and, as a result, the ionization efficiency (defined as the ratio of analyte ions detected to initial atoms loaded on a filament) remain relatively constant. In standard single filament analysis the sample is deposited on the filament surface where it will be evaporated and ionized. Surface conditions of the filament (e.g., temperature, crystalline structure, and work function) change as the analysis progresses; these parameters have a profound effect on ionization efficiency and mass bias. The TE method, while not optimal for traditional single filament analysis, was selected to ensure the entire sample was exhausted.

Static, multi-collector measurements were employed to simultaneously monitor the sample ion beams using the Faraday cup detectors, exclusively. The collector array configuration used for uranium and plutonium analyses are listed in Table 4.1. Individual isotope ratios were calculated for each five second integration period (i.e., one cycle). Final isotope ratio values were determined by taking the ratio of the summed signal intensities at the end of

Table 4.1: Faraday cup position/nuclide assignments used in the analysis of uranium and plutonium isotopic standards

Element	Collector position (isotope)								
	L3	L2	—	Axial	H1	H2	H3	H4	H5
U	233	234	—	235	236	—	238	—	
Pu	—	238	—	239	240	241	242	—	244

analysis. Isotope ratio measurements were conducted over a period ranging from March 2014 to July 2014. Measured isotope ratios and certificate values were decay corrected to 1 May, 2015, the data analysis date, for comparison. Half-life values used for decay corrections were obtained from the Decay Data Evaluation Project (DDEP) recommended data [132]

4.2.5 Mass bias correction

Raw data were corrected for mass fractionation via internal normalization (i.e., corrections were made on a case-by-case comparison with a known value) using the empirically determined mass bias correction laws presented in the literature [4, 7]. Theses include the Linear law;

$$
\begin{aligned}
R_{ij}^{C} &= R_{ij}^{M}\left[1+\alpha_L^{i,j}\Delta m_{ij}\right] \\
\alpha_L^{i,j} &= \frac{\alpha_L^{u,v}}{1-\alpha_L^{u,v}\Delta m_{vj}} \\
\alpha_L^{u,v} &= \frac{\left(R_{uv}^{N}/R_{uv}^{M}\right)-1}{\Delta m_{uv}}
\end{aligned}
\tag{4.1}
$$

the Power law;

$$\begin{aligned} R_{ij}^{C} &= R_{ij}^{M}\left[1+\alpha_P\right]^{\Delta m_{ij}} \\ \alpha_P &= \left(R_{uv}^{N}/R_{uv}^{M}\right)^{1/\Delta m_{uv}} - 1 \end{aligned} \tag{4.2}$$

and the Exponential law.

$$\begin{aligned} R_{ij}^{C} &= R_{ij}^{M}\left(\frac{m_i}{m_j}\right)^{\beta} \\ \beta &= \frac{\ln[R_{uv}^{N}/R_{uv}^{M}]}{\ln[m_u/m_v]} \\ \alpha_E &= \frac{\beta}{m_j} \end{aligned} \tag{4.3}$$

Here, Δm_{ij} is the difference in masses m_i and m_j of isotopes i and j; Δm_{uv} represents the difference in masses m_u and m_v of isotopes u and v; R_{ij}^{M} and R_{ij}^{C} are the measured and corrected isotope ratio of isotopes i and j with masses m_i and m_j, respectively; R_{uv}^{M} is the measured isotope ratio of isotopes u and v with masses m_u and m_v and R_{uv}^{N} is the accepted or known ratio (e.g., the certified isotope ratio) of isotopes u and v. Isotopic mass values used for calculations are from the Atomic Mass Data Center (AMDC) files [133].

Fractionation factors, F (in units of ‰ amu^{-1}), were determined using standard delta (δ) notation divided by the difference in isotopic masses;

$$\begin{aligned}\delta &= \left[\frac{({}^{i}A/{}^{j}A)_M}{({}^{i}A/{}^{j}A)_N} - 1\right] \times 1000 \\ F &= \frac{\delta}{\Delta m}\end{aligned} \tag{4.4}$$

The subscripts, M and N represent the measured and certified isotope ratio values; Δm is the difference in isotopic masses; the superscripts i and j represent isotopes of an element, A.

4.3 Results and discussion

Prior to mass bias corrections, raw data were corrected for abundance sensitivity. Data were then plotted in three-isotope space, the resulting distributions were examined for linearity. Data plotted in this manner resulting in a linear distribution, within the limits of experimental error, can be interpreted as isotopic fractionation resulting from a Rayleigh distillation process [5]. Uranium, ^{233}U/^{238}U, and plutonium, ^{240}Pu/^{244}Pu, isotopic ratios were corrected for mass bias using Equations 4.1, 4.2, and 4.3 in conjunction with the measured and certified ^{235}U/^{238}U and ^{242}Pu/^{244}Pu ratios, respectively.

4.3.1 Plutonium

Multiple trials (N=13) were conducted using CRM 144 plutonium isotopic reference standard; three trials at 5 ng mass loading levels of plutonium and ten trials at 10 ng. Plutonium isotope ratio data, corrected for abundance sensitivity, are presented numerically in Table 4.2. Figure 4.1 illustrates the data plotted in three-isotope space. Plutonium sample mass loading level has a significant effect on the degree of mass bias; ^{240}Pu/^{244}Pu isotope ratios exhibited average instrumental mass fractionation factors of 0.94 ‰ amu^{-1} and 1.25 ‰ amu^{-1} for 5 ng and 10 ng sample sizes, respectively. Despite a 25 % reduction in fractionation factor exhibited by 5 ng samples relative to 10 ng samples, the data, when plotted on a three-isotope diagram, fractionates in a highly linear fashion. Least squares regression analysis of the data yielded a trend line that extends through the ratio of certified isotope ratio values, within the stated uncertainty, reported at the 95 % confidence level, with a correlation coefficient, R^2, of 0.998 77. Data, plotted in three-isotope space, that falls on a fractionation line extending through the certificate value indicates that the major source of error in plutonium isotope ratios measured using PIEs is a result of mass fractionation effects. Isotope ratio data corrected for fractionation using each of the aforementioned mass-bias correction laws are plotted in Figure 4.2. The decay corrected certified ^{240}Pu/^{240}Pu isotope ratio

Table 4.2: Plutonium isotope ratio data obtained from replicate analyses of CRM 144 using PIEs.

Analysis			$\frac{^{240}\text{Pu}}{^{244}\text{Pu}}$	$\frac{^{242}\text{Pu}}{^{244}\text{Pu}}$
number	date	sample mass		
1	2014-03-07	5 ng	1.882 560 1	2.626 989 4
2	—	—	1.882 378 6	2.626 930 2
3	—	—	1.880 883 2	2.625 863 5
		mean	1.881 940 6	2.626 594 4
		%RSD	0.039 926 1	0.019 698 2
4	2014-03-20	10 ng	1.877 946 6	2.623 748 6
5	—	—	1.879 753 2	2.625 059 3
6	—	—	1.879 917 8	2.625 074 3
7	—	—	1.878 455 8	2.624 159 9
8	—	—	1.880 243 6	2.625 393 6
		mean	1.879 263 4	2.624 687 1
		%RSD	0.047 684 5	0.023 771 6
9	2014-07-02	10 ng	1.879 328 5	2.624 815 2
10	—	—	1.879 357 0	2.624 755 5
11	—	—	1.882 358 7	2.626 808 8
12	—	—	1.879 354 5	2.624 664 2
13	—	—	1.879 270 6	2.624 639 9
		mean	1.879 933 8	2.625 136 7
		%RSD	0.064 514 1	0.031 937 0
mean			1.880 139 1	2.625 300 2
SD			0.001 437 0	0.001 011 5
%RSD			0.076 431 4	0.038 530 0

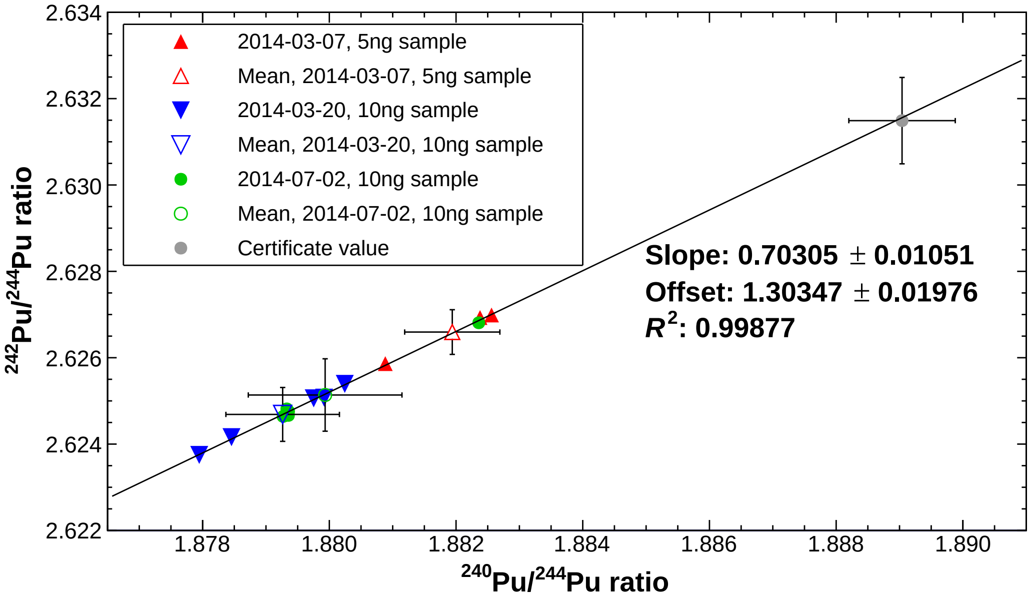

Figure 4.1: Raw plutonium isotope ratio data plotted in three-isotope space. Also plotted is the ratio of certified values along with associated uncertainties.

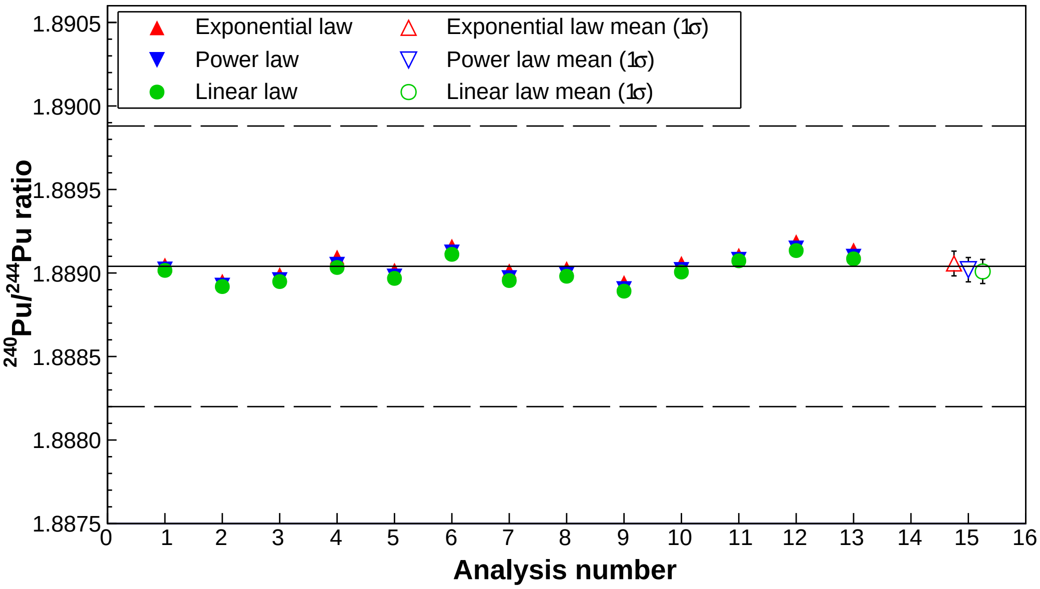

Figure 4.2: High precision data, obtained using PIE sources, corrected for mass bias. The solid line represents the certified isotope ratio; uncertainty in the certified ratio is shown by the dashed line.

value, 1.889 04(85), is represented by the solid line; the dashed lines represent the upper and lower bounds of the uncertainty in the certificate value. Each of the mass-bias correction laws used herein generated isotope ratio data that, on average, were statically identical to one another as well as the certified value. Average ^{240}Pu/^{240}Pu ratio values of 1.889 019 9(728), 1.889 056 9(741), and 1.889 009 2(722) were determined using the Power, Exponential, and Linear laws, respectively. The data indicate that the Power law most accurately describes the fractionation behavior of CRM 144 plutonium isotopic standard loaded atop PIE equipped filaments with a deviation from the certificate value of −0.008 78 ‰. Deviations from the certificate value were determined to be 0.010 81 ‰ and −0.014 47 ‰ for the Exponential and Linear laws, respectively. Assuming that the true instrumental fractionation does follow the Power law, the *error* that would be introduced by correcting raw isotope ratio data using the Linear or Exponential laws would be approximately 0.0014 ‰ amu^{-1} and 0.0050 ‰ amu^{-1}, respectively. Average mass bias corrected isotope ratio values along with associated uncertainties are listed in Table 4.3. Due to the concordance between isotope ratio data corrected for mass bias using the Power, Exponential, and Linear laws further investigation into fractionation law selection was conducted. This was accomplished by fitting a straight line to the natural logarithms of the ratio data, plotted against one another, on a

Table 4.3: Mean values for ^{240}Pu/^{244}Pu isotope ratio data corrected for mass bias using the Power, Exponential, and Linear laws of fractionation.

$\frac{^{240}\text{Pu}}{^{244}\text{Pu}}$	Mass bias correction law			Certificate value
	Linear	Power	Exponential	
mean	1.889 009 2	1.889 019 9	1.889 056 9	1.889 04
SD	0.000 072 2	0.000 072 8	0.000 074 1	
%RSD	0.003 822 9	0.003 851 8	0.003 924 2	
Deviation from cert. value (‰)	−0.014 47	−0.008 78	0.010 81	

three-isotope diagram, as shown in Figure 4.3. The slope, 0.503 543(7528), of the resultant trend line was then compared to the slopes of lines predicted by the Exponential law and the Power and Linear laws. Slope values of 0.497 996 and 0.500 067 were determined by the Exponential law and the Power and Linear laws, respectively. This analysis confirms that the data are best described by the Power law which provides a better fit than the Exponential law, however, both values fall within the uncertainty in the slope value determined for the the line of best fit to the data.

4.3.2 Uranium

Repeat fractionation trials (N=7) were conducted using 50 ng sample mass loadings of IRM 199 uranium isotopic reference material. Analytic conditions for uranium trials were similar to those employed during plutonium analyses; a key difference being the larger sample size used during uranium analysis.

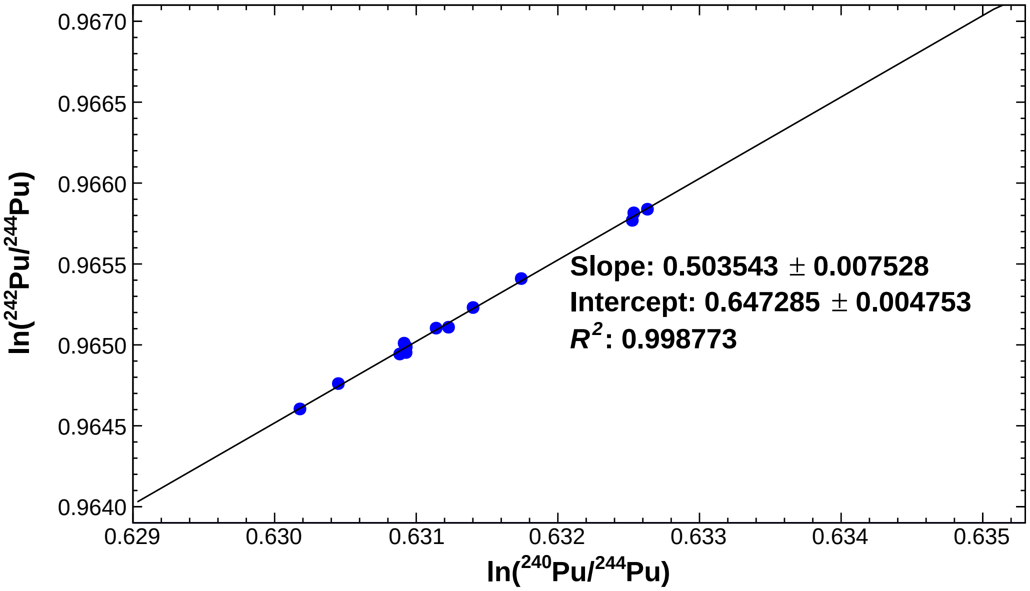

Figure 4.3: Plutonium three-isotope diagram. Plotted are the natural logarithms of the raw plutonium isotope ratio data.

As expected, the relatively larger samples exhibited a significant degree of fraction. An average fractionation factor of 1.67 ‰ amu^{-1} was determined for the $^{233}\mathrm{U}/^{238}\mathrm{U}$ isotopic ratio using Equation 4.4. Raw isotope ratio data is listed in Table 4.4. Despite the samples being relatively heavily fractionated, the data plotted on a three-isotope diagram are fit well by a straight line, R^2=0.995 63. The line fit to the data does not, however, project through the certified value within the stated uncertainty, reported at the 95 % confidence level, indicating significant residual bias. Data was corrected for residual bias after mass bias correction. Figure 4.4 shows the uranium data, corrected for abundance sensitivity and decay, plotted in three-isotope space along with

Table 4.4: Raw uranium isotope ratio data acquired from repeat measurements of IRM 199 using PIEs.

Analysis			$\frac{^{233}\mathrm{U}}{^{238}\mathrm{U}}$	$\frac{^{235}\mathrm{U}}{^{238}\mathrm{U}}$
number	date	sample mass		
1	2014-03-19	50 ng	0.991 371 9	0.995 114 8
2	—	—	0.991 112 8	0.994 972 1
3	—	—	0.991 726 0	0.995 339 7
4	—	—	0.991 236 0	0.995 137 9
5	—	—	0.991 948 3	0.995 564 0
		mean	0.991 479 0	0.995 221 7
		%RSD	0.031 442 7	0.020 659 3
6	2014-06-10	50 ng	0.991 602 5	0.995 288 7
7	—	—	0.991 636 4	0.995 302 7
		mean	0.991 619 4	0.995 295
		%RSD	0.001 710 9	0.000 703 2
mean			0.991 519 1	0.995 242 8
SD			0.000 271 2	0.000 177 0
%RSD			0.027 347 7	0.017 784 2

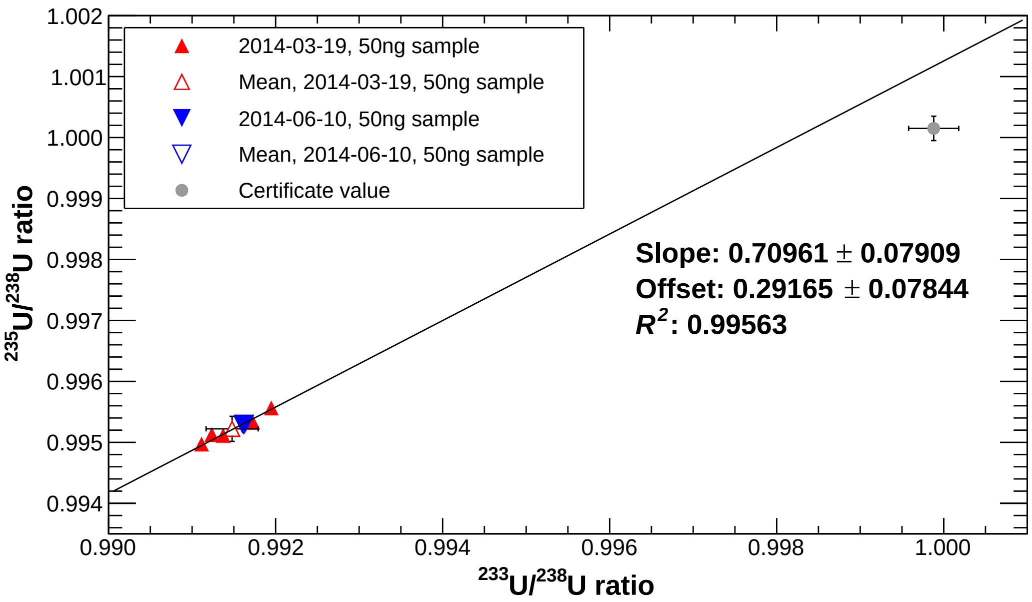

Figure 4.4: Raw uranium isotope ratio data plotted in three-isotope space. Also plotted is the ratio of certified values along with associated uncertainties.

the fractionation line and pertinent fitting parameters. As with plutonium isotope ratio data, uranium isotope ratios, measured using PIEs, indicate that mass-dependent fractionation is a significant source of measurement error. Because sample runs exhibited a relatively high degree of fractionation, the Exponential law was expected to most satisfactorily account for uranium fractionation behavior. Analysis of the data, however, revealed that all mass bias correction laws investigated herein rendered average ^{233}U/^{238}U isotope ratio values that were statistically identical to that of the decay corrected certificate value of ^{233}U/^{238}U=0.999 88(30). Mean isotope ratio data corrected for fractionation is presented in Table 4.5. Data corrected for fractionation

Table 4.5: Mean $^{233}\text{U}/^{230}\text{U}$ isotope ratio values corrected for mass bias using the Linear, Power, and Exponential laws of fractionation.

$\frac{^{233}\text{U}}{^{235}\text{U}}$	Mass bias correction law			Certificate value
	Linear	Power	Exponential	
mean	0.999 851 5	0.999 864 9	0.999 900 0	0.999 88
SD	0.000 065 4	0.000 065 8	0.000 066 4	
%RSD	0.006 536 8	0.006 578 4	0.006 635 9	
Deviation from cert. value (‰)	−0.030 07	−0.016 67	0.018 40	

using the Power law exhibited the smallest deviation for the certificate value followed by the Exponential and Linear laws. Deviations of −0.016 67 ‰, 0.018 40 ‰, −0.030 07 ‰ and −0.030 07 ‰ were calculated, using δ notation, for the Power, Exponential, and Linear laws, respectively, indicating that the Power law most accurately describes uranium fractionation behavior under the current set of analytical conditions. Fractionation corrected data are illustrated in Figure 4.5.

Fractionation law selection was further tested in the same manner described for plutonium in section 4.3.1 of this work. The natural logarithms of uranium isotope ratio data, plotted on a three-isotope diagram is illustrated in Figure 4.6. Slopes of the trend lines predicted by the Exponential and the Power and Linear laws were found to be 0.597 48 and 0.600 03, respectfully. The slope of the regression line fit to the natural logarithms of the measured isotope ratio data was determined to be 0.635 04(7881). Slopes predicted

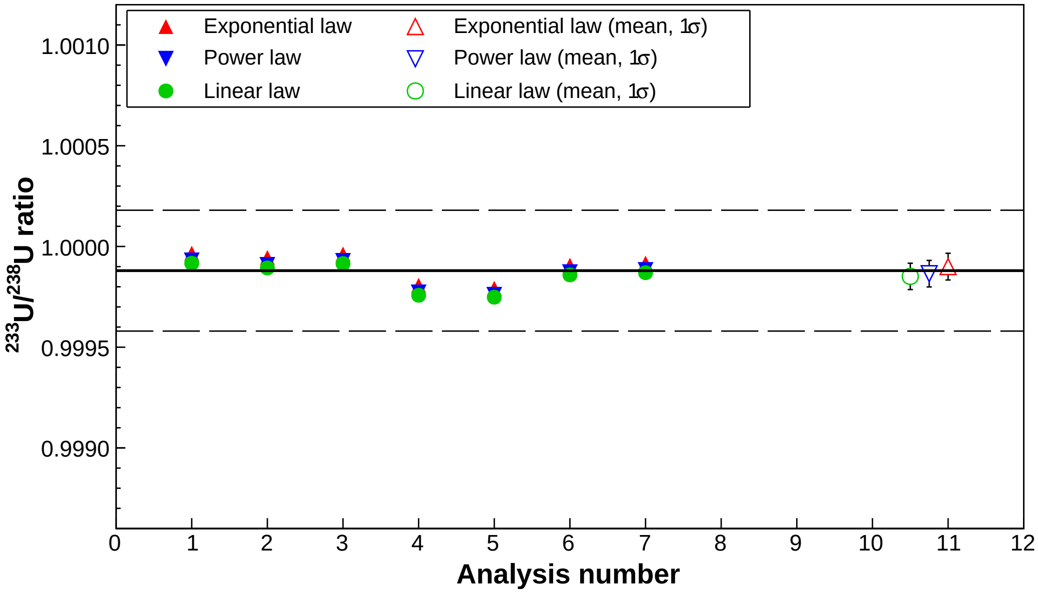

Figure 4.5: High precision uranium isotope ratio data corrected for mass and residual bias. The solid line represents the certified isotope ratio; uncertainty in the certified ratio is shown by the dashed line.

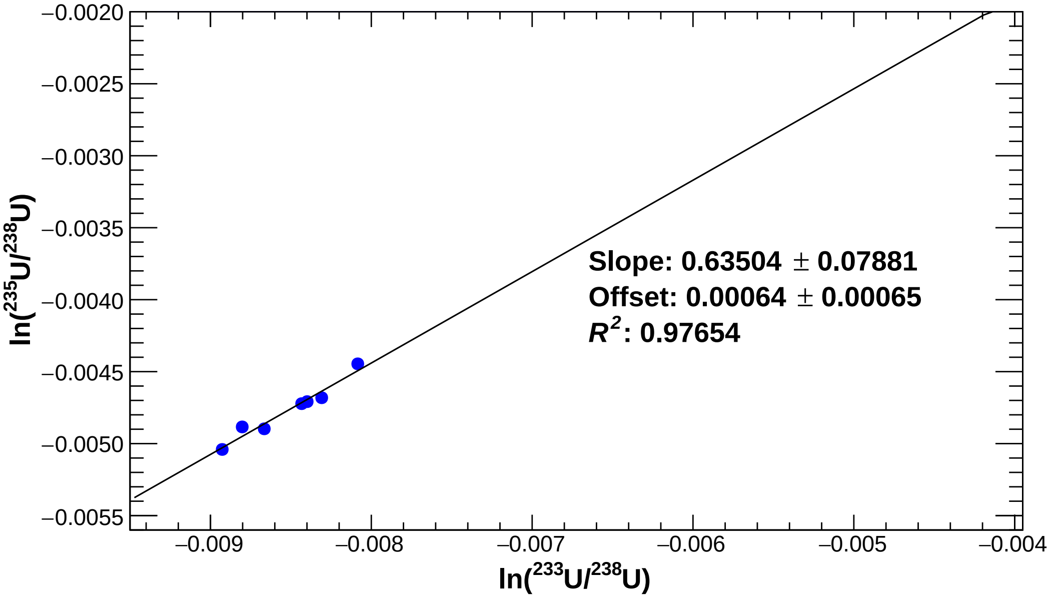

Figure 4.6: The natural logarithms of uranium isotope ratio data plotted in three-isotope space.

by each of the empirical laws were statistically identical to the slope of the fractionation line of the data, yielding no definitive conclusion on the selection of fractionation law.

4.4 Future work

An alternative strategy for mass bias correction that makes it possible to avoid the normalization procedure has been demonstrated by Cavazzini [134]. This approach is contingent on the line linear hypothesis of instrumental isotopic fractionation being satisfied and the sample is composed of a minimum of three isotopes. The linear hypothesis requires that raw isotope ratio data follow a linear distribution when plotted on an x_m vs. x_m/y_m diagram, where x_m and y_m represent two measured isotope ratios; data presented herein satisfies this requirement.

4.5 Conclusions

We have determined that the commonly employed empirical mass bias correction laws presented in the literature have proven adequate for correcting mass-induced fractionation behavior of uranium and plutonium samples associated with the use of PIEs as TIMS sources. Analysis of CRM 144 plutonium and IRM 199 uranium isotopic standards using PIE sources have yielded isotope ratio values are in excellent agreement with the certificate values, once corrected for mass fractionation using each of the mass-bias correction laws presented herein. The suite of plutonium and uranium samples, analyzed under the set of analytic conditions described herein, are most accurately described by the Power law of isotopic fractionation. Additional efforts are required to fully understand the effects that sample size and isotopic composition have on mass bias associated with PIEs. Furthermore, efforts to optimize the analytical procedure should be put forth to minimize instrumentally induced mass bias in order to maximize the accuracy and precision of isotope ratio data measured using PIEs.

Chapter 5

Comparison of porous ion emitter and traditional TIMS ion sources for determining the model-ages of four uranium standard reference materials

A manuscript entitled "Determining the model-ages of uranium reference materials using PIEs as TIMS sources" by Matthew L. Baruzzini, Howard L. Hall, Khalil J. Spencer, and Floyd E. Stanley, based on the work presented in this chapter is in preparation for submission to the *International Journal of Mass Spectrometry* to be considered for publication.

My contributions to this work include: Preparation of PIE stock materials; traditional and PIE filament preparation; sample preparation and loading; mass spectrometric analyses; processing, analyzing, and interpretation of experimental data; and the writing of the manuscript.

The institutional number for this manuscript, "Comparison of porous ion emitter and traditional TIMS ion sources for determining the model-ages of four uranium standard reference materials", is LA-UR-15-29427

Abstract

This paper describes a preliminary investigation into the use of PIE thermal ion sources for the model-age determination of uranium-bearing materials employing the ^{230}Th/^{234}U chronometer. All uranium measurements were carried out using standard rhenium triple filament assemblies. PIE equipped filaments were used for thorium isotope ratio measurements; for comparison, thorium analyses were also conducted using traditional (i.e., a zone-refined

rhenium filament ribbon plus carbon additive) single filaments. The obtained ratios were used to calculate the model-ages of four distinct uranium standard reference materials of varying enrichments ranging from 2.038–20.013 at% ^{235}U (0.0125–0.1246 at% ^{234}U) containing ultra-trace quantities, approximately 85–300 fg), of ^{230}Th to simulate very young material. All age data are decay corrected to a reference date of 31 August, 2014. Calculated model-ages were then compared to an assumed known purification date. In cases where the purification date was not known, the date the material was retrieved from the K-25 enrichment cascade in Oak Ridge, TN was used for age comparison.

5.1 Introduction

Radiochronometric dating of nuclear material, either interdicted or collected, is a fundamental tool in the portfolio of techniques available for nuclear forensic investigations. Determining the “age” of a sample can provide valuable information about a material such as origin, process history, and intended use [11, 12]. In this context a material's age refers to the time elapsed since a radionuclide of interest was chemically and/or physically separated from its decay products. The ^{230}Th/^{234}U daughter-parent isotope pair provides one of the most valued and widely used chronometers in modern nuclear forensic and safeguards research [11, 13]. These two isotopes, ^{234}U and ^{230}Th, represent the longest-lived intermediate decay products of the 4n + 2 decay series of ^{238}U, illustrated in Figure 5.1, also known as the radium series. Due to the relatively rapid ingrowth of ^{230}Th, this chronometer has been successfully applied for the determination of sample ages ranging from a few years to several hundred thousand years old [2, 14, 15].

The accuracy of model-ages determined using the ^{230}Th/^{234}U chronometer rely heavily on the assumptions that the parent has been completely purified from residual impurities or decay products, the system remains closed post-purification (i.e., no parent-daughter fractionation following purification), and daughter-parent isotope ratio measurements are precise and accurate. Previous studies have demonstrated that closed system behavior is a reasonable assumption for reference materials; however, complete initial purification, even for uranium certified reference materials, is not [135]. Any residual ^{230}Th in a uranium-bearing sample will result in a positive age bias; the material will appear to be older than its true age. This effect is greatly magnified in young materials. A complementary uranium age-dating strategy employing inductively coupled plasma mass spectrometry (ICP-MS), gamma and alpha spectroscopy has been demonstrated by Varga et al. that circumvents the challenge of incomplete zeroing when interrogating uranium ore concentrates [136], this method, however, was not employed in during this work.

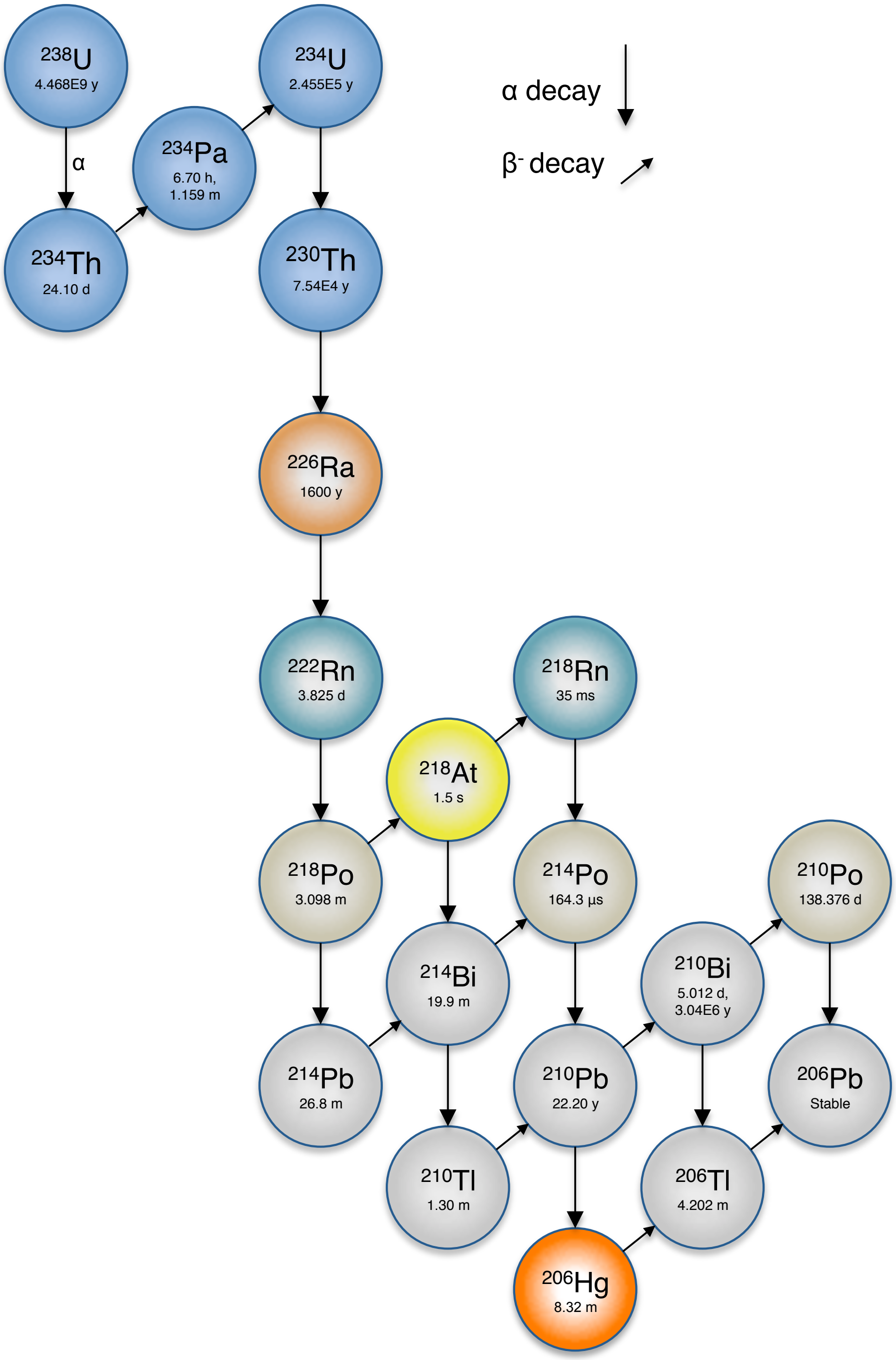

Figure 5.1: The 4n + 2 decay series with half-life and decay mode mode information. After uranium purification, ^{230}Th slowly grows in and can be used to determine time elapsed since purification.

Thorium has proven to be incredibly difficult to thermally ionize and is arguably the most difficult element to analyze via TIMS. Previous studies using PIE thermal ion sources have demonstrated significant enhancement in ionization efficiency relative to traditional filaments at the picogram mass loading level of thorium [2, 10]. The objective of this study is to capitalize on the enhanced thorium sample utilization associated with PIE thermal ion sources demonstrated by Stanley et al. [10] in an effort to improve precision and accuracy of model-age determination of uranium materials using the ^{230}Th/^{234}U chronometer containing trace quantities of thorium. Stanley et al. reported that in addition to exhibiting a trend of increased sample utilization as sample size decreases, a relative enhancement in sample utilization was also boosted as analyte loading levels were reduced [10]. These findings indicate that PIE filaments should significantly outperform traditional filaments in their ability to produce ions at femtogram mass loading levels of thorium. This boost in ion yield should translate to a more stable ion beam at higher target intensity yielding more precise and accurate isotope ratios.

5.2 Materials and experimental methods

5.2.1 Reagents, spikes, and uranium isotopic standards

The ^{233}U spike was prepared in-house at LANL and calibrated against a solution prepared from NBS-U960 uranium metal assay standard. The ^{229}Th spike used for ^{230}Th measurements was obtained from NBL, and cross-calibrated against a natural thorium standard (Spex Certipriep Inc., Metuchen, NJ; USA). Lewatit anion exchange resin (MP5080, 60–120 mesh) was used for ion chromatography. All acids used were Optima™ grade purchased from Fisher Scientific (Pittsburgh, PA; USA). Platinum powder (325 mesh), rhenium powder (325 mesh), and water soluble Poly(4-styrenesulfonic acid) solution cation exchange resin (M_w=75 000, 18 wt% in H_2O) were all acquired from Sigma Aldritch (St. Louis, MO; USA). High-purity zone-refined rhenium filament ribbons were purchased from H. Cross Co. (Moonachie, NJ; USA). Graphite for the colloidal carbon solution was obtained from Ultra Carbon Corporation (Bay City, MI; USA). All dilutions were made using 18 MΩ DI water. Four distinct uranium standard reference materials (SRMs), obtained from the United States NBS (now distributed by NBL as CRMs) were used in this study; U020, U050, U100 and U200. Certificates for each of these uranium isotopic standards can be found in Appendices D.2, D.3, D.4, and D.5.

5.2.2 Sample preparation for ^{234}U analysis

Three aliquots from each of the four uranium standard solutions were partitioned to contain microgram levels of uranium. Each sample fraction was transferred to an individual spike vial containing a known quantity of ^{233}U tracer for thermal ionization isotope dilution mass spectrometry (IDMS) analyses. The spiked samples were weighed, equilibrated, evaporated to dryness, reconstituted in concentrated HNO_3 to ensure conversion to nitrate form and dried down a second time. The fractions were then dissolved in 1 M HNO_3 and brought to a final concentration of approximately $200\,\mathrm{ng}\,\mu\mathrm{L}^{-1}$ for subsequent filament loading. Because each aliquot contained only ultra-trace amounts of thorium (i.e., $N_U \gg N_{Th}$) uranium-thorium separations were not carried out on uranium sample cuts prior to TIMS analysis.

Filament preparation, sample loading, and TIMS analysis

Uranium analyses were conducted using triple filament assemblies constructed using high-purity zone-refined rhenium filament ribbons. Prior to sample loading, filament ribbons and support posts were submerged in acetone and sonicated for approximately ten minutes. Once cleaned, the filament assemblies were thoroughly dried in a laboratory convection oven. The assemblies were then placed in a GV Instruments Ltd (now IsotopX Ltd: Middlewich, Cheshire; UK) filament bake-out unit, brought under high vacuum, and degassed at 4.5 A for approximately 20 minutes to minimize uranium blank. After filament pretreatment, 1 µL of uranium solution was carefully pipetted directly onto a side filament, dried via gentle heating at a current of 1 A, and mounted on the sample turret in preparation for TIMS analysis.

Mass spectrometric analyses were carried out using a VG Sector 54 single-focusing magnetic sector TIMS from VG Micromass (now IsotopX Ltd: Middlewich, Cheshire; UK) equipped with a twenty position sample turret, five variable-position Faraday cup detectors (each equipped with a $10^{11}\,\Omega$ resistor) and a Daly detector fixed at the axial position. To ensure precision and accuracy of isotope ratio measurements Faraday cup inter-detector amplifier gains were calibrated each morning prior to sample analyses. The cold trap was filled with LN_2 as needed to minimize hydrocarbon background that may produce isobaric interference as well as keep source pressure to a minimum.

Each sample fraction was run in duplicate using the TE analytical technique [23]. The TE measurement method was chosen to achieve the best precision and accuracy by minimizing the effects of instrumental fractionation. The measured $n(^{233}\mathrm{U})/n(^{238}\mathrm{U})$ isotope ratios for each pair of samples were averaged; the resulting ratio was used for subsequent model-age calculations.

Static, multi-collection measurements, employing the Faraday cup collectors, were used for all detection positions; the major isotope, $^{238}U^{+}$, ion beam intensity was targeted at approximately 4 V. A standard sample bracketing method [137] was employed, using IRM 199 (Joint Research Centre; Geel, Belgium) uranium isotopic reference standard as a comparator, to evaluate instrument bias resulting from isotopic fractionation as well as a quality control standard. Mass bias was corrected using the linear mass bias correction law [4] in conjunction with the measured and decay corrected certified IRM 199 $n(^{233}U)/n(^{238}U)$ ratio.

5.2.3 Sample preparation for ^{230}Th analysis

Four aliquots, containing femtogram quantities of ^{230}Th, were prepared from each of the four uranium standard solutions for a total of sixteen thorium sample cuts; eight were analyzed using PIEs and eight using traditional filaments. Sample size requirements were estimated using the theoretical predicted in-growth of ^{230}Th and certificate value for ^{234}U abundance in each standard. Figure 5.2 illustrates the expected ^{230}Th in-growth, in $\mathrm{fg\,\mu g^{-1}U}$, as a function of material age. In preparation for IDMS analysis, sample cuts were spiked with known quantities of ^{229}Th, weighed, allowed to equilibrate and evaporated to dryness. The fractions were then re-dissolved in 12 M

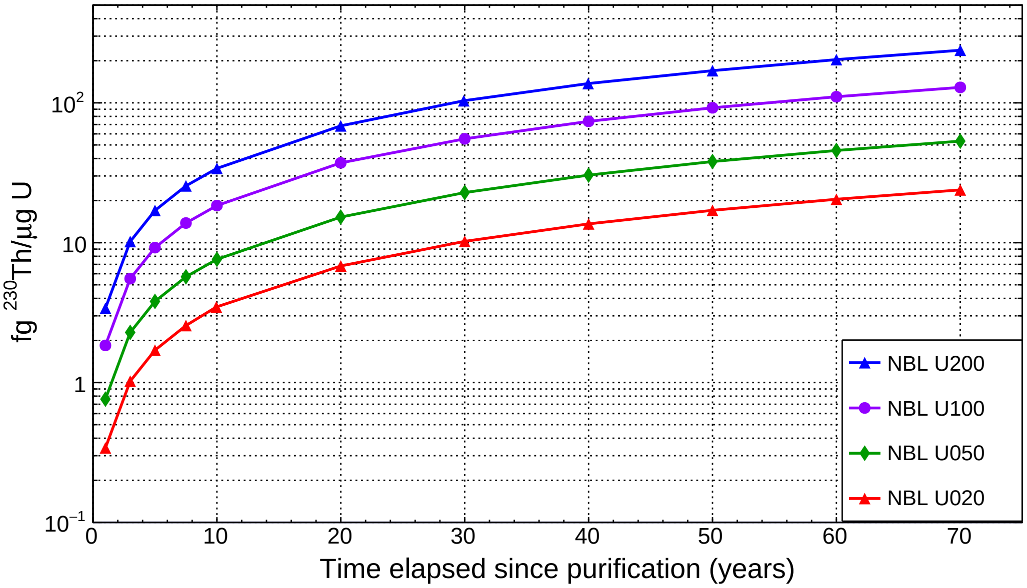

Figure 5.2: Predicted ^{230}Th in-growth, as a function of age, of the four NBL uranium reference materials used in this investigation.

hydrochloric acid (HCL) and dried a second time. Prior to separations, the samples were reconstituted in approximately 1 mL of 12 M HCL.

Thorium separations/purification

Thorium separations were carried out on a 2 mL Lewatit anion exchange resin bed. In-house performance evaluations of this Lewatit-based separation scheme have demonstrated a separation factor on the order of 10^5 and nearly 100 % thorium recovery. Separation factor is defined as the quotient of the thorium-uranium ratio in the initial material $(\mathrm{N_{Th}}/\mathrm{N_U})_i$ and in the final material $(\mathrm{N_{Th}}/\mathrm{N_U})_f$, after separation. Preceding sample introduction, each column was preconditioned with approximately 10 mL of concentrated HCL in order to convert the resin to chloride form as well as remove any thorium blank that may be present on the resin. Spiked aliquots were deposited on the columns followed by an additional two sample vial rinses. The rinsing process was carried out using 0.5 mL of concentrated HCL and serves to remove any residual thorium remaining in the sample vial. In chloride form, thorium is not retained on the column and was immediately collected into a pre-cleaned, conical bottom Savillex (Eden Prairie, MN; USA) vials. An additional 0.5 mL of concentrated HCL was added to the column to further elute any residual thorium.

The purified thorium fractions were evaporated to dryness and then dissolved in a few drops of HNO_3 in order to convert the sample to nitrate form. The samples were then heated and evaporated to near dryness, then treated with a drop, approximately 1 µL, of 0.3 M H_3PO_4. The H_3PO_4 was added to prevent the sample from completely drying as well as provide a visual indicator of the sample location in the vial. Great care was taken to ensure that the entire sample was located at the vertex of each conical vial. In preparation for filament loading, the samples were reconstituted in 1 µL of 1 M HNO_3 and allowed to equilibrate overnight.

Filament preparation and TIMS analysis

An Isoprobe-T™ single magnetic sector TIMS from GV Instruments Ltd (now IsotopX Ltd: Middlewich, Cheshire; UK) was employed for all thorium isotopic measurements. The ion detection system consists of nine variable-position Faraday cup detectors, each equipped with a $10^{11}\,\Omega$ resistor, and a single static, axial position ion counting Daly detector mounted behind a WARP energy filter. Instrument performance and programming were controlled via the GV Instruments IonVantage software package installed on a Dell Optiplex PC (Rock Round, TX; USA). Source pressure and hydrocarbon background were kept to a minimum with the aid of LN_2 added to the ion source cold trap as needed. Thermal ionization IDMS analyses of ^{234}U and ^{230}Th were conducted using ^{233}U and ^{229}Th spikes, respectively.

Thorium isotope ratio measurements were carried out using PIE and standard, single filament thermal ion sources. All filaments were pre-treated using a GV Instruments Ltd (now Isotopx: Middlewich, Cheshire; UK) filament bake-out unit evacuated to approximately 10^{-7} mbar (10^{-5} Pa). The filaments were slowly heated to 4.5 A and degassed at this temperature for at least ten minutes. PIEs were constructed from a 50/50 mixture, by mass, of rhenium and platinum metal powders that were mixed with a hot gluing agent and sintered atop a standard zone-refined rhenium filament. Two drops of a polystyrene sulfonic acid cation exchanger, diluted with DI water to a concentration of roughly 3 % by mass, were wicked into the PIEs and dried; the ion exchange resin is added to enhance thorium sample incorporation into the PIE. Explicit details of PIE filament preparation have been described previously [10, 71]. Samples were carefully loaded directly to the PIE structure and dried by gentle heating at 1 A. Traditional single filament assemblies were constructed from zone-refined rhenium filament ribbons; thorium samples were loaded with colloidal graphite and dried with a current of 1 A applied to the filament. Due to the trace quantities of thorium present in each sample, isotopic measurements were carried out exclusively using the Daly detector in conjunction with the WARP filter to maximized abundance sensitivity. A three step peak-jumping technique was employed for isotope detection; the Daly detector was sequentially exposed to ^{232}Th, ^{230}Th and ^{229}Th ion beams. A five second integration time was used for ^{232}Th and ^{229}Th ion beams, the ^{230}Th beam signal was integrated for ten seconds. Baseline and peak centering steps were included in this method preceding each block of ten, three-cycle isotopic measurements.

Due to the lack of a suitable certified thorium isotopic standard, no mass fractionation corrections were applied to the measured thorium isotope ratios. As a result, the largest contributor to the combined standard uncertainty in model-ages was the $n(^{230}\mathrm{Th})/n(^{229}\mathrm{Th})$ ratio measurement, which accounted for approximately 90 % of the total model-age uncertainty budget.

5.3 Results and discussion

The highest precision (i.e., the lowest %RSD) $n(^{230}\mathrm{Th})/n(^{229}\mathrm{Th})$ isotope ratio measurements using PIE filaments were obtained at a $^{229}\mathrm{Th}^+$ beam aiming intensities of approximately 3000 cps. Attempts at increasing aiming intensity resulted in ion beam instability leading to unacceptably poor measurement precision. Traditional filaments, on the other hand, exhibited the highest precision ratio results at 10 000 cps; this was the highest count rate attempted using traditional filaments during this investigation. The inability of PIE filaments to maintain stable ion beams at higher aiming intensities relative to traditional filaments was unexpected as previous ionization efficiency studies conducted using PIE sources at picogram mass loading levels of uranium [9], americium and plutonium [3], and, most notably, thorium [10] have demonstrated a substantial increase in sample utilization when compared to standard single rhenium filaments. Ionization efficiency studies presented in Chapter 3 of this Dissertation show that PIEs were not only capable of significantly boosting ion yield, but generating stable ion beams with several times the intensity of those emitted from standard filaments at mass loading levels of less than 10 pg as well. The addition of H_3PO_4 to thorium samples during this investigation is likely the culprit causing the substandard performance of PIE filaments as this is the primary difference between this and the aforementioned studies.

5.3.1 Model-age calculation

The expected ingrowth of ^{230}Th over time in a uranium sample can be expressed as;

$$\frac{N^t_{^{230}\mathrm{Th}}}{N^t_{^{234}\mathrm{U}}} = \frac{\lambda_{^{234}\mathrm{U}}}{\lambda_{^{230}\mathrm{Th}} - \lambda_{^{234}\mathrm{U}}}\left(1 - e^{(\lambda_{^{234}\mathrm{U}} - \lambda_{^{230}\mathrm{Th}})t}\right) + \frac{N^0_{^{230}\mathrm{Th}}}{N^t_{^{234}\mathrm{U}}} e^{-\lambda_{^{230}\mathrm{Th}} t}, \tag{5.1}$$

where $\lambda_{^{230}\mathrm{Th}}$ and $\lambda_{^{234}\mathrm{U}}$ are the decay constants of ^{230}Th and ^{234}U, respectively. The concentrations of ^{230}Th and ^{234}U in the sample are denoted by $N^t_{^{230}\mathrm{Th}}$ and $N^t_{^{234}\mathrm{U}}$, respectively. $N^0_{^{230}\mathrm{Th}}$ is the residual ^{230}Th remaining in a sample post-purification. Assuming complete initial separation (i.e., $N^0_{^{230}\mathrm{Th}} = 0$), Equation 5.1 can be solved for the time elapsed since purification, t;

$$t = \frac{1}{\lambda_{^{234}U} - \lambda_{^{230}Th}} \ln\left(1 - \frac{\lambda_{^{230}Th} - \lambda_{^{234}U}}{\lambda_{^{234}U}} R\right) \tag{5.2}$$

The sample model-age is calculated by substituting the measured daughter-parent ratio, R, decay corrected to the reference date, and the appropriate decay constant values into into Equation 5.2. A samples model-date can be obtained by subtracting t from the reference date. Model ages determined using Equation 5.2 should be thought of as a maximum possible material age, as residual thorium is not accounted for. Half-life values of 245 620(260) yr for ^{234}U and 75 584(110) yr for ^{230}Th [138] were used for model-age calculations; reported half-life uncertainties are at the 2σ level.

Elemental concentrations of uranium in each sample was determined using the standard IDMS equation;

$$c_s = \frac{c_y m_y}{m_s} \frac{R_y - R_b}{R_b - R_s} \frac{\Sigma R_{is}}{\Sigma R_{iy}} \tag{5.3}$$

where c_y is the concentration of element in the spike, m_s is the mass of the sample in the blend, m_y is the mass of the spike in the blend, R_s, R_y, and R_b are the isotope ratios in the sample, spike, and blend, respectively, ΣR_{is} is the sum of isotope ratios in the sample and ΣR_{iy} is the sum of the isotope ratios in the spike. The ^{234}U isotopic concentration, $N^t_{^{234}\mathrm{U}}$, was determined by multiplying the total concentration of uranium (in $\mathrm{g\,g^{-1}}$), obtained using Equation 5.3, with the isotopic abundance (in wt%) of ^{234}U in each sample. Uranium isotopic abundances were obtained from the decay corrected certificate values; certificates for the uranium isotopic standards are located in Appendix D, section D.2. Thorium concentrations were determined using Equation 5.4;

$$w_s = w_{x,s} \frac{M_s m_y}{M_x m_s a_{s,x}} \frac{R_y - R_b}{R_b - R_s}, \tag{5.4}$$

here $w_{y,x}$ is the mass fraction of isotope x in the spike; M_s and M_y are the standard atomic weights of the element in the sample and spike; m_x and m_y mass of the sample and mass of the spike solution; $a_{s,x}$ is the abundance of isotope x in the sample; R_s, R_y, and R_b are the isotope ratios in the sample, spike, and blend, respectively.

Uncertainties in isotope-amount ratios and sample model-ages uncertainties were calculated according to the Joint Committee for Guides in Metrology (JCGM) 100:2008, "evaluation of measurement data – guide to the expression of uncertainty in measurement (GUM)" [139] using commercially available software, GUM Workbench by Metrodata® [140]. Model-age results are summarized in Tables D.1–D.8 and plotted in Figure D.1 located in Appendix D. The paper age, in years, of each uranium standard was calculated using a reference date of 31 August, 2014.

5.3.2 U020

Records indicate that the material used to make NBL U020 was removed from the K-25 enrichment cascade on 21 January, 1958 [141]; the purification date was not reported. Because the purification date was not known, the date the material was removed from the enrichment cascade was used to determine the "age"; the paper age of U020 was calculated to be 56.6 years older than the reference date. The range of model dates calculated using thorium isotope ratio data obtained employing PIE sources extended from 01 March, 1958 to 18 June, 1962, yielding an average model-age of 54.2 ± 4.3 years old. This model-age is approximately two years younger than, but concordant with, the paper age of the stock material within expanded uncertainty. The reported uncertainty in the model-age is twice the standard deviation (2σ) of the population ($N = 6$). Sample UD Th1-U020 yielded a ^{230}Th concentration, thus model-age, that was lower than expected; careful examination of the measured $n(^{230}\text{Th})/n(^{229}\text{Th})$ raw isotope ratio data revealed that this sample was unable to maintain a stable $^{230}\text{Th}^{+}$ ion beam at the set $^{229}\text{Th}^{+}$ aiming intensity of 10 000 cps. Thorium sample ID Th3-U020 was analyzed using a $^{229}\text{Th}^{+}$ aiming intensity of 2000 cps; this filament generated a more stable ion beam and rendered a model-age much closer to the U020 paper age and the model-age determined using standard filaments. Thorium samples analyzed using traditional filaments resulted in an average model-age of 57.1 ± 2.2 years old, slightly older than, but statistically identical to, the know sample age once expanded standard uncertainty was accounted for; model-dates ranged from 12 May, 1956 to 8 October, 1958. Model-age results for individual trials, average model-ages, and paper age of NBL U020 are plotted in Figure 5.3 along with associated uncertainties. Data used to calculate the model-ages are summarized in Table D.1 and Table D.2 for PIE and standard filaments, respectively.

5.3.3 U050

Stock material used for the production of NBL U050 was reported to have been removed from the enrichment cascade on 4 October, 1957 [141] and purified between 7 October, 1957 and 7 November, 1957 [142] making the paper age of this material approximately 56.6 years older than the reference date. Previous age determinations of U050 conducted using MC-ICP-MS have reported model-dates spanning from 9 March, 1956 to 19 October, 1957 [142, 143]; The slight, positive age bias reported in [142, 143] were attributed to incomplete initial separation resulting in trace amounts of residual ^{230}Th being present in the stock material. The model-ages determined for U050 samples analyzed during the present investigation were found to be substantially older than both

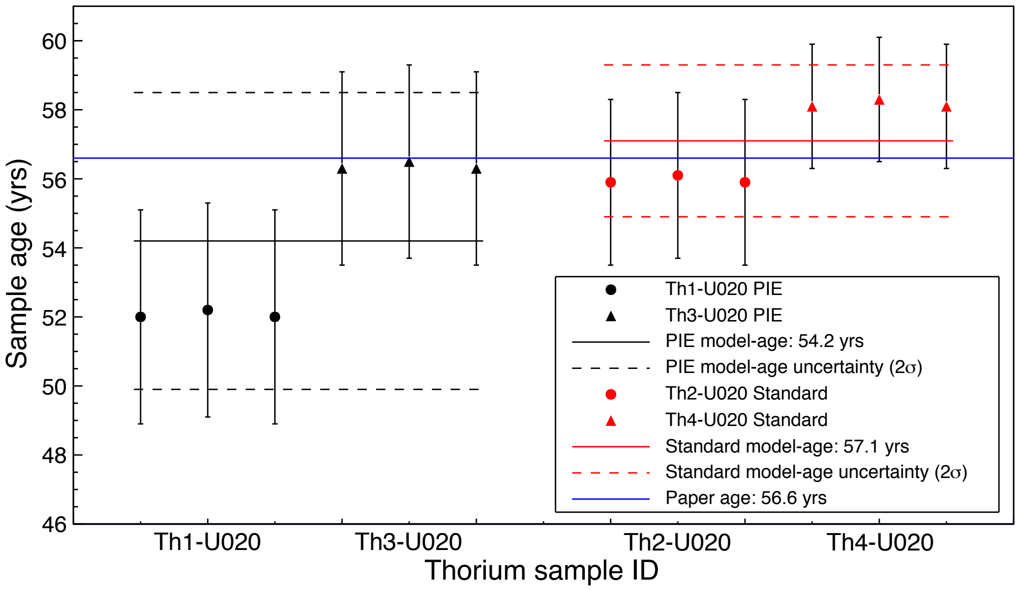

Figure 5.3: U020 Model-age results obtained using PIE and standard filaments with associated uncertainties. Reported uncertainty in model-ages are two standard deviations of the population.

the known age and previously reported age values; an approximately fifteen years positive age bias, on average, was observed. Standard and PIE filaments rendered model-dates spanning 21 January, 1941 to 15 March, 1942 and 11 November, 1941 to 12 May, 1944, respectively. Despite the significant bias, PIE and standard filaments rendered average model-ages that were statistically identical as illustrated in Figure 5.4. Also shown in Figure 5.4 are the results of individual trials and the paper age of U050. Reported uncertainties in model-are are at the 2σ level, where σ is the standard deviation of the population. Due to the large discrepancy of model-ages obtained during this work and those reported previously by multiple independent laboratories, we conclude

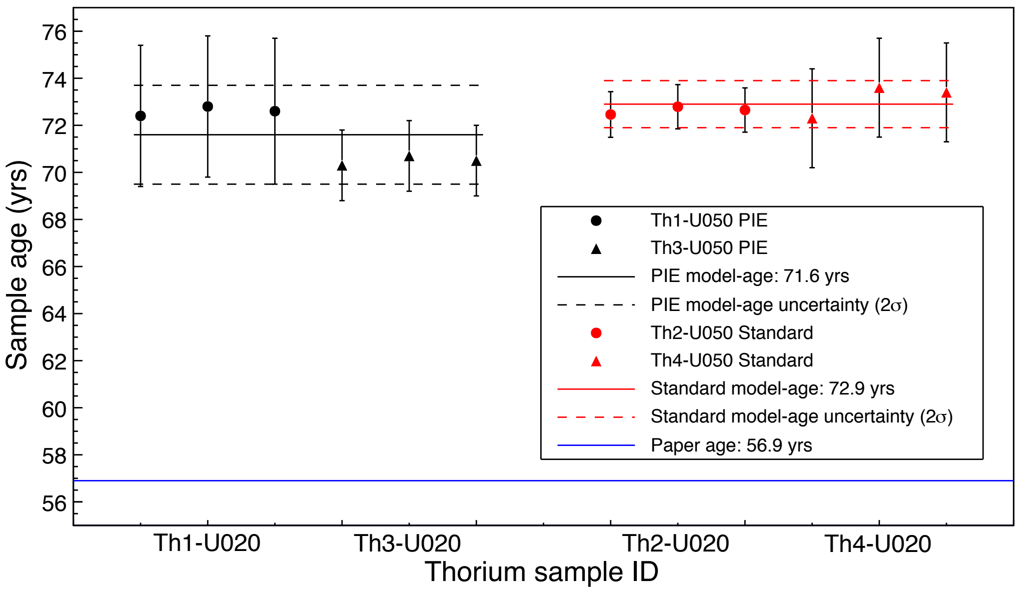

Figure 5.4: Model-age results of U050 using PIE and traditional filaments. Reported uncertainty in model-ages are two standard deviations of the population.

that this significant positive bias can be attributed to error(s) in thorium sample preparation. Possible sources of the significant positive bias include transcription errors (e.g., misweighing or mislabeling of the thorium stock) or the introduction of ^{230}Th to the stock solution; the source of "contamination" is not known at this time. Contamination from natural thorium is an unlikely culprit as the concentration of ^{232}Th in this sample is not systematically higher than any other sample analyzed during this study. Measurement data acquire for the age determination of U050 using PIEs and standard single filament assemblies can be found in Tables D.3 and D.4, respectively, located in Appendix D.

5.3.4 U100

Purification of the stock material used to make NBL U100 was reported to have been completed on 8 January, 1959 [135]. In previous work, Williams and Gaffney investigated the model-age of U100 using using the ^{230}Th/^{234}U chronometer, samples were analyzed via high resolution MC-ICP-MS. Model-dates were reported to be 16 February, 1959 and 6 March, 1959 [135]. These results are in excellent agreement with the reported purification date of 8 January, 1959, within analytical uncertainty. In the present investigation model-dates were determined to be 18 October, 1955 and 26 January, 1957 using PIE and standard filaments, respectively. The determined model-dates translate to material model-ages of 58.9 ± 1.2 and 57.59 ± 0.64 years; older than the reported age of U100, 55.6 years, by amounts greater than the expanded uncertainty, reported at the 2σ, where σ is the standard deviation of the population. On average, a two-and-a-half years year positive bias in material age was observed. Model-ages of U100 obtained during this study using PIE and traditional TIMS filaments were statistically identical. Figure 5.5 shows the reported material age, model-age results for individual trials, and average model-ages determined using PIEs and standard filaments along with associated uncertainties. The relatively large uncertainties associate with PIE trials are a result of poor counting statistics;

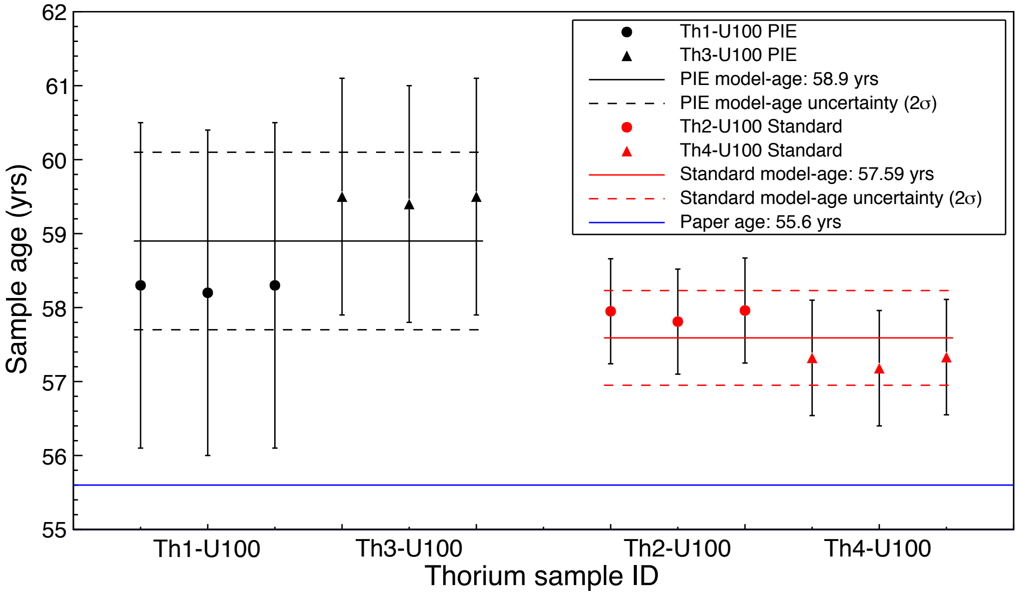

Figure 5.5: U100 model-ages determined using PIE and standard single filaments. Reported uncertainty in model-ages are two standard deviations of the population.

PIE sources were analyzed at an ion, $^{229}\text{Th}^{+}$, count rate of 3000 cps whereas traditional filaments trials were conducted at a count rate of 10 000 cps. Because of ion beam stability issues encountered in U020 and U050 trials using PIE sources no attempts at increasing ion beam intensity above 3000 cps were made during the investigation of U100. Model-age data and results for individual trials determined using PIE traditional filaments are listed in Tables D.5 and D.6, respectively, located in Appendix D.

5.3.5 U200

The data that purification of the stock material used to make NBL U200 was completed was not reported; therefore, the age of the material was calculated using 4 November, 1957, the date the stock was retrieved from the enrichment cascade at K-25 [141]. Assuming that the purification was completed near the date the material was retrieved from the K-25 enrichment cascade, we can estimate that the stock material is 56.8 years older than the 31 August, 2014 reference data. On average, samples analyzed using PIEs rendered model-ages of 56.3 ± 1.8 years, which corresponds to a model-date of 7 May, 1958. Thorium samples analyzed using traditional filaments yielded an average model-age of 57.1 ± 2.8 years old, this translates to a model-date of 12 July, 1957. After accounting for uncertainty, both standard and PIE filament analysis rendered average model-age results that were concordant with the paper age of U200. Individual trial results with associated uncertainties are plotted in Figure 5.6. Despite being in excellent agreement with the *known* material age, it is impossible to guarantee the accuracy of these results without knowing the actual purification date of the material used to make U200. Data used to calculate model-dates can be found in Appendix D. Data obtained using PIE and standard filaments are summarized in Table D.7 and Table D.8, respectively.

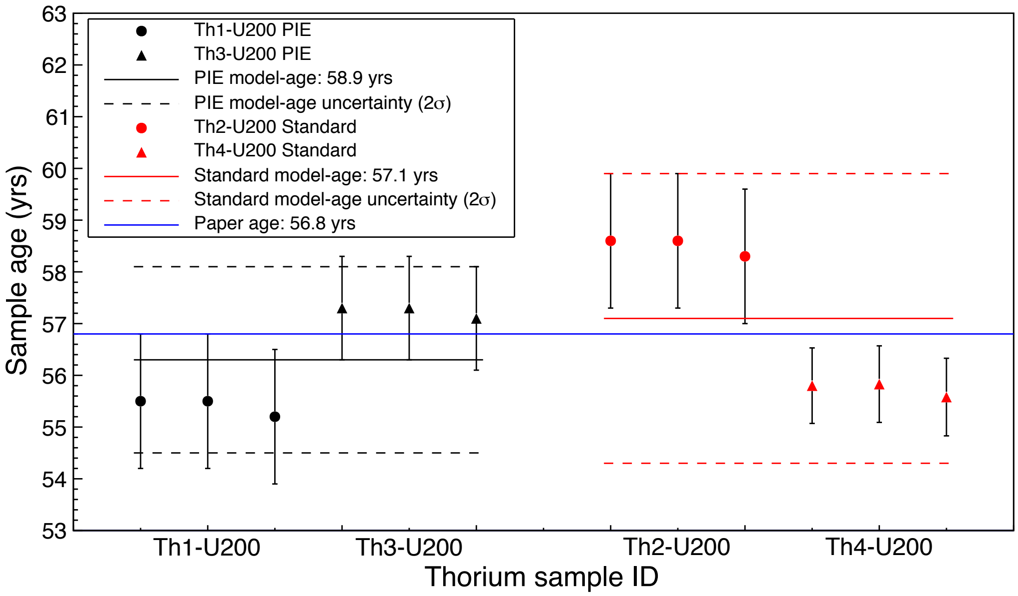

Figure 5.6: Model-age results of U200 determined using PIEs and traditional filaments. Reported uncertainty in model-ages are two standard deviations of the population.

5.4 Future work

The addition of H_3PO_4 appears to have a profound effect on a PIEs ability to generate and maintain a stable ion beam at higher count rates, >3000 cps for the thorium mass loading levels investigated during this study. To date, thorium analyses have never been conducted at such small quantities using PIEs; 30 pg mass loadings atop PIE filaments are the smallest quantity of thorium tested [10]. This is approximately one hundred times the size of thorium samples samples tested in this study. Ionization efficiency measurements described by Stanley et al. need to be extended to include femtogram mass loading levels to test the viability of PIE techniques at such low thorium mass loading levels.

The initial trials detailed in this paper were conducted using uranium isotopic standards; chronometric investigations are not the intended purpose of such samples. The ^{230}Th/^{234}U chronometer is highly sensitive to initial purification/purity of material, a decontamination factor of greater than 10^7 is required to eliminate positive bias caused by residual ^{230}Th in the material [14]. Future trials would greatly benefit from the implementation of certified uranium chronometric standards, which are highly purified and have precise, well-documented purification dates. Chronometric standards are necessary to truly determine the robustness of an age dating strategy. The development of such uranium standards have been described [13, 144] and preliminary trials have been conducted [14].

The ability to correct isotopic ratios for thermally induced fractionation, detailed in Chapter 4 of this work, is vital to attain high precision isotope ratios; this is especially important for ion counting methods. The fractionation behavior of thorium atop PIEs has yet to be investigated and is not known at this time. Unfortunately, such an investigation requires a well-characterized thorium isotopic standard for instrumental mass bias corrections suitable for TIMS that is not currently available.

5.5 Conclusions

The model-ages of four NBL certified uranium isotopic standards were determined using the ^{230}Th/^{234}U radiochronometer. Thorium isotope ratio measurements were conducted using standard single filaments and PIEs as TIMS sources.

The only samples to yield model-ages that were concordant, within analytical uncertainty, with the reported material ages were NBL U020, analyzed using traditional filaments, and NBL U200 analyzed using PIEs. Despite PIEs exhibiting enhanced ionization efficiencies relative to traditional filaments during the analyses of trace levels of thorium [10], findings herein suggest that, under the analytic conditions employed during this study, PIEs were unable to provide the anticipated improvements in thorium isotope measurements. Based on the results we can conclude that the thorium sample preparation method outlined in this paper is not suitable for analysis with PIEs and requires modification.

Chapter 6

Lead analysis using PIEs

6.1 Introduction

Lead isotopic signatures, commonly referred to as “fingerprints”, using the stable isotopes of lead can provide useful information for nuclear forensic analyses. Lead is composed of four stable isotopes; ^{204}Pb, ^{206}Pb, ^{207}Pb, and ^{208}Pb. Only ^{204}Pb is entirely primordial and nonradiogenic, being produced exclusively by s-process nucleosynthesis in stars. The remaining three isotopes are the end products of the ^{238}U (4n + 2; the Uranium or Radium Series), ^{235}U (4n + 3; the Actinium Series) and ^{232}Th (4n; the Thorium Series) decay chains, respectively. Large differences in half-lives coupled with natural variations of uranium and thorium isotopic composition based on global position have resulted in ore deposits with distinct lead signatures based on geolocation. Determination of geographic origin of uranium samples based on lead signatures have previously been demonstrated [16–22]. Signatures from anthropogenic lead (i.e., lead produced from fossil fuel combustion such as industrial processes and automobile exhaust) can also provide additional information about geographic origin as the isotopic composition will be different from that of naturally occurring deposits. Due to the relevance of lead isotopic signatures to the field of nuclear forensics, preliminary experiments were conducted to investigate the efficacy of PIE techniques for enhanced analysis of lead via TIMS.

6.2 Materials, methods, and insturmentation

A detailed description of PIE stock preparation can be found in 3.2.1. Standard and PIE filaments were pretreated and prepared by the methods described in 3.2.1 of this work. All isotopic measurements were conducted using an Isoprobe-T™ from GV Instruments Ltd. (now Isotopx: Middlewich, Cheshire; UK); specifications and tuning of this mass spectrometer are located in 3.2.3.

6.2.1 Preparation of silica gel

Silica gel was prepared by the hydrolysis of silicon tetrachloride $SiCl_4$ (Sigma Aldritch; St. Louis, MO) with 18 MΩ DI water. This reaction was carried out in a clean teflon vessel equipped with pressure relief valve; a 3-to-1 ratio of water to $SiCl_4$ was found to produce the most desirable results. A hot plate was used to gently heat the vessel in order to expedite the reaction, limiting the possibility of the silica get being contaminated. The resulting colloidal silica gel solution was sonicated for approximately ten minutes to break down larger particles and then allowed to settle overnight prior to use. Silica gel for sample loading was decanted from the top of the bulk solution; this was done to ensure that only the smallest silica gel particles were used in order to maximize the analyte-to-silica gel interaction.

6.2.2 Sample loading

Samples were loaded atop PIE and traditional filaments as an aqueous solution of 1 M HNO_3 containing 5 ng of SRM-981 common lead isotopic standard. The certificate for SRM-981 can be found in Appendix E. The samples were evaporated to dryness by running 1 A current through the filament. Silica gel (approximately 1 µL) was carefully pipetted over the top of each dried sample followed by a drop of 0.3 M H_3PO_4. The current applied to the filament was then slowly raised to 2 A in order to fume off the H_3PO_4 and dry the silica gel to roughly the color of bone china. All filaments were affixed to a sample turret which, in turn, was mounted in the mass spectrometer source housing.

6.3 Results

Traditional and PIE filaments were run side-by-side for direct comparison of performance. Traditional filaments performed as expected, generating steady ion beams for thirty minutes or longer; samples were not run to exhaustion. Filaments equipped with PIEs, on the other hand, were unable to reach the set ion beam aiming intensity and consistently failed within the first minute of analysis. After careful consideration, it is believed that, despite painstaking efforts to minimize the size of the particles in the silica gel, the addition of silica gel over the top of the PIE clogged the pores, trapping the majority of the sample within the porous structure of the PIEs. This theory could be tested by dissolving the filament, isolating the remaining lead and reanalyzing via the standard TIMS filamnts; however, due to time restrictions, we were unable to perform such analyses. We can conclude from this investigation that thebso-called silica gel technique used in conjunction with PIE filaments in the manner described herein is not a suitable the analysis of lead samples

Chapter 7

Conclusions

This work, project number LA13-FY13-123-PD08 entitled “Improved sample utilization in TIMS isotopic ratio measurements via refined development and application of porous ion emitters”, was conducted under the auspices of the DOEs NNSA Office of Proliferation Detection Research & Development (NA-22). The overarching theme of the research presented in this dissertation is the development of capabilities to bolster the current set of mass spectrometric techniques employed to detect useful nuclear forensic signatures using PIEs as TIMS ionization sources. Moreover, this work was designed to address the need for state-of-the-art mass spectrometric techniques that exhibit enhanced ionization efficiency during isotope ratio measurements. Specific objectives of this work included: 1) expanding the use of PIEs as TIMS sources for the isotopic analysis of samples contain trace quantities of actinides (see Chapter 3), 2) refine composition and preparation procedures for manufacturing PIEs to further enhance actinide ionization efficiency, thus reducing the sample quantity necessary to successfully obtain isotopic information (see Chapter 3), and 3) capitalize on the improved ionization efficiency associated with PIEs use for improved chronometric capabilities to address current challenges in uranium chronometry (detailed in Chapters 4 and 5). The series of investigations described herein were carefully designed to determine the viability of PIE sources for enhancing chronometric investigations of young materials with extreme parent/daughter ratios. In order to accomplish this, enhanced sample utilization and isotopic fractionation behavior of actinides associated with PIEs were studied in depth. A brief summary of each research component performed is presented below.

Americium and plutonium ionization efficiency. PIE techniques consistently demonstrated substantial improvements in sample utilization during the analyses of americium and plutonium in the 1–100 pg mass loading range when compared to traditional TIMS ion sources. The list of actinides successfully analyzed via PIE techniques include americium, plutonium, uranium, and thorium. Additional enhancements in ionization efficiency were observed during the analysis of 10 pg plutonium samples using a new type of PIE constricted completely from platinum. These preliminary trials suggest PIEs constructed of 100 % platinum may prove superior to Pt/Re PIEs for analyses of lower vapor pressure actinides (e.g., plutonium and americium). Further investigations using platinum PIEs should be conducted that include a wider range of plutonium sample mass loadings as well as applying them to americium analyses.

Fractionation of uranium and plutonium. The ability to make precise and accurate isotope ratio measurements (e.g., sample age-dating) is highly contingent on the ability to correct for the effects of mass fractionation. The extent of fractionation effects using PIEs as thermal ion sources was evaluated using plutonium and uranium isotope reference standard. Once corrected for mass fractionation using the appropriate law, the measured isotope ratio values are in excellent agreement with the certificate values. The Linear and Exponential laws were determined to provide the most accurate description of the isotopic fractionation behavior of plutonium and uranium, respectively.

Model-age determination of uranium isotopic standards. The determination of the model-ages of four distinct uranium isotopic standards, of varying enrichment, were determined using the ^{230}Th/^{234}U radiochronometer. Uranium isotope ratio measurements were carried out using triple filament assemblies. PIEs were used for thorium isotope ratio measurements; thorium measurements were also conducted using traditional filaments for a side-by-side comparison. Under the experimental conditions used in this study, the anticipated enhancement in thorium isotopic ratio measurements using PIEs were not realized. Theses results, while unexpected, lead to the conclusion that the methods for thorium sample preparation employed during this investigation requires modification for use with PIE techniques.

Bibliography

[1] S. Bürger, L. R. Riciputi, D. A. Bostick, S. Turgeon, E. H. McBay, and M. Lavelle, "Isotope ratio analysis of actinides, fission products, and geolocators by high-efficiency multi-collector thermal ionization mass spectrometry," *International Journal of Mass Spectrometry*, vol. 286, no. 2, pp. 70–82, 2009. 2, 13, 16, 28, 38, 40, 43, 53, 54, 65, 75, 79

[2] R. L. Edwards, J. H. Chen, and G. J. Wasserburg, "^{238}U–^{234}U–^{230}Th–^{232}Th systematics and the precise measurement of time over the past 500,000 years," *Earth and Planetary Science Letters*, vol. 81, no. 2, pp. 175–192, 1987. 2, 9, 16, 28, 40, 59, 77, 90, 115, 117

[3] D. M. Wayne, W. Hang, D. K. McDaniel, R. E. Fields, E. Rios, and V. Majidi, "The thermal ionization cavity (TIC) source: elucidation of possible mechanisms for enhanced ionization efficiency," *International Journal of Mass Spectrometry*, vol. 216, no. 1, pp. 41–57, 2002. 6, 51, 52, 59, 66, 75, 77, 80, 90

[4] G. Wasserburg, S. Jacousen, D. DePaolo, M. McCulloch, and T. Wen, "Precise determination of Sm/Nd ratios, Sm and Nd isotopic abundances in standard solutions," *Geochimica et Cosmochimica Acta*, vol. 45, no. 12, pp. 2311–2323, 1981. 8, 91, 97, 121

[5] G. Cavazzini, "Rayleigh's distillation law and linear hypothesis of isotope fractionation in thermal ionization mass spectrometry," *International Journal of Mass Spectrometry*, vol. 288, no. 1, pp. 84–91, 2009. 91, 99

[6] S. R. Hart and A. Zindler, "Isotope fractionation laws: a test using calcium," *International journal of mass spectrometry and ion processes*, vol. 89, no. 2, pp. 287–301, 1989. 91

[7] W. Russell, D. Papanastassiou, and T. Tombrello, "Ca isotope fractionation on the Earth and other solar system materials," *Geochimica et Cosmochimica Acta*, vol. 42, no. 8, pp. 1075–1090, 1978. 91, 97

[8] A. Eberhardt, R. Delwiche, and J. Geiss, "Isotopic effects in single filament thermal ion sources," *Zeitschrift für Naturforschung A*, vol. 19, no. 6, pp. 736–740, 1964. 8, 91

[9] M. G. Watrous and J. E. Delmore, "Measurement of trace uranium isotopes using a porous ion emitter," *International Journal of Mass Spectrometry*, vol. 303, no. 1, pp. 1–5, 2011. 8, 28, 33, 56, 66, 67, 92, 126

[10] F. E. Stanley, K. J. Spencer, D. S. Schwartz, M. G. Watrous, and J. E. Delmore, “Investigating enhanced thorium ionization in TIMS using Re/Pt porous ion emitters,” *Journal of Radioanalytical and Nuclear Chemistry*, vol. 299, no. 3, pp. 1447–1452, 2014. xxi, 8, 10, 28, 56, 58, 59, 66, 67, 83, 84, 117, 125, 126, 137, 139

[11] F. E. Stanley, “A beginner’s guide to uranium chronometry in nuclear forensics and safeguards,” *Journal of Analytical Atomic Spectrometry*, vol. 27, no. 11, pp. 1821–1830, 2012. 9, 114

[12] K. J. Moody, P. M. Grant, and I. D. Hutcheon, *Nuclear forensic analysis*. CRC Press, 2 ed., 2014. 9, 114

[13] Z. Varga, A. Nicholl, M. Wallenius, and K. Mayer, “Development and validation of a methodology for uranium radiochronometry reference material preparation,” *Anal. Chim. Acta*, vol. 718, pp. 25–31, Mar. 2012. 9, 114, 138

[14] Z. Varga, K. Mayer, C. Bonamici, A. Hubert, I. Hutcheon, W. Kinman, M. Kristo, F. Pointurier, K. Spencer, F. Stanley, *et al.*, “Validation of reference materials for uranium radiochronometry in the frame of nuclear forensic investigations,” *Applied Radiation and Isotopes*, vol. 102, pp. 81–86, 2015. 9, 115, 138

[15] S. P. LaMont and G. Hall, “Uranium age determination by measuring the ^{230}Th/^{234}U ratio,” *Journal of Radioanalytical and Nuclear Chemistry*, vol. 264, no. 2, pp. 423–427, 2005. 9, 115

[16] J. Švedkauskaitė-LeGore, *Development and validation of a method for origin determination of uranium-bearing material.* PhD thesis, University of Vilnius, Vilnius, Lithuania, 2007. 11, 141

[17] J. Švedkauskaitė-LeGore, G. Rasmussen, S. Abousahl, and P. van Belle, “Investigation of the sample characteristics needed for the determination of the origin of uranium-bearing materials,” *Journal of Radioanalytical and Nuclear Chemistry*, vol. 278, no. 1, pp. 201–209, 2008.

[18] E. Keegan, S. Richter, I. Kelly, H. Wong, P. Gadd, H. Kuehn, and A. Alonso-Munoz, “The provenance of australian uranium ore concentrates by elemental and isotopic analysis,” *Applied Geochemistry*, vol. 23, no. 4, pp. 765–777, 2008.

[19] Z. Varga, M. Wallenius, K. Mayer, E. Keegan, and S. Millet, "Application of lead and strontium isotope ratio measurements for the origin assessment of uranium ore concentrates," *Analytical Chemistry*, vol. 81, pp. 8327–8334, Oct. 2009.

[20] A. Fahey, N. Ritchie, D. Newbury, and J. Small, "The use of lead isotopic abundances in trace uranium samples for nuclear forensics analysis," *Journal of Radioanalytical and Nuclear Chemistry*, vol. 284, no. 3, pp. 575–581, 2010.

[21] E. Keegan, M. J. Kristo, M. Colella, M. Robel, R. Williams, R. Lindvall, G. Eppich, S. Roberts, L. Borg, A. Gaffney, *et al.*, "Nuclear forensic analysis of an unknown uranium ore concentrate sample seized in a criminal investigation in Australia," *Forensic Science International*, vol. 240, pp. 111–121, 2014.

[22] M. J. Kristo, E. Keegan, M. Colella, R. Williams, R. Lindvall, G. Eppich, S. Roberts, L. Borg, A. Gaffney, J. Plaue, *et al.*, "Nuclear forensic analysis of uranium oxide powders interdicted in Victoria, Australia," *Radiochimica Acta*, vol. 103, no. 7, pp. 487–500, 2015. 11, 141

[23] E. L. Callis and R. M. Abernathey, "High-precision isotopic analyses of uranium and plutonium by total sample volatilization and signal integration," *International Journal of Mass Spectrometry and Ion Processes*, vol. 103, no. 2, pp. 93–105, 1991. 14, 61, 96, 120

[24] S. Richter, H. Kühn, Y. Aregbe, M. Hedberg, J. Horta-Domenech, K. Mayer, E. Zuleger, S. Bürger, S. Boulyga, J. Köpf, A. Poths, and K. Mathew, "Improvements in routine uranium isotope ratio measurements using the modified total evaporation method for multi-collector thermal ionization mass spectrometry," *Journal of Analytical Atomic Spectrometry*, vol. 26, no. 3, pp. 550–564, 2011. 14, 61

[25] J. D. Fassett and W. R. Kelly, "Interlaboratory isotopic ratio measurement of nanogram quantities of uranium and plutonium on resin beads by thermal ionization mass spectrometry," *Analytical Chemistry*, vol. 56, no. 3, pp. 550–556, 1984. 14

[26] A. O. Nier, "The isotopic constitution of uranium and the half-lives of the uranium isotopes. I," *Physical Review*, vol. 55, no. 2, p. 150, 1939. 15

[27] T. Walczyk, "TIMS versus multicollector-ICP-MS: coexistence or struggle for survival?," *Analytical and bioanalytical chemistry*, vol. 378, no. 2, pp. 229–231, 2004. 15

[28] T. B. Coplen, "Atomic weights of the elements 1999," *Journal of Physical and Chemical Reference Data*, vol. 30, no. 3, pp. 701–712, 2001. 15

[29] F. Guthrie, "XXXI. On a relation between heat and static electricity," *Philosophical Magazine Series 4*, vol. 46, no. 306, pp. 257–266, 1873. 16

[30] O. W. Richardson, *The Emission of Electricity from Hot Bodies*. Longmans, Green and Company, 1921. 16

[31] A. J. Dempster, "A new method of positive ray analysis," *Physical Review*, vol. 11, no. 4, pp. 316–325, 1918. xvii, 16, 17

[32] F. A. White, "Multiple Cartridge Source for Mass Spectrometer," July 1956. US Patent 2,756,341. 19

[33] W. H. Christie and A. E. Cameron, "Reliable Sample Changer for Mass Spectrometer," *The Review of Scientific Instruments*, vol. 37, no. 3, pp. 336–337, 1966. 19

[34] K. Ingeneri, L. Riciputi, and P. Hedberg, "Preliminary results of uranium and plutonium efficiency measurements using a high efficiency cavity ion source interfaced with a Finnigan MAT 262 mass spectrometer," in *Proceedings of the Institute of Nuclear Materials Management*, pp. 24–27, 2002. xix, 20, 53

[35] L. R. Riciputi, K. B. Ingeneri, and P. M. L. Hedberg, "Advances in destructive and non-destructive analysis for environmental monitoring and nuclear forensics," in *Conference Proceeding IAEA-CN-98 P*, vol. 25, p. 347, 2003. 20, 28, 52, 53, 54

[36] D. Tuttas, J. Schwieters, N. Quaas, and C. Bouman, "Improvements in tims high precision isotope improvements in TIMS high precision isotope ratio measurements for small sample size," Tech. Rep. Application Note: 30136, Thermo Fisher Scientific, 2007. xvii, 22

[37] I. Langmuir and K. H. Kingdon, "Thermionic effects caused by vapours of alkali metals," *Proceedings of the Royal Society of London. Series A*, vol. 107, no. 741, pp. 61–79, 1925. 22

[38] M. Saha, “LIII. Ionization in the solar chromosphere,” *Philosophical Magazine Series 6*, vol. 40, no. 238, pp. 472–488, 1920. 22

[39] M. Saha, “On a physical theory of stellar spectra,” *Proceedings of the Royal Society of London. Series A*, vol. 99, no. 697, pp. 135–153, 1921. 22

[40] NIST, “Boltzmann constant in eV/K; `http://physics.nist.gov/cgi-bin/cuu/Value?tkev`.” 23

[41] C. Barshick, D. Duckworth, and D. Smith, *Inorganic Mass Spectrometry: Fundamentals and Applications*. CRC Press, Feb. 2000. 24

[42] H. Kawano, “Mean work functions effective for negative-ionic, electronic and positive-ionic emissions from polycrystalline surfaces,” *Applied Surface Science*, vol. 252, pp. 5233–5242, May 2006. xiv, 25, 82

[43] H. Kawano, “Effective work functions for ionic and electronic emissions from mono- and polycrystalline surfaces,” *Progress in Surface Science*, vol. 83, pp. 1–165, Feb. 2008. 25

[44] J. A. McHugh, “Surface ionization—the rhenium V-type single filament,” *International Journal of Mass Spectrometry and Ion Physics*, vol. 3, no. 3, pp. 267–276, 1969. xviii, 26, 36

[45] W. D. Davis, “Continuous mass spectrometric analysis of particulates by use of surface ionization,” *Environmental Science & Technology*, vol. 11, no. 6, pp. 587–592, 1977. 25, 47

[46] N. Sasaki, K. Kubo, and M. Asano, “A graphite filament method for improving the emission efficiency of U+ ions,” *Journal of Physics E: Scientific Instruments*, vol. 7, no. 5, p. 386, 1974. 27

[47] R. E. Perrin, G. W. Knobeloch, V. M. Armijo, and D. W. Efurd, “Isotopic analysis of nanogram quantities of plutonium by using a SID ionization source,” *International journal of mass spectrometry and ion processes*, vol. 64, no. 1, pp. 17–24, 1985. 28, 44, 49, 50

[48] Previous work done in-house at LANL. 28, 40

[49] D. J. Rokop, R. E. Perrin, G. W. Knobeloch, V. M. Armijo, and W. R. Shields, “Thermal ionization mass spectrometry of uranium with electrodeposition as a loading technique,” *Analytical Chemistry*, vol. 54, no. 6, pp. 957–960, 1982. 28, 50

[50] N. C. Fenner, "A method of increasing the production of uranium ions in a mass spectrometer source," *Journal of Scientific Instruments*, vol. 41, no. 1, p. 48, 1964. 28, 36, 41

[51] J. H. Chen and G. J. Wasserburg, "Isotopic determination of uranium in picomole and subpicomole quantities," *Anal. Chem.;(United States)*, vol. 53, no. 13, 1981. 28, 37

[52] S. J. Goldstein, M. T. Murrell, and D. R. Janecky, "Th and U isotopic systematics of basalts from the Juan de Fuca and Gorda Ridges by mass spectrometry," *Earth and Planetary Science Letters*, vol. 96, no. 1, pp. 134–146, 1989. 28, 33

[53] K. H. Rubin, "Analysis of ^{232}Th/^{230}Th in volcanic rocks: a comparison of thermal ionization mass spectrometry and other methodologies," *Chemical Geology*, vol. 175, pp. 723–750, June 2001. 28, 40

[54] M. H. Huyskens, T. Iizuka, and Y. Amelin, "Evaluation of colloidal silicagels for lead isotopic measurements using thermal ionisation mass spectrometry," *Journal of Analytical Atomic Spectrometry*, vol. 27, no. 9, pp. 1439–1446, 2012. 28, 46, 47

[55] *Alternative Sample Loading Preparation for Thermal Ionization Mass Spectrometry*, 2015. xviii, 30

[56] M. G. Inghram and W. A. Chupka, "Surface ionization source using multiple filaments," *Review of Scientific Instruments*, vol. 24, no. 7, pp. 518–520, 1953. 31

[57] R. Thomas, "Mass spectrometry." Radiochemistry Webinars. xviii, 32

[58] H. W. Wilson and N. R. Daly, "Mass spectrometry of solids," *J. Sci. Instrum.*, vol. 40, p. 273, June 1963. 33

[59] J. E. Delmore, A. D. Appelhans, and J. E. Olson, "Self imaging of surface ionization ion sources—where do the ions come from?," *International Journal of Mass Spectrometry and Ion Processes*, vol. 140, no. 1, pp. 111–122, 1994. 33

[60] H. Patterson and H. W. Wilson, "New mass spectrometer solid source arrangement for the simultaneous analysis of two samples," *Journal of Scientific Instruments*, vol. 39, no. 2, p. 84, 1962. 34

[61] F. A. White, T. L. Collins, and F. M. Rourke, “Search for possible naturally occurring isotopes of low abundance,” *Physical Review*, vol. 101, no. 6, p. 1786, 1956. 34

[62] T. Prohaska, J. Irrgeher, A. Zitek, and N. Jakubowski, *Sector Field Mass Spectometry for Elemental and Isotopic Analysis*. Royal Society of Chemistry, 2014. xix, 35

[63] L. A. Dietz, “Ion Optics for the V-Type Surface Ionization Filament Used in Mass Spectrometry,” *Review of Scientific Instruments*, vol. 30, no. 4, pp. 235–241, 1959. 36

[64] J. J. Stoffels and C. R. Lagergren, “Fabrication of V-type filaments for surface ionization mass spectrometry,” *International journal of mass spectrometry and ion processes*, vol. 55, no. 2, pp. 217–219, 1984. 37

[65] T. M. Esat, D. E. Brownlee, D. A. Papanastassiou, and G. J. Wasserburg, “Magnesium isotopic composition of interplanetary dust particles,” *Science*, vol. 206, no. 4415, pp. 190–197, 1979. 37

[66] T. M. Esat, “Charge collection thermal ion mass spectrometry of thorium,” *International journal of mass spectrometry and ion processes*, vol. 148, no. 3, pp. 159–170, 1995. 37

[67] D. H. Smith, “Mass Spectrometric Investigation of Surface Ionization. X. Desorption of Uranium Ions and Neutrals from Carburized Rhenium,” *The Journal of Chemical Physics*, vol. 55, no. 8, pp. 4152–4154, 1971. 39, 41

[68] J. M. Kelley and D. M. Robertson, “Plutonium ion emission from carburized rhenium mass spectrometer filaments,” *Analytical Chemistry*, vol. 57, no. 1, pp. 124–130, 1985. 39, 40

[69] P. G. Pallmer, R. L. Gordon, and M. J. Dresser, “The emissivity of carburized rhenium,” *Journal of Applied Physics*, vol. 51, no. 3, pp. 1798–1801, 1980. 41, 42

[70] M. H. Studier, E. N. Sloth, and L. P. Moore, “The chemistry of uranium in surface ionization sources,” *The Journal of Physical Chemistry*, vol. 66, no. 1, pp. 133–134, 1962. 39, 40

[71] M. G. Watrous, J. E. Delmore, and M. L. Stone, “Porous ion emitters – A new type of thermal ion emitter,” *International Journal of Mass Spectrometry*, vol. 296, no. 1, pp. 21–24, 2010. 44, 56, 58, 71, 82, 94, 125

[72] R. Jakopič, S. Richter, H. Kühn, and Y. Aregbe, "Isotope ratio measurements of pg-size plutonium samples using tims in combination with "multiple ion counting" and filament carburization," *International Journal of Mass Spectrometry*, vol. 279, no. 2, pp. 87–92, 2009. 39

[73] M. H. Kakazu, N. M. P. Moraes, S. S. Iyer, and C. Rodrigues, "Reduction of oxide ions of uranium in single-filament surface-ionization mass spectrometry with application to rock samples," *Analytica Chimica Acta*, vol. 132, pp. 209–213, 1981. 39, 40

[74] M. G. Watrous and J. E. Delmore, "Metal dicarbides as intermediate species in thermal ion formation mechanisms," *International Journal of Mass Spectrometry*, vol. 286, no. 1, pp. 7–10, 2009. 39, 40, 41

[75] M. T. M. S. J. Goldstein, "Th and U isotopic systematics of basalts from the Juan de Fuca and Gorda Ridges by mass spectrometry," *Earth and Planetary Science Letters*, pp. 134–146, 1989. 40

[76] M. Kraiem, K. Mayer, T. Gouder, A. Seibert, T. Wiss, H. Thiele, and J.-P. Hiernaut, "Experimental investigation of the ionization mechanisms of uranium in thermal ionization mass spectrometry in the presence of carbon," *International Journal of Mass Spectrometry*, vol. 289, no. 2, pp. 108–118, 2010. 40, 41

[77] M. Kraiem, K. Mayer, T. Gouder, A. Seibert, T. Wiss, and J.-P. Hiernaut, "Filament chemistry of uranium in thermal ionisation mass spectrometry," *Journal of Analytical Atomic Spectrometry*, vol. 25, no. 7, pp. 1138–1144, 2010. 40

[78] P. G. Pallmer, R. L. Gordon, and M. J. Dresser, "The work function of carburized rhenium," *Journal of Applied Physics*, vol. 51, no. 7, pp. 3776–3779, 1980. 42

[79] R. L. Gordon, "Kinetics of the surface ionization of plutonium on carburized rhenium," *International Journal of Mass Spectrometry and Ion Processes*, vol. 55, no. 1, pp. 31–46, 1983. 41

[80] D. H. Smith and J. A. Carter, "A simple method to enhance thermal emission of metal ions," *International Journal of Mass Spectrometry and Ion Physics*, vol. 40, no. 2, pp. 211–215, 1981. 42, 44

[81] R. W. Gurney, "Theory of Electrical Double Layers in Adsorbed Films," *Phys. Rev.*, vol. 47, pp. 479–482, Mar. 1935. 42

[82] D. H. Freeman, L. A. Currie, E. C. Kuehner, H. D. Dixon, and R. A. Paulson, "Development and characterization of ion-exchange bead microstandards," *Analytical Chemistry*, vol. 42, no. 2, pp. 203–209, 1970. 42

[83] R. L. Walker, R. E. Eby, C. A. Pritchard, and J. A. Carter, "Simultaneous plutonium and uranium isotopic analysis from a single resin bead-a simplified chemical technique for assaying spent reactor fuels," *Analytical Letters*, vol. 7, no. 8-9, pp. 563–574, 1974. 42, 43

[84] R. L. Walker, J. L. Botts, J. A. Carter, and D. A. Costanzo, "Mass Spectrometric Determination of Zirconium from a Resin Bead," *Analytical Letters*, vol. 10, no. 4, pp. 251–262, 1977. 42

[85] T. J. Anderson and R. L. Walker, "Determination of picogram amounts of technetium-99 by resin bead mass spectrometric isotope dilution," *Analytical Chemistry*, vol. 52, no. 4, pp. 709–713, 1980. 42

[86] K. O. Buesseler and J. E. Halverson, "The mass spectrometric determination of fallout ^{239}Pu and ^{240}Pu in marine samples," *Journal of environmental radioactivity*, vol. 5, no. 6, pp. 425–444, 1987. 43

[87] J. A. Carter, R. L. Walker, D. H. Smith, and W. H. Christie, "Isotope Dilution Resin Bead Mass Spectrometry—An Ultra Trace Technique for Measuring Nuclides in Three-Mile Island Water," *International Journal of Environmental Analytical Chemistry*, vol. 8, no. 4, pp. 241–248, 1980. 43

[88] D. H. Smith, W. H. Christie, and R. E. Eby, "The resin bead as a thermal ion source: A SIMS study," *International Journal of Mass Spectrometry and Ion Physics*, vol. 36, no. 3, pp. 301–316, 1980.

[89] J. A. Carter, R. L. Walker, R. E. Eby, and C. A. Pritchard, "Safeguarding Nuclear Materials," *IAEA-201/9*, vol. 11, p. 461, 1976. 43

[90] R. E. Perrin, D. J. Rokop, J. H. Cappis, and W. R. Shields, "Electro-Deposition as a Sample Mounting Technique for U and Pu Isotopic Analysis," in *Am. Soc. Mass Spectrom., Twenty-Ninth Annual Conf., Mass Spectrometry and Allied Topics, Minneapolis, Minnesota*, pp. 422–423, 1981. 44, 49

[91] P. A. Akishin, O. T. Nikitin, and G. M. Panchenkov, “A new effective ionic emitter for the isotopic analysis of lead,” *Geochemistry*, vol. 5, pp. 500–505, 1957. 45

[92] T. Huett, J. C. Ingram, and J. E. Delmore *International journal of mass spectrometry and ion processes*, vol. 146, pp. 5–14, 1995. 45, 47

[93] G. F. Kessinger, T. Huett, and J. E. Delmore, “Ag ion formation mechanisms in molten glass ion emitters,” *International Journal of Mass Spectrometry*, vol. 208, no. 1, pp. 37–57, 2001. 45

[94] G. F. Kessinger and J. E. Delmore, “High temperature chemistry of molten glass ion emitters,” *International Journal of Mass Spectrometry*, vol. 213, no. 1, pp. 63–80, 2002. 45, 47

[95] F. E. Stanley, A. M. Stalcup, and H. B. Spitz, “A brief introduction to analytical methods in nuclear forensics,” *Journal of Radioanalytical and Nuclear Chemistry*, vol. 295, no. 2, pp. 1385–1393, 2013. 45

[96] A. E. Cameron, D. H. Smith, and R. L. Walker, “Mass spectrometry of nanogram-size samples of lead,” *Analytical Chemistry*, vol. 41, no. 3, pp. 525–526, 1969. 45

[97] H. Gerstenberger and G. Haase, “A highly effective emitter substance for mass spectrometric Pb isotope ratio determinations,” *Chemical Geology*, vol. 136, no. 3, pp. 309–312, 1997. 46, 47

[98] Y. Koide and E. Nakamura, “Lead isotope analyses of standard rock samples,” *Journal of the Mass Spectrometry Society of Japan*, vol. 38, no. 5, pp. 241–252, 1990. 46

[99] S. Nohda, “Precise isotopic measurements of lead by fused silicagel,” *Geochemical journal: journal of the Geochemical Society of Japan*, vol. 33, pp. 133–139, 1999. 46

[100] T. Kani and S. Nohda, “Pb isotope analyses using bead method: Application to BCR-1 and GSJ standard rock samples,” *Journal of the Mass Spectrometry Society of Japan*, vol. 50, no. 4, pp. 199–203, 2002. 46

[101] T. Miyazaki, M. Yoshikawa, and T. Sakamoto, “Evaluation of silica-gel activator in order to find the optimal silica-gel activator for lead isotope measurement by thermal ionization mass spectrometer (TIMS),” *Frontier Research on Earth Evolution*, vol. 2. 47

[102] T. Miyazaki, T. Shibata, and M. Yoshikawa, "New synthesis method of silica-gel for lead isotope analysis," *Proceedings of the Japan Academy, Series B*, vol. 79, no. 2, pp. 58–62, 2003.

[103] S. Nohda, B. Wang, C. You, and R. Shinjo, "New supplemental activator for lead isotope analysis using TIMS," *Geochemical journal: journal of the Geochemical Society of Japan*, vol. 45, no. 2, pp. 169–174, 2011. 47

[104] I. D. Baikie, U. Petermann, A. Speakman, B. Lagel, K. M. Dirscherl, and P. J. Estrup, "Work function study of rhenium oxidation using an ultra high vacuum scanning Kelvin probe," *Journal of Applied Physics*, vol. 88, no. 7, pp. 4371–4375, 2000. 47

[105] W. G. Myers and F. A. White, "Diffusion-thermal ionization source for mass spectrometric assay of trace metals," *Analytical Chemistry*, vol. 41, no. 13, pp. 1861–1864, 1969. 48

[106] J. R. Rec, W. G. Myers, and F. A. White, "Diffusion controlled, thermal ionization source for mass spectrometric analysis of trace metals," *Analytical Chemistry*, vol. 46, no. 9, pp. 1243–1247, 1974. 48

[107] D. W. Efurd, J. Drake, F. R. Roensch, J. H. Cappis, and R. E. Perrin, "Measurement of neptunium-237 by SID ionization source," *International journal of mass spectrometry and ion processes*, vol. 74, no. 2, pp. 309–315, 1986. 50

[108] G. J. Beyer, E. Herrmann, A. Piotrowski, V. J. Raiko, and H. Tyrroff, "A new method for rare-earth isotope separation," *Nuclear Instruments and Methods*, vol. 96, no. 3, pp. 437–439, 1971. 50, 51

[109] P. G. Johnson, A. Bolson, and C. M. Henderson, "A high temperature ion source for isotope separators," *Nuclear Instruments and Methods*, vol. 106, no. 1, pp. 83–87, 1973. 50, 51

[110] A. Latuszynski and V. I. Raiko, "Studies of the ion source with surface-volume ionization," *Nuclear Instruments and Methods*, vol. 125, no. 1, pp. 61–66, 1975. 51

[111] R. Kirchner and A. Piotrowski, "Thermal ionization in a hot cavity," *Nuclear Instruments and Methods*, vol. 153, no. 1, pp. 291–292, 1978. 51

[112] R. Kirchner, "On the thermoionization in hot cavities," *Nuclear Instruments and Methods in Physics Research Section A: Accelerators,*

Spectrometers, Detectors and Associated Equipment, vol. 292, no. 2, pp. 203–208, 1990.

[113] Y. Duan, R. E. Danen, X. Yan, R. Steiner, J. Cuadrado, D. Wayne, V. Majidi, and J. A. Olivares, "Characterization of an improved thermal ionization cavity source for mass spectrometry," *Journal of the American Society for Mass Spectrometry*, vol. 10, no. 10, pp. 1008–1015, 1999. 51, 54

[114] J. Cesario, Y. Boulin, and B. Landeau, "An improved surface ionization ion source," *International Journal of Mass Spectrometry and Ion Physics*, vol. 46, pp. 35–38, 1983. 51

[115] Y. Duan, E. P. Chamberlin, and J. Olivares, "Development of a new high-efficiency thermal ionization source for mass spectrometry," *International journal of mass spectrometry and ion processes*, vol. 161, no. 1, pp. 27–39, 1997. 51, 52

[116] D. M. Wayne, W. Hang, D. K. McDaniel, R. E. Fields, E. Rios, and V. Majidi, "A linear time-of-flight mass analyzer for thermal ionization cavity mass spectrometry," *Spectrochimica Acta Part B: Atomic Spectroscopy*, vol. 56, no. 7, pp. 1175–1194, 2001. 52, 54

[117] S. Bürger, L. R. Riciputi, S. Turgeon, D. Bostick, E. McBay, and M. Lavelle, "A high efficiency cavity ion source using TIMS for nuclear forensic analysis," *Journal of Alloys and Compounds*, vol. 444, pp. 660–662, 2007. 53

[118] Z. Li-hua, D. Hu, W. Guan-yi, L. Zhi-ming, W. Chang-hai, L. Xue-song, Z. Guo-qing, S. Yong-yang, and Z. Zi-bin, "A new, ohmic-heating based thermal ionization cavity source for mass spectrometry," *International Journal of Mass Spectrometry*, vol. 305, no. 1, pp. 45–49, 2011. 54

[119] J. D. Fassett and P. J. Paulsen, "Isotope dilution mass spectrometry for accurate elemental analysis," *Analytical chemistry*, vol. 61, no. 10, pp. 643A–649A, 1989. 61

[120] M. L. Baruzzini, H. L. Hall, M. G. Watrous, K. J. Spencer, and F. E. Stanley, "Enhanced ionization efficiency in TIMS analyses of plutonium and americium using porous ion emitters," *International Journal of Mass Spectrometry*, vol. 412, pp. 8–13, January 2017. 64

[121] R. Deissenberger, S. Köhler, F. Ames, K. Eberhardt, N. Erdmann, H. Funk, G. Herrmann, H.-J. Kluge, M. Nunnemann, G. Passler, *et al.*, "First determination of the ionization potential of americium and curium," *Angewandte Chemie International Edition in English*, vol. 34, no. 7, pp. 814–815, 1995. 75

[122] J. Chrzanowski, Y. Kravtsov, and B. Bieg, "Application of the work function to study the percentage composition of aluminum alloys," *Zeszyty Naukowe/Akademia Morska w Szczecinie*, vol. 38, no. 110, pp. 27–31, 2014. 75

[123] M. G. Watrous, *Characterization of the Resin Bead and Development and Application of the Porous Ion Emitter for Thermal Ionization Mass Spectrometry*. PhD thesis, University of Idaho, 2010. 80

[124] NIST, "Atomic data for plutonium (Pu); `http://physics.nist.gov/PhysRefData/Handbook/Tables/plutoniumtable1.htm`." 80

[125] H. C. Urey, "The thermodynamic properties of isotopic substances," *Journal of the Chemical Society*, pp. 562–581, 1947. 90

[126] F. Albarède, P. Telouk, J. Blichert-Toft, M. Boyet, A. Agranier, and B. Nelson, "Precise and accurate isotopic measurements using multiple-collector ICPMS," *Geochimica et Cosmochimica Acta*, vol. 68, no. 12, pp. 2725–2744, 2004. 91

[127] C. M. Johnson and B. L. Beard, "Correction of instrumentally produced mass fractionation during isotopic analysis of fe by thermal ionization mass spectrometry," *International Journal of Mass Spectrometry*, vol. 193, no. 1, pp. 87–99, 1999. 91

[128] K. Habfast, "Fractionation correction and multiple collectors in thermal ionization isotope ratio mass spectrometry," *International journal of mass spectrometry*, vol. 176, no. 1, pp. 133–148, 1998.

[129] H. Ramebäck, M. Berglund, R. Kessel, and R. Wellum, "Modelling isotope fractionation in thermal ionisation mass spectrometry filaments having diffusion controlled emission," *International Journal of Mass Spectrometry*, vol. 216, no. 2, pp. 203–208, 2002.

[130] R. Andreasen and M. Sharma, "Fractionation and mixing in a thermal ionization mass spectrometer source: Implications and limitations for

high-precision nd isotope analyses," *International Journal of Mass Spectrometry*, vol. 285, no. 1, pp. 49–57, 2009. 91

[131] R. Fiedler, D. Donohue, G. Grabmueller, and A. Kurosawa, "Report on preliminary experience with total evaporation measurements in thermal ionization mass spectrometry," *International Journal of Mass Spectrometry and Ion Processes*, vol. 132, no. 3, pp. 207–215, 1994. 96

[132] "Decay data evaluation project." 97

[133] M. Wang, G. Audi, A. Wapstra, F. Kondev, M. MacCormick, X. Xu, and B. Pfeiffer, "The ame2012 atomic mass evaluation," *Chinese Physics C*, vol. 36, no. 12, p. 1603, 2012. 98

[134] G. Cavazzini, "A method for determining isotopic composition of elements by thermal ionization source mass spectrometry: Application to strontium," *International Journal of Mass Spectrometry*, vol. 240, no. 1, pp. 17–26, 2005. 110

[135] R. W. Williams and A. M. Gaffney, "^{230}Th-^{234}U model ages of some uranium standard reference materials," *Proceedings in Radiochemistry A Supplement to Radiochimica Acta*, vol. 1, no. 1, pp. 31–35, 2011. 115, 134

[136] Z. Varga, M. Wallenius, K. Mayer, and E. Hrnecek, "Alternative method for the production date determination of impure uranium ore concentrate samples," *Journal of Radioanalytical and Nuclear Chemistry*, vol. 290, no. 2, pp. 485–492, 2011. 115

[137] M. Sargent, R. Harte, and C. Harrington, *Guidelines for achieving high accuracy in isotope dilution mass spectrometry (IDMS)*, vol. 11. Royal Society of Chemistry, 2002. 121

[138] H. Cheng, R. L. Edwards, C. Shen, V. J. Polyak, Y. Asmerom, J. Woodhead, J. Hellstrom, Y. Wang, X. Kong, C. Spötl, *et al.*, "Improvements in ^{230}Th dating, ^{230}Th and ^{234}U half-life values, and U–Th isotopic measurements by multi-collector inductively coupled plasma mass spectrometry," *Earth and Planetary Science Letters*, vol. 371, pp. 82–91, 2013. 128

[139] BIPM, *evaluation of measurement data — guide to the expression of uncertainty in measurement.* JCGM 100, 2008. 129

[140] GUM Workbench. Metrodata GmbH. 129

[141] R. Essex. New Brunswick Laboratory. private communication, July 2012. 130, 131, 136

[142] A. M. Gaffney, A. Hubert, W. S. Kinman, M. Magara, A. Okubo, F. Pointurier, K. C. Schorzman, R. E. Steiner, and R. W. Williams, "Round-robin ^{230}Th–^{234}U age dating of bulk uranium for nuclear forensics," *Journal of Radioanalytical and Nuclear Chemistry*, pp. 1–6, 2015. 131

[143] R. W. Williams, A. M. Gaffney, K. C. Schorzman, and A. C. Villa, "Age dating of SRM U050: LLNL results," Tech. Rep. LLNL-TR-642914, Lawrence Livermore National Laboratory (LLNL), 2013. 131

[144] Z. Varga, C. Venchiarutti, A. Nicholl, J. Krajkó, R. Jakopič, K. Mayer, S. Richter, and Y. Aregbe, "Irmm-1000a and irmm-1000b uranium reference materials certified for the production date. part i: methodology, preparation and target characteristics," *Journal of Radioanalytical and Nuclear Chemistry*, pp. 1–9, 2015. 138

[145] G. H. Fontaine, *Fundamental Studies on Mass Bias Variability in Multi Collector-Inductively Coupled Plasma Mass Spectrometry and the Use of Isotope Ratios in Gem Authentication*. PhD thesis, Eidgenössische Technische Hochschule (ETH) Zürich, 2010. xxiii, 169

[146] N. Daly, "Scintillation type mass spectrometer ion detector," *Review of Scientific Instruments*, vol. 31, pp. 264–267, March 1960. xxiii, 174

Appendix

Appendix A

Magnetic mass filtering

Ions accelerated through a potential difference (V) leaving the mass spectrometer source housing will have a kinetic energy described by Equation A.1;

$$E_k = zV = \frac{mv^2}{2} \tag{A.1}$$

where m, v and z are the ion mass, velocity and charge, respectively. As the moving charges enter the magnetic sector they experience a force;

$$\boldsymbol{F_B} = z\boldsymbol{v} \times \boldsymbol{B} \tag{A.2}$$

with magnitude;

$$F_B = zvB \tag{A.3}$$

where B is the strength of the magnetic field, v is the ion velocity and z is the ion charge. Because the magnetic field is uniform and perpendicular to the direction of travel, ion are deflected to a circular path of radius (R), similar to a ball at the end of swinging string; as a result, an expression for centripetal force (F_c) can be used;

$$F_c = \frac{m\boldsymbol{v} \cdot \boldsymbol{v}}{R} = \frac{mv^2}{R} \tag{A.4}$$

Ion trajectory is determined by equilibrium of the magnetic and centripetal forces. By setting Equations A.3 and A.4 equal to one another,

$$\frac{mv^2}{R} = zvB \tag{A.5}$$

an expression for ion velocity (v) is obtained;

$$v = \frac{zRB}{m} \tag{A.6}$$

Substituting A.6 into Equation A.1 and rearranging yields the result presented in Chapter 2, Equation 2.1

$$\frac{m}{z} = \frac{R^2B^2}{2V} \tag{A.7}$$

In TIMS, ion charge is almost exclusively equal to 1, therefore, the radius followed by an ion in a constant magnetic field is determined by its momentum.

This can be shown by solving Equation A.5 for R;

$$R = \frac{mv}{B} \tag{A.8}$$

Upon Inspection of Equation A.8, its apparent that ions with less momentum (i.e., lighter isotopes) will follow a path with smaller radius than heavier isotopes. This is illustrated in Figure A.1

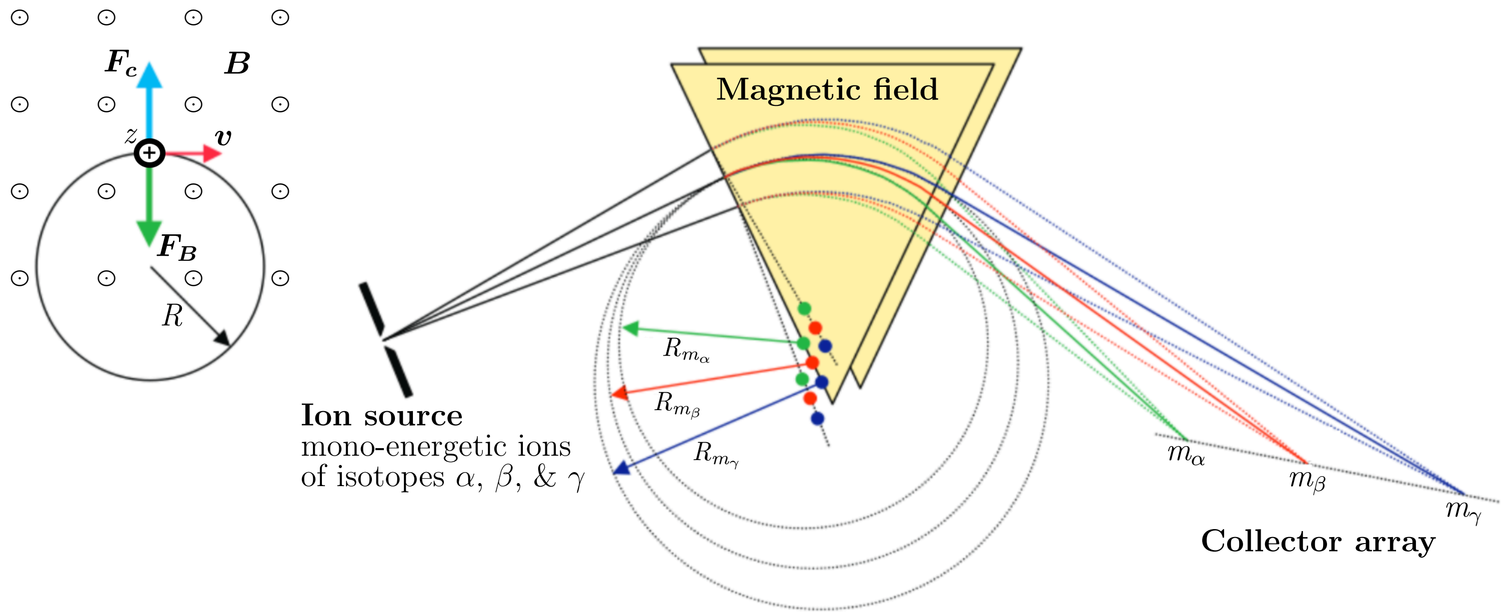

Figure A.1: Separation of a hypothetical sample composed of isotopes α, β, and γ wqith masses m_α, m_β, and m_γ, respectively, where $m_\alpha < m_\beta < m_\gamma$. Ions follow a circular path of radius R in the magnetic field $\boldsymbol{B}$; ions with the same mass-to-charge ratio m/z are focussed to the same collector. This Figure adapted was adapted from reference [145]

Appendix B

Ion detection

B.1 Faraday cup detector

A Faraday cup detector, illustrated in Figure B.1, is a remarkably simple, robust and relatively inexpensive device that can be used for the detection of positive or negative ions. They consist of a metal or carbon cup with a small entrance opening designed to prevent secondary electrons from escaping the detector. Ions entering the Faraday cup and are neutralized by either accepting electrons from or donating electrons to the detector wall. The current generated by the detector is related to the number of incident ions; this relationship is shown in Equation B.1;

$$\frac{N}{t} = \frac{I}{e} \tag{B.1}$$

where N is the number of ions detected, t is the ion collection time in seconds, I is the induced current in amperes, and e is the elementary charge in coulombs. Because ion detection is based solely on charge, there is no mass, velocity, or energy discrimination, allowing for very precise measurements.

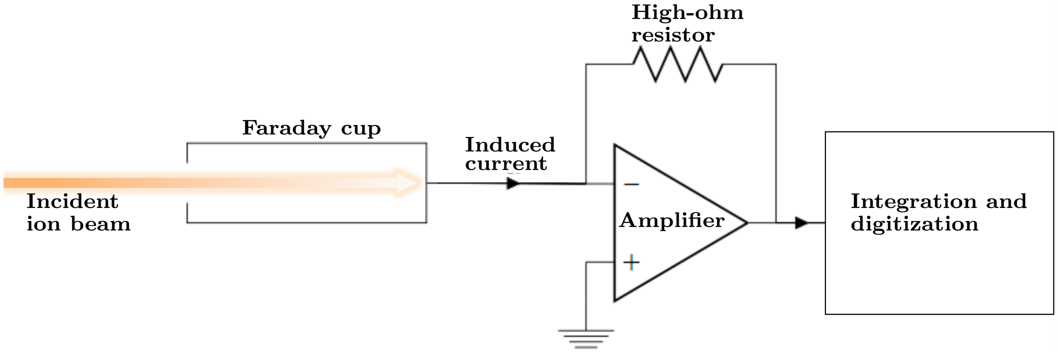

Figure B.1: A simple schematic diagram of a Faraday cup detector and associated electronics

B.2 Ion counting Daly detector

A Daly detector is a simple device used for the detection of positive ions. It consists of a negatively charged highly polished door knob shaped metal conversion dynode, an organic scintillator, and a photomultiplier tube (PMT). Positive ions from the mass spectrometer enter the detector and are accelerated via a high potential, striking the Daly knob, resulting in the release of secondary electrons. These secondary electrons are accelerated by the same potential and impinge on a scintillator which generates a light signal that is detected/amplified by the PMT; the output signal from the PMT is counted via pulse counting electronics. Figure B.2 illustrates the operation of Daly detector.

Advantages of using Daly detector include minimal mass discrimination, a high conversion efficiency scintillator, and high sensitivity allowing for precise measurements of very small samples of low abundance isotopes within a sample. Additionally, the PMT is mounted outside the vacuum system allowing for access/repairs without breaking system vacuum. With respect to electron multipliers, Daly detectors generate a pulse height distribution more suitable for discrimination between ion currents and dark currents.

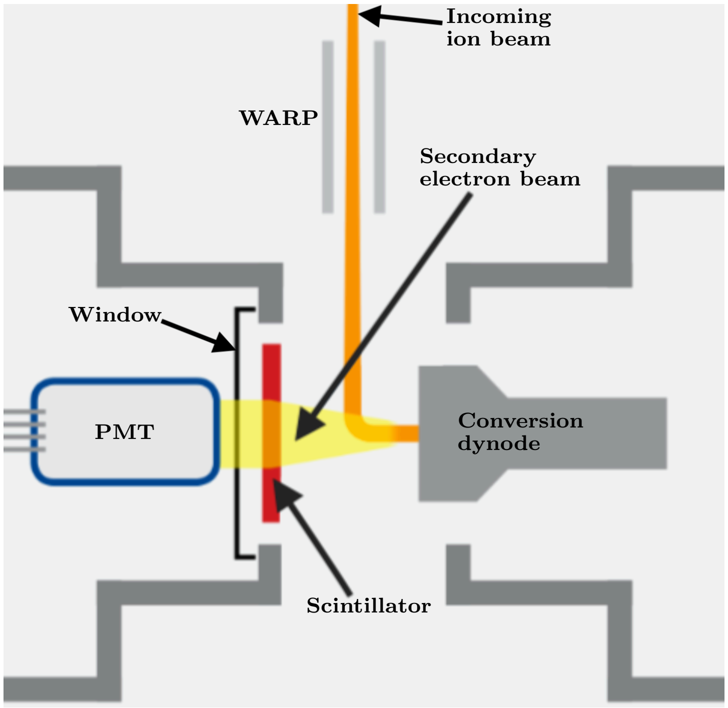

Figure B.2: An illustration of an ion counting Daly detector adapted from reference [146].

B.2.1 WARP filter

The WARP is mounted in front of the Daly detector array and provides a potential barrier that allows only a specific, narrow range of ion energy to pass. Low energy ions produced from collisions with the sides of flight tube or residual gas molecules in the analyzer are skimmed off the beam and not detected. This type of filter significantly improves abundance sensitivity, approximately two orders of magnitude, without compromising ion transmission.

Appendix C

Certificates of isotopic standards used in fractionation studies

C.1 IRMM-199

Commission of the European Communities
**JOINT
RESEARCH
CENTRE**

Geel Establishment
Central Bureau for Nuclear Measurements
Steenweg op Retie, 2440 Geel, Belgium
Tel. (014) 571.211 - Telex 33589 EURAT B

CERTIFICATE

ISOTOPIC REFERENCE MATERIAL EC NRM 199

The IRM is supplied with atomic isotope ratios certified as:

^{233}U/^{238}U = 1.000 01 +/- 0.000 30
^{234}U/^{238}U = 0.002 05 +/- 0.000 01
^{235}U/^{238}U = 1.000 15 +/- 0.000 20
^{236}U/^{238}U = 0.000 25 +/- 0.000 01

This corresponds to the isotopic composition:

	Isotopic Atom %	Isotopic Mass %	uncertainties
^{233}U/U	33.306 4	32.975 6	+/- 0.005 9
^{234}U/U	0.068 3	0.067 9	+/- 0.000 3
^{235}U/U	33.311 0	33.263 9	+/- 0.004 0
^{236}U/U	0.008 2	0.008 2	+/- 0.000 3
^{238}U/U	33.306 1	33.684 4	+/- 0.004 9

The atomic weight of the uranium is 235.377 23 +/- 0.000 24

The concentration is specified as: 1.899 +/- 0.002 . 10^{-3} kg U/kg solution

The IRM is intended for:

a) calibration of isotope dilution measurements
b) verification of the dependence of mass discrimination upon mass.

Notes

1. All uncertainties indicated are accuracies, computed on a 2s basis.

2. The relative atomic masses, used in the calculations, are:

^{233}U : 233.039 628 0 +/- 0.000 006 0
^{234}U : 234.040 946 8 +/- 0.000 004 8
^{235}U : 235.043 924 2 +/- 0.000 004 8
^{236}U : 236.045 562 7 +/- 0.000 004 6
^{238}U : 238.050 784 7 +/- 0.000 004 6

3. The Reference Material consists of a uranylnitrate solution. The amount of U per unit is 10 mg.

4. The IRM solution has a molality of 6 m HNO_3 (i.e. 6 mol $HNO_3 \cdot kg^{-1}$ of solvent) or a molarity of 5 M HNO_3 (i.e. 5 mol $HNO_3 \cdot l^{-1}$ of solution).

Chemical purification of the $^{233}U_3O_8$, $^{235}U_3O_8$ and $^{238}U_3O_8$ starting materials was performed by Willy Lycke. Preparation of the mixture was performed by Frans Hendrickx and Willy Lycke. Isotopic measurements of the starting materials were performed by Kevin Rosman and René Damen. Verification measurements on the IRM were done by René Damen.

The overall technical coordination of the establishment of this IRM, was performed by Willy Lycke.

B - 2440 Geel
1 November 1985

Paul De Bièvre
Head
CBNM Mass Spectrometry

C.2 CRM-144

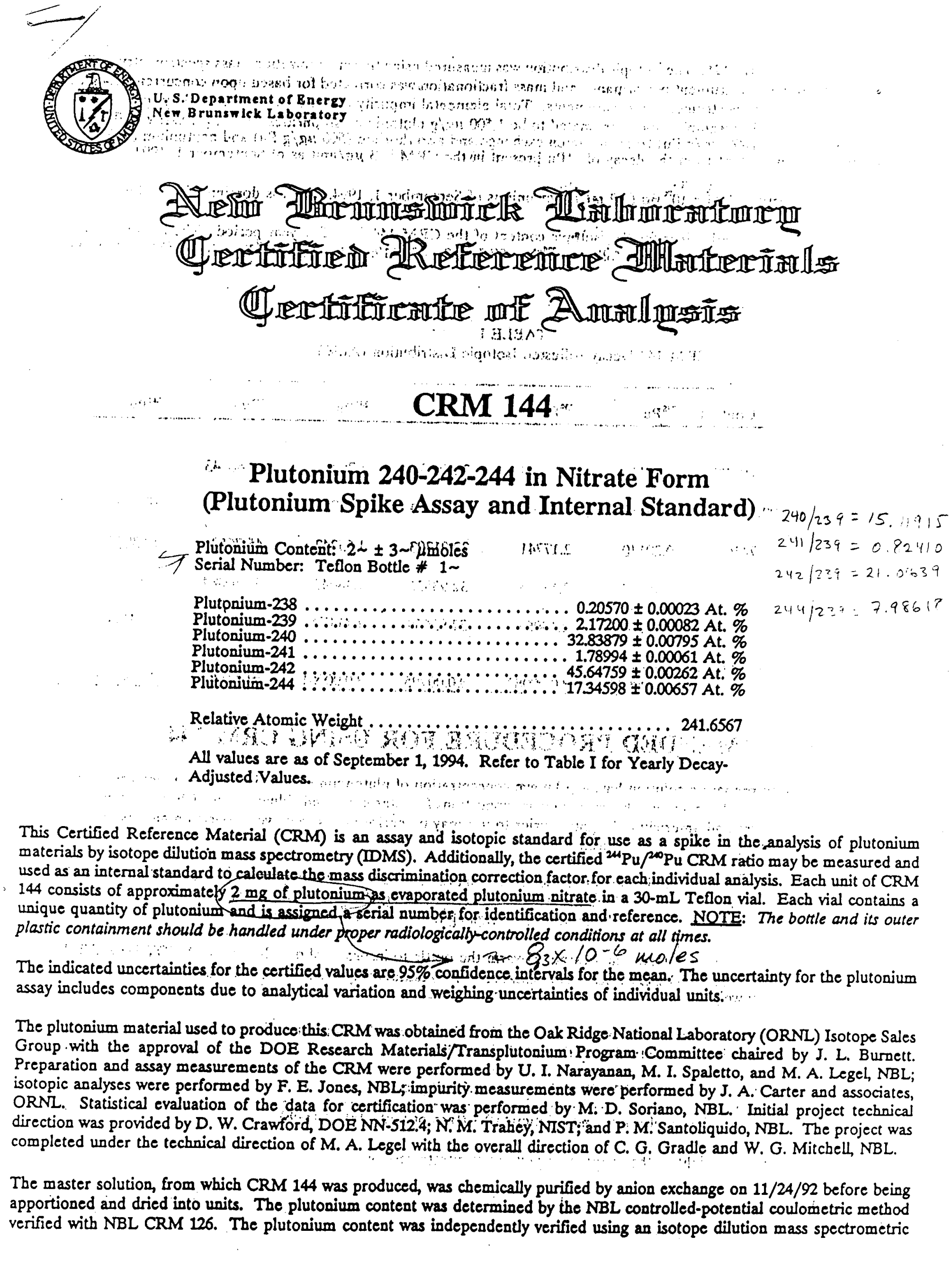

U. S. Department of Energy
New Brunswick Laboratory

New Brunswick Laboratory
Certified Reference Materials
Certificate of Analysis

CRM 144

Plutonium 240-242-244 in Nitrate Form
(Plutonium Spike Assay and Internal Standard)

240/239 = 15.11915
241/239 = 0.82410
242/239 = 21.0639
244/239 = 7.98617

Plutonium Content: 2~ ± 3~ µmoles
Serial Number: Teflon Bottle # 1~

Plutonium-238	0.20570 ± 0.00023 At. %
Plutonium-239	2.17200 ± 0.00082 At. %
Plutonium-240	32.83879 ± 0.00795 At. %
Plutonium-241	1.78994 ± 0.00061 At. %
Plutonium-242	45.64759 ± 0.00262 At. %
Plutonium-244	17.34598 ± 0.00657 At. %

Relative Atomic Weight 241.6567

All values are as of September 1, 1994. Refer to Table I for Yearly Decay-Adjusted Values.

This Certified Reference Material (CRM) is an assay and isotopic standard for use as a spike in the analysis of plutonium materials by isotope dilution mass spectrometry (IDMS). Additionally, the certified ^{244}Pu/^{240}Pu CRM ratio may be measured and used as an internal standard to calculate the mass discrimination correction factor for each individual analysis. Each unit of CRM 144 consists of approximately 2 mg of plutonium as evaporated plutonium nitrate in a 30-mL Teflon vial. Each vial contains a unique quantity of plutonium and is assigned a serial number for identification and reference. NOTE: *The bottle and its outer plastic containment should be handled under proper radiologically-controlled conditions at all times.*

$\rightarrow$ 8.3×10^{-6} moles

The indicated uncertainties for the certified values are 95% confidence intervals for the mean. The uncertainty for the plutonium assay includes components due to analytical variation and weighing uncertainties of individual units.

The plutonium material used to produce this CRM was obtained from the Oak Ridge National Laboratory (ORNL) Isotope Sales Group with the approval of the DOE Research Materials/Transplutonium Program Committee chaired by J. L. Burnett. Preparation and assay measurements of the CRM were performed by U. I. Narayanan, M. I. Spaletto, and M. A. Legel, NBL; isotopic analyses were performed by F. E. Jones, NBL; impurity measurements were performed by J. A. Carter and associates, ORNL. Statistical evaluation of the data for certification was performed by M. D. Soriano, NBL. Initial project technical direction was provided by D. W. Crawford, DOE NN-512.4; N. M. Trahey, NIST; and P. M. Santoliquido, NBL. The project was completed under the technical direction of M. A. Legel with the overall direction of C. G. Gradle and W. G. Mitchell, NBL.

The master solution, from which CRM 144 was produced, was chemically purified by anion exchange on 11/24/92 before being apportioned and dried into units. The plutonium content was determined by the NBL controlled-potential coulometric method verified with NBL CRM 126. The plutonium content was independently verified using an isotope dilution mass spectrometric technique traceable to NBL CRM 126. The isotopic distribution was measured using thermal ionization mass spectrometry. NBL CRM 137 was used to monitor instrument performance and mass fractionation was corrected for based upon concurrent analyses of NBL CRM 128 for all mass spectrometric measurements. Total elemental impurity content was determined by spark source mass spectrometry on selected subsamples and is estimated to be 1,500 μg/g plutonium. Impurities consist primarily of fluoride (>500 μg/g Pu) and chloride (300 μg/g Pu) from the anion exchange and also thorium (500 μg/g Pu) and neptunium (100 μg/g Pu). The calculated ^{241}Am content from the decay of ^{241}Pu present in the CRM is 3 μg/unit as of September 1, 1994.

CRM 144 had a radioactivity of 1.44×10^8 Bq (3.9 mCi) per unit as of September 1, 1994, which is dominated by ^{241}Pu.

Table I provides the decay-adjusted values for the isotopic content of the CRM 144 for a five-year period. The half-life values (in years) used for the decay calculations are as follows: ^{238}Pu - 87.7; ^{239}Pu - 24,119; ^{240}Pu - 6,563; ^{241}Pu - 14.35; ^{242}Pu - 373,300; and ^{244}Pu - 8.26×10^7.

TABLE I

CRM 144 Decay-Adjusted Isotopic Distribution (At.%)

Date	Pu Content	^{238}Pu	^{239}Pu	^{240}Pu	^{241}Pu	^{242}Pu	^{244}Pu
September 1, 1995	99.9107%	0.20427	2.17388	32.86476	1.70713	45.68843	17.36153
September 1, 1996	99.8251%	0.20283	2.17569	32.88954	1.62786	45.72763	17.37646
September 1, 1997	99.7436%	0.20140	2.17741	32.91303	1.55242	45.76504	17.39070
September 1, 1998	99.6656%	0.19997	2.17905	32.93536	1.48043	45.80084	17.40434
September 1, 1999	99.5911%	0.19855	2.18063	32.95659	1.41172	45.83511	17.41740
95% Confidence Interval for Certified Values:		±0.00023	±0.00082	±0.00795	±0.00061	±0.00262	±0.00657

RECOMMENDED PROCEDURE FOR USING CRM 144

The package is designed to prepare a solution having a known concentration of plutonium on a weight basis. Once prepared, it is suggested that all the solution be immediately distributed as subportions for later use as individual spikes. Chemical separation of plutonium from its uranium and americium daughters prior to use may be performed to remove isobaric impurities, however this step is not critical if ^{241}Pu is not to be measured.

Locate the plutonium nitrate material within the bottle and assure that the bulk is not in the cap area. Wipe the Teflon vial with a damp cloth to dissipate any static charge or alternatively remove static by using ^{210}Po sources at close range. This step assures that the sample will not be expelled from the vial on opening. Weighing the Teflon vial is not recommended, as static charge can give the false appearance of stable balance readings. Transfer of the solution to another tared container is recommended for dilution. Initially, add 5-10 mL of 8 $\underline{M}$ HNO_3 and carefully warm the bottle to insure total dissolution. DO NOT HEAT THE BOTTLE ABOVE 150° C TO AVOID BOTTLE DEFORMATION! Quantitatively transfer the solution to a tared container and make a final dilution by weight to calculate the plutonium concentration.

Shake vigorously to homogenize the contents and distribute all the solution as weighed portions into suitable containers for use as spikes. Calculate the plutonium concentration of the solution as follows:

$$\text{Plutonium, } \mu\text{moles/g} = \frac{\text{(Certified Pu content of unit, } \mu\text{moles)}}{\text{(mass of bottle and solution,[g]) - (tare of bottle,[g] - 0.0048)}}$$

in which 0.0048 is the nominal weight of the evaporated plutonium nitrate residue.

September 1, 1994
Argonne, Illinois

Carleton D. Bingham
Director

Appendix D

^{230}Th/^{234}U chronometry study

D.1 Results

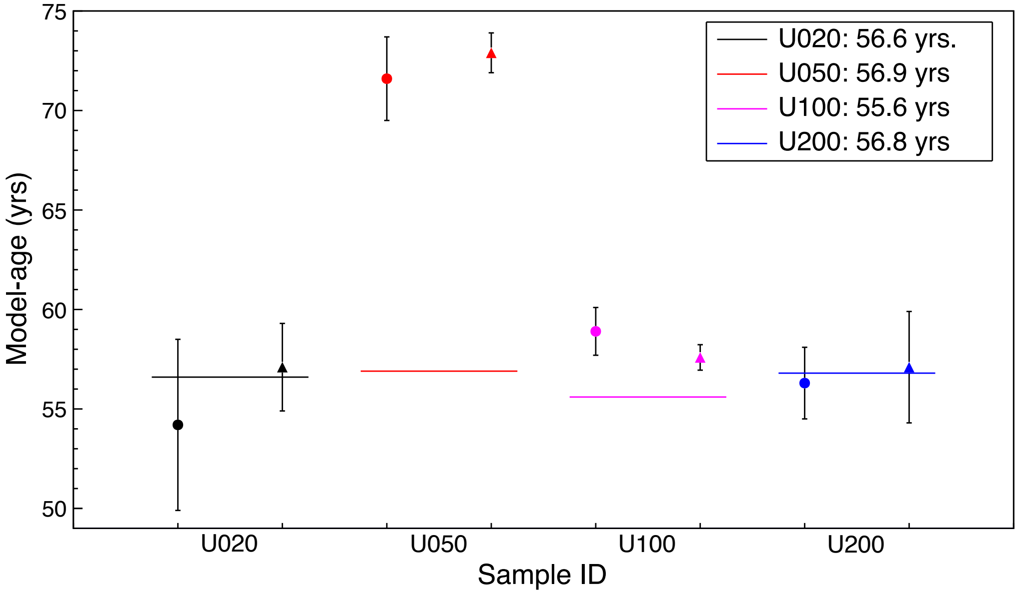

Figure D.1: Average model-age results using PIEs and standard filaments.

Table D.1: ^{230}Th and ^{234}U concentrations and model ages of NBL U020 determined using PIEs. Expanded uncertainties ($k = 2$) are given in parentheses.

Sample ID		^{234}U	^{230}Th	^{230}Th/^{234}U	model age	model
Uranium fraction	Thorium fraction	(atoms/g)	(atoms/g)	(measured)	(years before 2014-08-31)	date
U020-1-5155	Th1-U020	$3.111(50) \times 10^{11}$	$4.57(26) \times 10^{7}$	$1.470(87) \times 10^{-4}$	52.0 ± 3.1	1962-08-31
	Th3-U020		$4.95(23) \times 10^{7}$	$1.591(78) \times 10^{-4}$	56.3 ± 2.8	1958-05-13
U020-2-5156	Th1-U020	$3.102(50) \times 10^{11}$	$4.57(26) \times 10^{7}$	$1.474(87) \times 10^{-4}$	52.2 ± 3.1	1962-06-18
	Th3-U020		$4.95(23) \times 10^{7}$	$1.595(78) \times 10^{-4}$	56.5 ± 2.8	1958-03-01
U020-3-5157	Th1-U020	$3.113(50) \times 10^{11}$	$4.57(26) \times 10^{7}$	$1.469(87) \times 10^{-4}$	52.0 ± 3.1	1962-08-31
	Th3-U020		$4.95(23) \times 10^{7}$	$1.590(78) \times 10^{-4}$	56.3 ± 2.8	1958-05-13
			average		54.2 ± 4.3	1960-06-18

Table D.2: ^{230}Th and ^{234}U concentrations and model ages of NBL U020 determined using standard filaments. Expanded uncertainties ($k = 2$) are given in parentheses.

Sample ID		^{234}U	^{230}Th	^{230}Th/^{234}U	model age	model
Uranium fraction	Thorium fraction	(atoms/g)	(atoms/g)	(measured)	(years before 2014-08-31)	date
U020-1-5155	Th2-U020	$3.111(50) \times 10^{11}$	$4.91(20) \times 10^{7}$	$1.577(68) \times 10^{-4}$	55.9 ± 2.4	1958-10-06
	Th4-U020		$5.10(14) \times 10^{7}$	$1.641(51) \times 10^{-4}$	58.1 ± 1.8	1956-07-24
U020-2-5156	Th2-U020	$3.102(50) \times 10^{11}$	$4.91(20) \times 10^{7}$	$1.582(68) \times 10^{-4}$	56.1 ± 2.4	1958-07-35
	Th4-U020		$5.10(14) \times 10^{7}$	$1.645(51) \times 10^{-4}$	58.3 ± 1.8	1956-05-12
U020-3-5157	Th2-U020	$3.113(50) \times 10^{11}$	$4.91(20) \times 10^{7}$	$1.576(68) \times 10^{-4}$	55.9 ± 2.4	1958-10-06
	Th4-U020		$5.10(14) \times 10^{7}$	$1.640(51) \times 10^{-4}$	58.1 ± 1.8	1956-07-24
			average		57.1 ± 2.2	1957-08-06

Table D.3: ^{230}Th and ^{234}U concentrations and model ages of NBL U050 determined using PIEs. Expanded uncertainties ($k = 2$) are given in parentheses.

Sample ID		^{234}U	^{230}Th	^{230}Th/^{234}U	model age	model
Uranium fraction	Thorium fraction	(atoms/g)	(atoms/g)	(measured)	(years before 2014-08-31)	date
U050-1-5154	Th1-U050	$1.3294(96) \times 10^{12}$	$2.72(11) \times 10^{8}$	$2.044(85) \times 10^{-4}$	72.4 ± 3.0	1942-04-06
	Th3-U050		$2.638(54) \times 10^{8}$	$1.984(42) \times 10^{-4}$	70.3 ± 1.5	1944-05-12
U050-2-5153	Th1-U050	$1.3232(96) \times 10^{12}$	$2.72(11) \times 10^{8}$	$2.054(85) \times 10^{-4}$	72.8 ± 3.0	1941-11-11
	Th3-U050		$2.638(54) \times 10^{8}$	$1.994(43) \times 10^{-4}$	70.7 ± 1.5	1943-12-18
U050-3-5152	Th1-U050	$1.3258(96) \times 10^{12}$	$2.72(11) \times 10^{8}$	$2.049(85) \times 10^{-4}$	72.6 ± 3.1	1942-01-23
	Th3-U050		$2.638(54) \times 10^{8}$	$1.990(43) \times 10^{-4}$	70.5 ± 1.5	1944-02-29
			average		71.6 ± 2.1	1943-02-11

Table D.4: ^{230}Th and ^{234}U concentrations and model ages of NBL U050 determined using standard filaments.Expanded uncertainties ($k = 2$) are given in parentheses.

Sample ID		^{234}U	^{230}Th	^{230}Th/^{234}U	model age	model
Uranium fraction	Thorium fraction	(atoms/g)	(atoms/g)	(measured)	(years before 2014-08-31)	date
U050-1-5154	Th2-U050	$1.3294(96) \times 10^{12}$	$2.718(29) \times 10^8$	$2.044(27) \times 10^{-4}$	72.46 ± 0.97	1942-03-15
	Th4-U050		$2.747(76) \times 10^8$	$2.066(59) \times 10^{-4}$	72.3 ± 2.1	1941-06-18
U050-2-5153	Th2-U050	$1.3232(96) \times 10^{12}$	$2.718(29) \times 10^8$	$2.054(26) \times 10^{-4}$	72.79 ± 0.94	1941-11-15
	Th4-U050		$2.747(76) \times 10^8$	$2.076(60) \times 10^{-4}$	73.6 ± 2.1	1941-01-23
U050-3-5152	Th2-U050	$1.3258(96) \times 10^{12}$	$2.718(29) \times 10^8$	$2.050(26) \times 10^{-4}$	72.65 ± 0.94	1942-01-05
	Th4-U050		$2.747(76) \times 10^8$	$2.072(59) \times 10^{-4}$	73.4 ± 2.1	1941-04-06
			average		72.9 ± 1.0	1941-08-24

Table D.5: ^{230}Th and ^{234}U concentrations and model ages of NBL U100 determined using PIEs. Expanded uncertainties ($k = 2$) are given in parentheses.

Sample ID		^{234}U (atoms/g)	^{230}Th (atoms/g)	^{230}Th/^{234}U (measured)	model age (years before 2014-08-31)	model date
Uranium fraction	Thorium fraction					
U100-1-5163	Th1-U100	$3.433(21) \times 10^{12}$	$5.65(21) \times 10^{8}$	$1.645(61) \times 10^{-4}$	58.3 ± 2.2	1956-05-12
	Th3-U100		$5.77(15) \times 10^{8}$	$1.680(45) \times 10^{-4}$	59.5 ± 1.6	1955-03-01
U100-2-5166	Th1-U100	$3.442(21) \times 10^{12}$	$5.65(21) \times 10^{8}$	$1.641(61) \times 10^{-4}$	58.2 ± 2.2	1956-06-18
	Th3-U100		$5.77(15) \times 10^{8}$	$1.675(45) \times 10^{-4}$	59.4 ± 1.6	1955-04-07
U100-3-5159	Th1-U100	$3.432(21) \times 10^{12}$	$5.65(21) \times 10^{8}$	$1.645(61) \times 10^{-4}$	58.3 ± 2.2	1956-05-12
	Th3-U100		$5.77(15) \times 10^{8}$	$1.680(45) \times 10^{-4}$	59.5 ± 1.6	1955-03-01
			average		58.9 ± 1.2	1955-10-18

Table D.6: ^{230}Th and ^{234}U concentrations and model ages of NBL U100 determined using standard filaments. Expanded uncertainties ($k = 2$) are given in parentheses.

Sample ID		^{234}U	^{230}Th	^{230}Th/^{234}U	model age	model
Uranium fraction	Thorium fraction	(atoms/g)	(atoms/g)	(measured)	(years before 2014-08-31)	date
U100-1-5163	Th2-U100	$3.433(21) \times 10^{12}$	$5.613(60) \times 10^{8}$	$1.635(20) \times 10^{-4}$	57.95 ± 0.71	1956-09-17
	Th4-U100		$5.552(68) \times 10^{8}$	$1.617(22) \times 10^{-4}$	57.32 ± 0.78	1957-05-05
U100-2-5166	Th2-U100	$3.442(21) \times 10^{12}$	$5.613(60) \times 10^{8}$	$1.631(20) \times 10^{-4}$	57.81 ± 0.71	1956-11-07
	Th4-U100		$5.552(68) \times 10^{8}$	$1.613(22) \times 10^{-4}$	57.18 ± 0.78	1957-06-26
U100-3-5159	Th2-U100	$3.432(21) \times 10^{12}$	$5.613(60) \times 10^{8}$	$1.635(20) \times 10^{-4}$	57.96 ± 0.71	1956-09-14
	Th4-U100		$5.552(68) \times 10^{8}$	$1.618(22) \times 10^{-4}$	57.33 ± 0.78	1957-05-02
			average		57.59 ± 0.64	1957-01-26

Table D.7: ^{230}Th and ^{234}U concentrations and model ages of NBL U200 determined using PIEs. Expanded uncertainties ($k = 2$) are given in parentheses.

Sample ID		^{234}U	^{230}Th	^{230}Th/^{234}U	model age	model
Uranium fraction	Thorium fraction	(atoms/g)	(atoms/g)	(measured)	(years before 2014-08-31)	date
U200-1-5160	Th1-U200	$4.606(22) \times 10^{12}$	$7.21(16) \times 10^{8}$	$1.565(38) \times 10^{-4}$	55.5 ± 1.3	1959-03-01
	Th3-U200		$7.44(13) \times 10^{8}$	$1.616(29) \times 10^{-4}$	57.3 ± 1.0	1957-05-13
U200-2-5164	Th1-U200	$4.604(23) \times 10^{12}$	$7.21(16) \times 10^{8}$	$1.565(38) \times 10^{-4}$	55.5 ± 1.3	1959-03-01
	Th3-U200		$7.44(13) \times 10^{8}$	$1.617(29) \times 10^{-4}$	57.3 ± 1.0	1957-05-13
U200-3-5167	Th1-U200	$4.624(26) \times 10^{12}$	$7.21(16) \times 10^{8}$	$1.558(38) \times 10^{-4}$	55.2 ± 1.3	1959-06-19
	Th3-U200		$7.44(13) \times 10^{8}$	$1.610(29) \times 10^{-4}$	57.1 ± 1.0	1957-07-25
			average		56.3 ± 1.8	1958-05-07

Table D.8: ^{230}Th and ^{234}U concentrations and model ages of NBL U200 determined using standard filaments. Expanded uncertainties ($k = 2$) are given in parentheses.

Sample ID		^{234}U	^{230}Th	^{230}Th/^{234}U	model age	model
Uranium fraction	Thorium fraction	(atoms/g)	(atoms/g)	(measured)	(years before 2014-08-31)	date
U200-1-5160	Th2-U200	$4.606(22) \times 10^{12}$	$7.61(17) \times 10^{8}$	$1.652(37) \times 10^{-4}$	58.6 ± 1.3	1956-01-24
	Th4-U200		$7.252(88) \times 10^{8}$	$1.575(21) \times 10^{-4}$	55.80 ± 0.73	1958-11-12
U200-2-5164	Th2-U200	$4.604(23) \times 10^{12}$	$7.61(17) \times 10^{8}$	$1.653(37) \times 10^{-4}$	58.6 ± 1.3	1956-01-24
	Th4-U200		$7.252(88) \times 10^{8}$	$1.575(21) \times 10^{-4}$	55.83 ± 0.74	1958-11-01
U200-3-5167	Th2-U200	$4.624(26) \times 10^{12}$	$7.61(17) \times 10^{8}$	$1.645(37) \times 10^{-4}$	58.3 ± 1.3	1956-05-12
	Th4-U200		$7.252(88) \times 10^{8}$	$1.568(21) \times 10^{-4}$	55.58 ± 0.75	1959-01-31
			average		57.1 ± 2.8	1957-07-18

D.2 Certificates

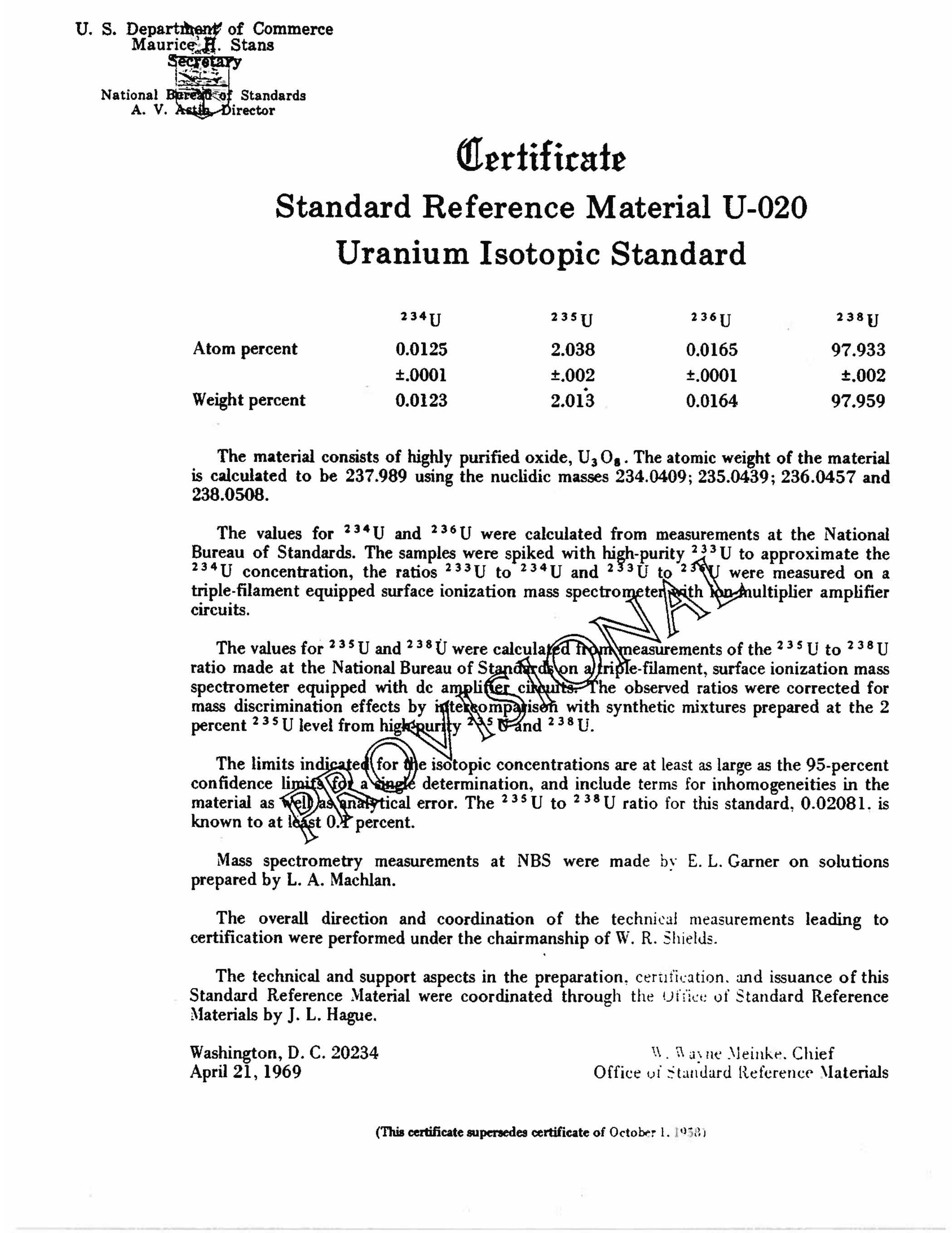

U. S. Department of Commerce
Maurice H. Stans
Secretary

National Bureau of Standards
A. V. Astin, Director

Certificate

Standard Reference Material U-020
Uranium Isotopic Standard

	^{234}U	^{235}U	^{236}U	^{238}U
Atom percent	0.0125	2.038	0.0165	97.933
	±.0001	±.002	±.0001	±.002
Weight percent	0.0123	2.013	0.0164	97.959

The material consists of highly purified oxide, U_3O_8. The atomic weight of the material is calculated to be 237.989 using the nuclidic masses 234.0409; 235.0439; 236.0457 and 238.0508.

The values for ^{234}U and ^{236}U were calculated from measurements at the National Bureau of Standards. The samples were spiked with high-purity ^{233}U to approximate the ^{234}U concentration, the ratios ^{233}U to ^{234}U and ^{233}U to ^{236}U were measured on a triple-filament equipped surface ionization mass spectrometer with ion-multiplier amplifier circuits.

The values for ^{235}U and ^{238}U were calculated from measurements of the ^{235}U to ^{238}U ratio made at the National Bureau of Standards on a triple-filament, surface ionization mass spectrometer equipped with dc amplifier circuits. The observed ratios were corrected for mass discrimination effects by intercomparison with synthetic mixtures prepared at the 2 percent ^{235}U level from high-purity ^{235}U and ^{238}U.

The limits indicated for the isotopic concentrations are at least as large as the 95-percent confidence limits for a single determination, and include terms for inhomogeneities in the material as well as analytical error. The ^{235}U to ^{238}U ratio for this standard, 0.02081, is known to at least 0.1 percent.

PROVISIONAL

Mass spectrometry measurements at NBS were made by E. L. Garner on solutions prepared by L. A. Machlan.

The overall direction and coordination of the technical measurements leading to certification were performed under the chairmanship of W. R. Shields.

The technical and support aspects in the preparation, certification, and issuance of this Standard Reference Material were coordinated through the Office of Standard Reference Materials by J. L. Hague.

Washington, D. C. 20234
April 21, 1969

W. Wayne Meinke, Chief
Office of Standard Reference Materials

(This certificate supersedes certificate of October 1, 1958)

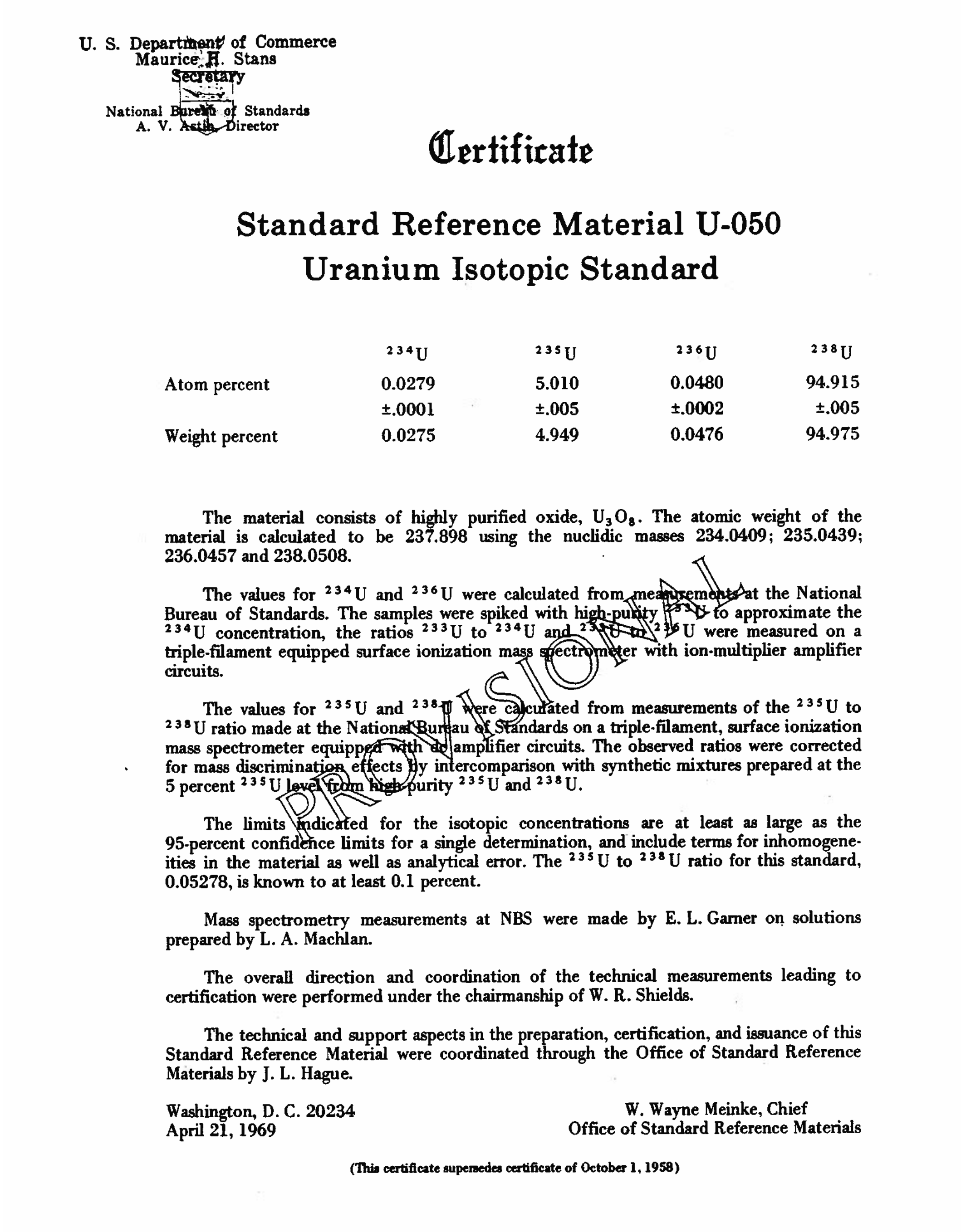

U. S. Department of Commerce
Maurice H. Stans
Secretary

National Bureau of Standards
A. V. Astin, Director

Certificate

Standard Reference Material U-050
Uranium Isotopic Standard

	^{234}U	^{235}U	^{236}U	^{238}U
Atom percent	0.0279	5.010	0.0480	94.915
	±.0001	±.005	±.0002	±.005
Weight percent	0.0275	4.949	0.0476	94.975

The material consists of highly purified oxide, U_3O_8. The atomic weight of the material is calculated to be 237.898 using the nuclidic masses 234.0409; 235.0439; 236.0457 and 238.0508.

The values for ^{234}U and ^{236}U were calculated from measurements at the National Bureau of Standards. The samples were spiked with high-purity ^{233}U to approximate the ^{234}U concentration, the ratios ^{233}U to ^{234}U and ^{233}U to ^{236}U were measured on a triple-filament equipped surface ionization mass spectrometer with ion-multiplier amplifier circuits.

The values for ^{235}U and ^{238}U were calculated from measurements of the ^{235}U to ^{238}U ratio made at the National Bureau of Standards on a triple-filament, surface ionization mass spectrometer equipped with dc amplifier circuits. The observed ratios were corrected for mass discrimination effects by intercomparison with synthetic mixtures prepared at the 5 percent ^{235}U level from high-purity ^{235}U and ^{238}U.

PROVISIONAL

The limits indicated for the isotopic concentrations are at least as large as the 95-percent confidence limits for a single determination, and include terms for inhomogeneities in the material as well as analytical error. The ^{235}U to ^{238}U ratio for this standard, 0.05278, is known to at least 0.1 percent.

Mass spectrometry measurements at NBS were made by E. L. Garner on solutions prepared by L. A. Machlan.

The overall direction and coordination of the technical measurements leading to certification were performed under the chairmanship of W. R. Shields.

The technical and support aspects in the preparation, certification, and issuance of this Standard Reference Material were coordinated through the Office of Standard Reference Materials by J. L. Hague.

Washington, D. C. 20234
April 21, 1969

W. Wayne Meinke, Chief
Office of Standard Reference Materials

(This certificate supersedes certificate of October 1, 1958)

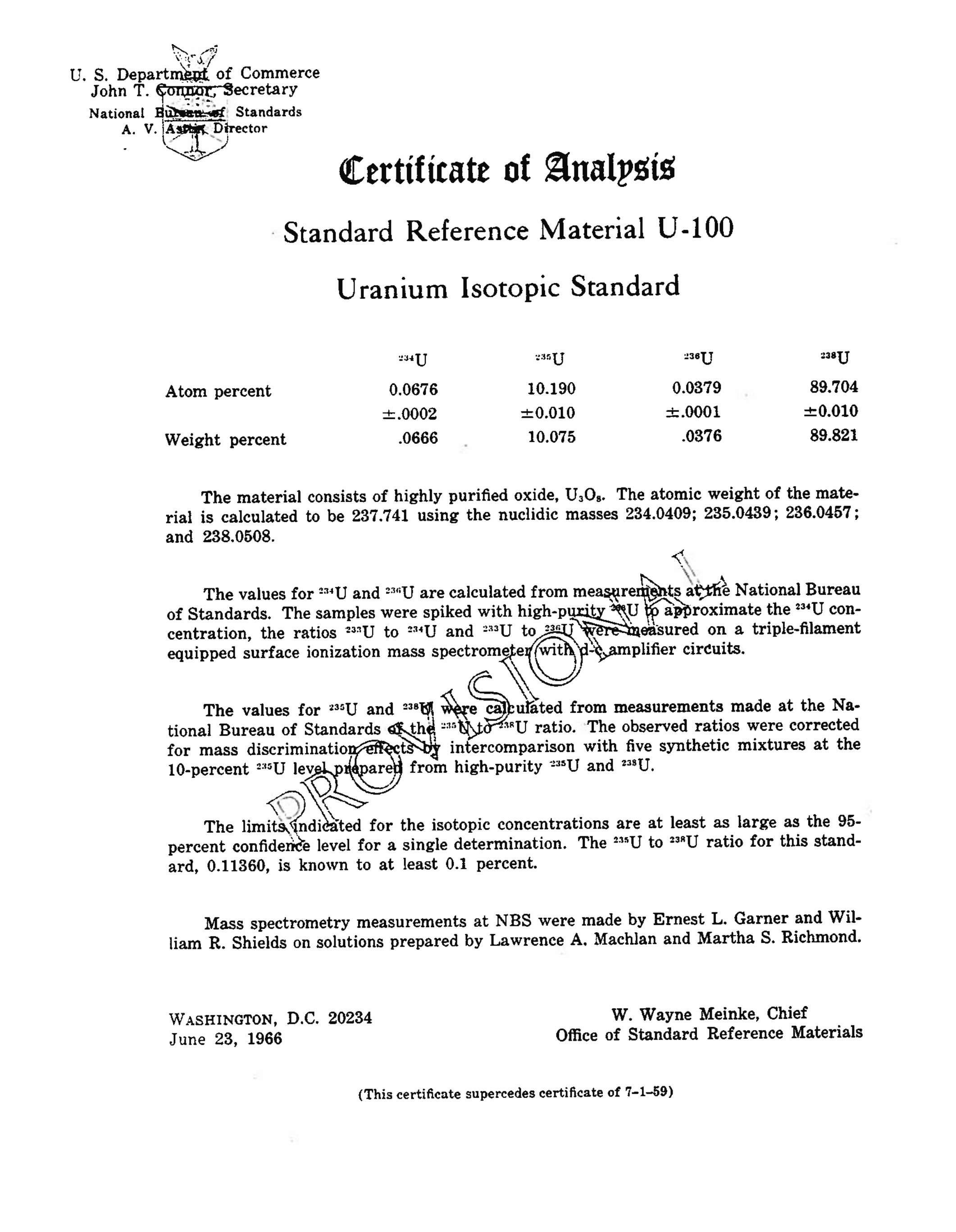

U. S. Department of Commerce
John T. Connor, Secretary
National Bureau of Standards
A. V. Astin, Director

Certificate of Analysis

Standard Reference Material U-100

Uranium Isotopic Standard

	^{234}U	^{235}U	^{236}U	^{238}U
Atom percent	0.0676	10.190	0.0379	89.704
	±.0002	±0.010	±.0001	±0.010
Weight percent	.0666	10.075	.0376	89.821

The material consists of highly purified oxide, U_3O_8. The atomic weight of the material is calculated to be 237.741 using the nuclidic masses 234.0409; 235.0439; 236.0457; and 238.0508.

The values for ^{234}U and ^{236}U are calculated from measurements at the National Bureau of Standards. The samples were spiked with high-purity ^{233}U to approximate the ^{234}U concentration, the ratios ^{233}U to ^{234}U and ^{233}U to ^{236}U were measured on a triple-filament equipped surface ionization mass spectrometer with d-c amplifier circuits.

The values for ^{235}U and ^{238}U were calculated from measurements made at the National Bureau of Standards of the ^{235}U to ^{238}U ratio. The observed ratios were corrected for mass discrimination effects by intercomparison with five synthetic mixtures at the 10-percent ^{235}U level prepared from high-purity ^{235}U and ^{238}U.

PROVISIONAL

The limits indicated for the isotopic concentrations are at least as large as the 95-percent confidence level for a single determination. The ^{235}U to ^{238}U ratio for this standard, 0.11360, is known to at least 0.1 percent.

Mass spectrometry measurements at NBS were made by Ernest L. Garner and William R. Shields on solutions prepared by Lawrence A. Machlan and Martha S. Richmond.

WASHINGTON, D.C. 20234
June 23, 1966

W. Wayne Meinke, Chief
Office of Standard Reference Materials

(This certificate supercedes certificate of 7-1-59)

U. S. Department of Commerce
John T. Connor, Secretary
National Bureau of Standards
A. V. Astin, Director

Certificate of Analysis

Standard Reference Material U-200

Uranium Isotopic Standard

	^{234}U	^{235}U	^{236}U	^{238}U
Atom percent	0.1246	20.013	0.2116	79.651
	±.0003	±0.020	±.0006	±0.021
Weight percent	.1229	19.811	.2103	79.856

The material consists of highly purified oxide, U_3O_8. The atomic weight of the material is calculated to be 237.440 using the nuclidic masses 234.0409; 235.0439; 236.0457; and 238.0508.

The values for ^{234}U and ^{236}U are calculated from measurements at the National Bureau of Standards. The samples were spiked with high-purity ^{233}U to approximate the ^{234}U concentration, the ratios ^{233}U to ^{234}U and ^{233}U to ^{236}U were measured on a triple-filament equipped surface ionization mass spectrometer with d-c amplifier circuits.

The values for ^{235}U and ^{238}U are derived from measurements made at the National Bureau of Standards, at Union Carbide Nuclear Co., Oak Ridge, Tenn., and at Goodyear Atomic Corp., Portsmouth, Ohio, each laboratory's value being given equal weight. Values obtained at NBS are the result of direct measurement of the ^{235}U to ^{238}U ratio using triple filament thermal ionization. The observed ratios were corrected for mass discrimination effects by determining the system bias from measurements on standards U-500 and U-100. Experience at NBS has shown, through intercomparison of the standards, and synthetic mixtures at the 10-, 50-, and 90-percent ^{235}U level prepared from high-purity ^{235}U and ^{238}U isotopes, that a constant bias for a given procedure can be maintained over the range of 5- to 95-percent ^{235}U. Values from Union Carbide and Goodyear Atomic are based on direct determinations of the ^{235}U concentration by oxide dilution and UF_6 analysis, and then the ratio calculated using the NBS values for ^{234}U and ^{236}U, and the ^{238}U value obtained by difference.

PROVISIONAL

The limits indicated for the isotopic concentrations are at least as large as the 95-percent confidence level for a single determination. The ^{235}U to ^{238}U ratio for this standard, 0.25126, is known to at least 0.1 percent; at the same time the pooled variance for the calibration system is significantly smaller.

Mass spectrometry measurements at NBS were made by Ernest L. Garner and William R. Shields on solutions prepared by Lawrence A. Machlan and Martha S. Richmond.

WASHINGTON, D.C. 20234
June 1, 1966

W. Wayne Meinke, Chief
Office of Standard Reference Materials

(This certificate supersedes certificate of 10-1-58)

Appendix E

Certificate for SRM-981 lead isotopic standard

National Institute of Standards & Technology

Certificate of Analysis

Standard Reference Material 981

Common Lead Isotopic Standard

This Standard Reference Material (SRM) is intended primarily for use as an isotopic standard. SRM 981 consists of 1 gram of a commercially available, high purity lead metal, of 99.9 + percent purity, that was extruded into wire form. The atomic weight of the material is calculated to be 207.215 using the nuclidic masses 203.973044, 205.974468, 206.975903, and 207.976650. The certified isotopic compositions are given below.

Atomic Abundance Ratio, Lead-204/Lead-206	0.059042 ± 0.000037
Atomic Abundance Ratio, Lead-207/Lead-206	0.91464 ± 0.00033
Atomic Abundance Ratio, Lead-208/Lead-206	2.1681 ± 0.0008
Lead-204, atom percent	1.4255 ± 0.0012
Lead-206, atom percent	24.1442 ± 0.0057
Lead-207, atom percent	22.0833 ± 0.0027
Lead-208, atom percent	52.3470 ± 0.0086

Overall limits of error are based on 95 percent confidence limits for the mean of the ratio measurements and on allowances for the known sources of possible systematic error.

Measurements for certification were by triple filament solid-sample mass spectrometry. Mixtures with known ^{208}Pb/^{206}Pb ratio, prepared from high-purity separated isotope solutions, were used as comparison standards. Details of the preparation and measurements were published by E.J. Catanzaro, T.J. Murphy, W.R. Shields, and E.L. Garner, J. Research NBS 72A, No. 3,261 (1968).

The analytical measurements leading to the certification of this material were performed in the NIST Inorganic Analytical Research Division.

The overall coordination of efforts leading to the update and revision of this certificate was coordinated through the Standard Reference Materials Program by T. E. Gills.

Gaithersburg, MD 20899
March 25, 1991
(Revision of certificate dated 4-10-73)

William P. Reed, Chief
Standard Reference Materials Program

Vita

Matthew Louis Baruzzini was born in St. Louis, Missouri, to parents Louis and Deborah Baruzzini. He attended Riverview Gardens Senior High School, St. Louis, Missouri, graduating in 1998. After graduation, he attended Ranken Technical College in St. Louis, MO, earning an Associates degree in Automotive Maintenance Technology in June, 2000. During the following four years, he was employed as an automotive technician. In the fall of 2004, Matthew decided to continue his education and enrolled in the University of Missouri – St. Louis/Washington University Joint Engineering Program focusing on electrical engineering. Matthew decided to change his major to nuclear engineering and transferred to the University of Wisconsin – Madison in the fall semester of 2006. While at Wisconsin Matthew earned a Bachelor of Science with a major in Nuclear Engineering and a Master of Science with a major in Nuclear Engineering & Engineering Physics; both degrees were awarded concurrently in August of 2011. Upon completion of his

Bachelor and Master degrees, Matthew moved to Oak Ridge, Tennessee and enrolled at University of Tennessee – Knoxville to pursue a PhD in nuclear engineering. Matthew lives in Los Alamos, New Mexico and is employed in the Advanced Nuclear Technology group (NEN-2) within the Nuclear Engineering & Nonproliferation division at Los Alamos National Laboratory.